Metabolic Systems Biology for Stem Cell Bioprocesses

João Alberto Pacheco Marques de Vasconcelos e Sá

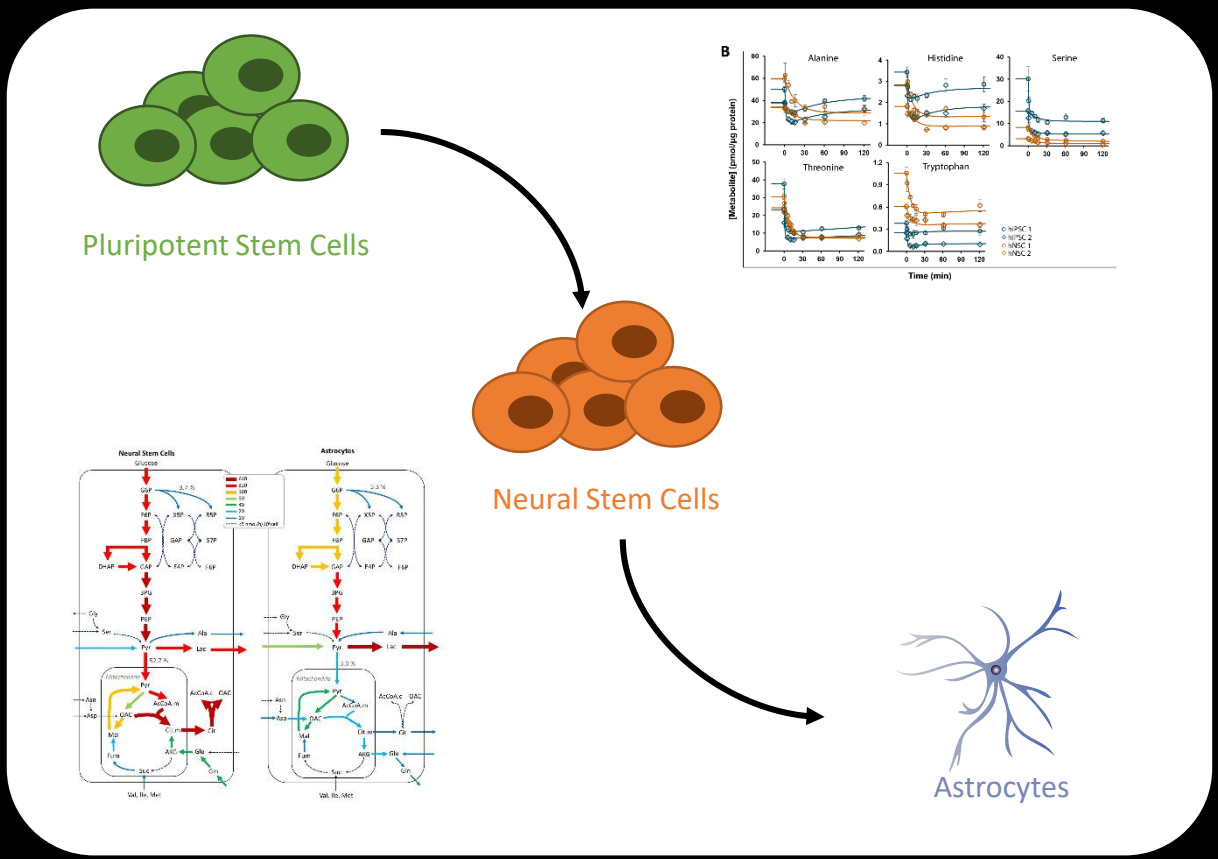

Dissertation presented to obtain the Ph.D degree in Bioengineering

Instituto de Tecnologia Química e Biológica António Xavier | Universidade Nova de Lisboa

Oeiras,
April, 2020

UNIVERSIDADE NOVA DE LISBOA

Metabolic Systems Biology for Stem Cell Bioprocesses

João Alberto Pacheco Marques de Vasconcelos e Sá

Dissertation presented to obtain the Ph.D degree in Bioengineering

Instituto de Tecnologia Química e Biológica António Xavier | Universidade Nova de Lisboa

Oeiras, April, 2020

Metabolic Systems Biology for Stem Cell Bioprocesses

João Alberto Pacheco Marques de Vasconcelos e Sá

The work developed in this thesis was supervised by:

- **Professor Manuel José Teixeira Carrondo,** Instituto de Tecnologia Química e Biológica António Xavier, Universidade Nova de Lisboa (ITQB NOVA) and Instituto de Biologia Experimental e Tecnológica (iBET)
- **Doctor Inês Azevedo Isidro,** Instituto de Tecnologia Química e Biológica António Xavier, Universidade Nova de Lisboa (ITQB NOVA) and Instituto de Biologia Experimental e Tecnológica (iBET)

Metabolic Systems Biology for Stem Cell Bioprocesses

Instituto de Tecnologia Química e Biológica António Xavier

Universidade Nova de Lisboa

Financial support from:

Fundação para a Ciência e Tecnologia (FCT)

Ph.D Grant PD/BD/52474/2014

iNOVA4Health (UID/Multi/04462/2019), a program financially supported by Fundação para a Ciência e Tecnologia/Ministério da Educação e Ciência, through national funds and co-funded by FEDER under the PT2020 Partnership Agreement

Aos meus pais que investiram na minha educação

Acknowledgements

I would like to express my gratitude to all the people who, directly or indirectly, have helped me during these years and contributed to this thesis.

To my supervisor Professor Manuel Carrondo for the opportunity to work in an inspiring and excellent scientific environment at the Animal Cell Technology Unit. Thank you for your supervision and your unique way of looking to projects in a strategic way, not just by analyzing if a project is scientifically possible. Your example of founding such a high-grade scientific institute in a place like Portugal 25 years ago is inspiring. Thank you for inspiring me to work harder and better over the years.

To Dr. Paula M Alves for your supervision, guidance and numerous opportunities throughout the years such as courses and conferences, that contributed to my development as a scientist.

To my co-supervisor Dr. Inês Isidro for your supervision in the last two years. Your attention to details and to scientific rigor have been very instructive. Moreover, I am extremely grateful for giving me the liberty to change gears during the last two years of my thesis, into a rather uncharted field. That liberty helped me also to gain responsibility and grow as person.

To Dr. Catarina Brito firstly for making me aware of the scientific competition and therefore prevent going into shark-infested waters. Secondly, to be able to collaborate and offer important insights into the work. Thirdly, to call my attention that perfection is paralyzing.

To Dr. Ana Teixeira for your supervision in the first two years and especially for the excellent lesson of how scientific output is always higher that it what seems. Your confidence in our scientific results led to the publication of my first research article as main author. In addition, I am

thankful for including me in the collaboration project with Konstanz University and NTNU University in the neural stem cell project. It was a very fruitful collaboration.

To Dr. Susanne Kleiderman, Dr. Marcel Leist and Dr. Ursula Sonnewald for all the support during our collaboration.

A very warm thanks to Dr. Daniel Simão for believing me more that I believed in myself. Without you, the last thesis' article would not have existed. It has been a great pleasure to work with you.

To my colleagues and friends Dr. Marta Silva, Dr. Ana Paula Terrasso for their constant great help and support. Without you, the last article wouldn't exist.

To the direction of the Ph.D program in BioEngineering – Cell Therapies & Regenerative Medicine – for the great content and invited speakers. The classes were very useful to perform an "investment" analysis of my scientific course.

To iBET direction for the excellent conditions provided and the instilment of scientific rigor. iBET is indeed one of the best places to work in Portugal. I will be always available to support iBET's mission, in accordance with my means and possibilities.

To my colleagues at Animal Cell Technology Unit for your ability to share scientific protocols and knowledge, permitting thus that any scientist in the lab can access to several fields. This creates a great balance between specialization and "know little about everything". To my collaborators in Advanced Cell Models group and Stem Cell Bioengineering for receiving me with open arms and teaching me.

Thank you Marta for your understanding and abnegation of so many weekends that we didn't spend together so that I could work on this thesis.

To my family and friends, thank you for understanding my absence over the last year.

I would like to thank also to the Portuguese and European tax payers that indirectly provided the funding and salary for my PhD thesis. I hope my work can be of use for the development of the regenerative medicine field in Europe.

Abstract

The application of stem cell-derived products for human health is in its infancy. Different applications of stem cell bioprocesses – cell therapy, discovery of new targets for regenerative medicine, disease modeling, drug and toxicity testing – have common hurdles. The most relevant hurdle is the lack of quality of cell products due to inefficient and ineffective stem cell differentiation procedures. Differentiated cells *in vitro* do not behave similarly to mature cells *in vivo* despite presenting similar surface and intracellular protein biomarkers. Our current weak understanding of cell "behavior" contributes to lack of cell functionality of produced cells and make these inadequate for cell therapy, disease modeling, drug screening and toxicity. Cells communicate with the environment and with neighboring cells, usually through secreted factors and through metabolites. This communication is guaranteed by an adjustable and controlled internal system in which metabolism is very important. Therefore, as complement to protein biomarkers, stem cell bioprocesses should be monitored and optimized by evaluating metabolic systemic characteristics. Thus, metabolism constitutes a needed toolbox for understanding and improving stem cell bioprocesses.

The work developed in this thesis aimed firstly to demonstrate how metabolic systems biology can differentiate between different stages in a neural differentiation process, and secondly, based on the obtained results, to propose new metabolic-based strategies to optimize stem cell bioprocesses. To achieve these goals, two different metabolic characterization approaches were pursued: metabolic flux analysis (MFA) of neural stem cells (NSC) and astrocytes, and dynamic metabolomics of pluripotent and neural stem cells.

In the first approach, ^{13}C-MFA was used to show that the fluxomes of neural stem cells and of astrocytes are distinct. The observed astrocytic

fluxome shows a significant glycolytic rate, citrate release, glutamine synthesis and secretion and residual TCA activity. Relevant fluxomic characteristics of NSC include reductive carboxylation, significant lipid synthesis and high upstream TCA cycle activity. The obtained fluxomes are distinct, with special incidence in amino acid metabolism. Therefore, these differences could be exploited to optimize neural stem cell bioprocessing. To improve astrocytic culture purity to enable more precise drug testing and toxicity results, glutamine deprivation or enzymatic blockage of fatty acid synthesis could be employed to starve off NSC.

A second more novel approach, focused on characterizing the intracellular metabolic control of a cell. The hypothesis postulates that each type of cell presents metabolic pools with specific, and therefore characteristic, control dynamics. This is based on present knowledge of the influence of several metabolites in the fate of specific cells. To identify candidates with regulatory potential, an extracellular step stimulus was applied. A relatively large number of metabolites, with a broad chemical range, was followed after the extracellular pulse. The first important observation was that metabolic pool levels changed but cell phenotype did not. This means that “static” characterization methods quantifying metabolic pools are only focusing on one possible metabolic pool set. Secondly, some metabolic pool changes were conserved between different cell lines of hiPSC and hNSC, implying that some metabolic pools have controlled steady-state changes while other metabolic pools are “free” to change their pool level. Interestingly, when mapping the ratio of metabolic pool levels after and before the pulse onto a metabolic network, flux results from literature could be reproduced. Consequently this pulse approach could be used to determine active fluxes, which consumes less computational time and is cheaper as ^{13}C-labelling is not required. Finally, characterization at the metabolic level was achieved by modelling the dynamic data of each

metabolic pool to a classical process dynamics equation. Fitting of most amino acid dynamic profiles showed cell-specific curves, a result with strong implications: the capture the dynamic behavior of amino acid metabolic pools over time after a perturbation might be a critical complementary method to characterize a given cell. Analytical methods for amino acids are abundant, precise and accurate, and there are several molecular methods to probe and study amino acid metabolism. These methods could be used, as a complementary way, to characterize cells.

Overall, it is expected that this thesis has demonstrated the value of metabolic systems biology as a cell characterization tool and its potential for the design of strategies for improving bioprocesses. In particular, we have shown, through two different metabolic characterization methods, that amino acids features, be it fluxes or intracellular pool dynamics, seem to be specific for each cell type.

The search of metabolism-based strategies for optimizing stem cell processes can benefit from the wide distribution of amino acids over the metabolic network and the existing mature methodology to analyse amino acids.

Resumo

O uso de produtos derivados de células estaminais na saúde humana está em franco crescimento. As diferentes aplicações de bioprocessos de células estaminais – terapia celular, descoberta de novos alvos para medicina regenerativa, modelação de doenças, testes de eficácia e toxicidade de drogas – apresentam dificuldades. O obstáculo mais relevante é a falta de qualidade dos produtos celulares devido a uma diferenciação ineficaz e ineficiente a partir de células estaminais. Células diferenciadas *in vitro* não se comportam da mesma maneira do que células *in vivo* apesar de apresentarem um perfil semelhante de proteínas membranares e intracelulares. A falta de funcionalidade das células produzidas, portanto inadequadas para terapia celular, modelação de doença, testes de eficácia e toxicidade de drogas, reside em parte no mau conhecimento do comportamento celular. As células comunicam com o ambiente exterior e com as células vizinhas, normalmente através de factores secretados e de metabolitos. Esta comunicação é garantida por um sistema interno ajustável e controlado no qual o metabolismo é extremamente importante. Consequentemente, e como complemento aos biomarcadores proteicos, os bioprocessos de células estaminais deveriam ser monitorizados e optimizados através da medição de características metabólicas sistémicas. Desta forma, o metabolismo pode apresentar-se como um potencial arsenal necessário para a compreensão e melhoria dos bioprocessos baseados em células estaminais.

O objectivo desta tese foi demonstrar, em primeiro lugar, que a biologia de sistemas focada no metabolismo consegue diferenciar entre diferentes estágios celulares do processo de diferenciação neural. Em segundo lugar, com base nos resultados obtidos, propor novas estratégias inspiradas pelo metabolismo para optimização de bioprocessos de células estaminais. Para

tal, recorreu-se a duas abordagens de caracterização metabólica: análise de fluxos metabólicos (MFA) de células estaminais neurais (NSC) e de astrócitos, e análises de dinâmicas metabólicas em células estaminais pluripotentes e neurais.

Na primeira abordagem, ^{13}C-MFA foi usado para mostrar que os fluxomas das células estaminais neurais e dos astrócitos são distintos. Os astrócitos apresentam um fluxo glicolítico considerável, secreção de citrato, síntese e secreção de glutamina, e actividade residual no ciclo de TCA. Características relevantes identificadas ao nível do fluxoma das NSC incluem a carboxilação reductiva, síntese lipídica significativa e uma alta taxa de actividade na parte superior do ciclo de TCA. Portanto, os fluxomas obtidos são diferentes, e as maiores diferenças em termos de taxas concentram-se na classe metabólica dos amino ácidos. Consequentemente, estas diferenças poderão ser exploradas para optimizar o bioprocesso de células estaminais neurais. De forma a aumentar a pureza de culturas astrocíticas em vista a resultados mais precisos de testes de eficiências e toxicidade de drogas, privação de glutamina no meio extracelular ou bloqueio da actividade enzimática na síntese de ácidos gordos poderiam ser utilizados para induzir a morte das NSC.

Uma segunda e nova abordagem focou-se na caracterização do controlo dos níveis metabólicos intracelulares. A hipótese postula que cada célula possui certos metabolitos com dinâmicas de controlo específicas, e portanto caracterizadoras das células. Esta hipótese é baseada no conhecimento actual sobre a influência de variados metabolitos na determinação do destino celular. Para identificar metabolitos com potencial poder regulador, aplicou-se um estímulo extracelular, após este estímulo, um elevado número de metabolitos, de diferentes classes metabólicas, foi acompanhado ao longo do tempo. Em primeiro lugar, observou-se que as quantidades intracelulares dos metabolitos se alteraram mas o fenótipo celular manteve-

se. Isto significa que os métodos de caracterização “estática”, através da quantificação dos níveis metabólicos, apenas determinam um conjunto de valores num conjunto alargado de possibilidades metabólicas para o mesmo tipo celular. Em segundo lugar, para alguns metabolitos, as alterações da sua concentração intracelular foi conservada entre diferentes linhas de hiPSC, e entre diferentes linhas de hNSC. Este resultado é relevante, indicando que alguns metabolitos têm alterações de estado estacionário controladas enquanto outros metabolitos têm mais liberdade operacional para os novos estados estacionários. De realçar que, quando se sobrepõe numa rede metabólica os rácios das concentrações metabólicas antes e depois do estímulo, obtém-se uma figura semelhante aos resultados de fluxomas presentes na literatura. Uma potencial aplicação desta estratégia é assim usar esta abordagem de estímulos para determinar fluxos intracelularmente activos. Esta abordagem a análises de fluxos metabólicos permitiria uma redução do tempo de resolução computacional e seria menos dispendioso porque o uso de marcação com ^{13}C já não seria necessário. Finalmente, foi efectuada uma caracterização das células ao nível metabólico, através da modelação dos dados dinâmicos de cada metabolito a uma equação clássica na área de dinâmicas de processo. Os perfis dinâmicos simulados da maior parte dos amino ácidos sugerem que estes perfis são específicos de cada tipo celular. Este resultado tem implicações importantes pois significa que para caracterizar um determinado tipo celular, talvez seja suficiente determinar o comportamento dinâmico intracelular dos amino ácidos, após uma perturbação extracelular. Afinal, os métodos analíticos para quantificação de amino ácidos são abundantes, precisos e exactos e, adicionalmente, existe uma variedade de métodos moleculares para sondar e estudar o metabolismo dos amino ácidos.

Em resumo, espera-se que o trabalho nesta tese tenha demonstrado o valor da biologia de sistemas, focado em metabolismo, como ferramenta

para a caracterização celular e o seu potencial para o desenho de estratégias para optimização de bioprocessos. Em particular, demonstra-se, através de dois diferentes métodos de caracterização metabólica, que os amino ácidos parecem ser fundamentais para uma eficiente caracterização celular, seja através de fluxos ou de dinâmicas intracelulares.

Atendendo ao facto de os amino ácidos estarem bem distribuídos pela rede metabólica humana e conjugando-a com a existência de métodos consolidados para a análise de amino ácidos, esta aposta na caracterização celular pelos amino ácido poderá ajudar a focar a procura e acelerar o aparecimento de estratégias para a optimização de bioprocessos de células estaminais.

Thesis Publications

Kleiderman S. , **Sá J. V.**, Teixeira A. P., Brito C. , Gutbier S. , Evje L. G., Hadera M. G., Glaab E. , Henry M. , Sachinidis A. , Alves P. M., Sonnewald U., Leist M. (2016), Functional and phenotypic differences of pure populations of stem cell-derived astrocytes and neuronal precursor cells. *Glia*, 64: 695-715. doi:10.1002/glia.22954

Sá J.V., Kleiderman S., Brito C., Sonnewald, U., Leist M., Teixeira A.P., Alves P.M. (2017) Quantification of Metabolic Rearrangements During Neural Stem Cells Differentiation into Astrocytes by Metabolic Flux Analysis. *Neurochem Res* 42: 244. https://doi.org/10.1007/s11064-016-1907-z.

Sá J.V.*, Simão D.*, Terrasso A.P., Silva M.M., Brito C., Isidro I.A., Alves P.M., Carrondo M.J.T. (2020) Unveiling Dynamic Metabolic Signatures in Human Induced Pluripotent and Neural Stem Cells. *PLOS Comp Biol.* (*Accepted)*

*These authors contributed equally to this work.

Additional Publications

Sá J.V., Duarte T.M., Carrondo M.J.T., Alves P.M., Teixeira A.P. (2015) Metabolic Flux Analysis: A Powerful Tool in Animal Cell Culture. In: Al-Rubeai M. (eds) Animal Cell Culture. Cell Engineering, vol 9. Springer, Cham.

Kleiderman S., Gutbier S., Ugur Tufekci K., Ortega F., **Sá J. V.**, Teixeira A. P., Brito C., Glaab E., Berninger B., Alves P. M., Leist M. (2016) Conversion of Nonproliferating Astrocytes into Neurogenic Neural Stem Cells: Control by FGF2 and Interferon-γ. *Stem Cells*, 34: 2861-2874. doi:10.1002/stem.2483

Table of Contents

List of Figures

List of Tables

List of Abbreviations

^{13}C-MFA	^{13}Carbon based Metabolic Flux Analysis
Ac-Orn	Acetylornithine
ADMA	Asymmetric dimethylarginine
Ala	Alanine
Alpha-AAA	Alpha-Aminoadipic acid
Arg	Arginine
Asn	Asparagine
Asp	Aspartate
Ast	Astrocytes
C0	Carnitine (free)
C2	Acetylcarnitine
C3	Propionylcarnitine
C3:1	Propenoylcarnitine
C3-OH	Hydroxypropionylcarnitine
C4	Butyrylcarnitine / Isobutyrylcarnitine
C4:1	Butenoylcarnitine
C4-OH (C3-DC)	Hydroxybutyrylcarnitine (Malonylcarnitine)
C5	Isovalerylcarnitine / 2-Methylbutyrylcarnitine / Valerylcarnitine
C5:1	Tiglylcarnitine / 3-Methyl-crotonylcarnitine
C5:1-DC	Glutaconylcarnitine / Mesaconylcarnitine
C5-DC (C6-OH)	Glutarylcarnitine (Hydroxyhexanoylcarnitine [= Hydroxycaproylcarnitine])
C5-M-DC	Methylglutarylcarnitine
C5-OH (C3-DC-M)	Hydroxyisovalerylcarnitine / Hydroxy-2-methylbutyryl / Hydroxyvalerylcarnitine (Methylmalonylcarnitine)

C6 (C4:1-DC)	Hexanoylcarnitine [= Caproylcarnitine] (Fumarylcarnitine)
C6:1	Hexenoylcarnitine
C7-DC	Pimelylcarnitine
C8	Octanoylcarnitine [= Caprylylcarnitine]
C9	Nonanoylcarnitine [= Pelargonylcarnitine]
C10	Decanoylcarnitine [= Caprylcarnitine]
C10:1	Decenoylcarnitine
C10:2	Decadienoylcarnitine
C12	Dodecanoylcarnitine [= Laurylcarnitine]
C12:1	Dodecenoylcarnitine
C12-DC	Dodecanedioylcarnitine
C14	Tetradecanoylcarnitine [= Myristylcarnitine]
C14:1	Tetradecenoylcarnitine [= Myristoleylcarnitine]
C14:1-OH	Hydroxytetradecenoylcarnitine [= Hydroxymyristoleylcarnitine]
C14:2	Tetradecadienoylcarnitine
C14:2-OH	Hydroxytetradecadienoylcarnitine
C16	Hexadecanoylcarnitine [= Palmitoylcarnitine]
C16:1	Hexadecenoylcarnitine [= Palmitoleylcarnitine]
C16:1-OH	Hydroxyhexadecenoylcarnitine [= Hydroxypalmitoleylcarnitine]
C16:2	Hexadecadienoylcarnitine
C16:2-OH	Hydroxyhexadecadienoylcarnitine
C16-OH	Hydroxyhexadecanolycarnitine [= Hydroxypalmitoylcarnitine]
C18	Octadecanoylcarnitine [= Stearylcarnitine]
C18:1	Octadecenoylcarnitine [= Oleylcarnitine]
C18:1-OH	Hydroxyoctadecenoylcarnitine [= Hydroxyoleylcarnitine]
C18:2	Octadecadienoylcarnitine [= Linoleylcarnitine]
Cit	Citrulline

c4-OH-Pro	cis-4-Hydroxyproline
DOPA	Dihydroxyphenylalanine
Gln	Glutamine
Glu	Glutamate
Gly	Glycine
H1	Hexoses
hiPSC	Human induced Pluripotent Stem Cells
His	Histidine
hNSC	Human Neural Stem Cells
Ile	Isoleucine
Kyn	Kynurenine
Leu	Leucine
Lys	Lysine
LysoPC a Cx:y	Lysophosphatidylcholine with acyl residue, with x carbons and with y double bonds
MFA	Metabolic Flux Analysis
Met	Methionine
Met-SO	Methionine-Sulfoxide
Nitro-Tyr	Nitrotyrosine
NSC	Neural Stem Cells
Orn	Ornithine
PC aa Cx:y	Phosphatidylcholine with diacyl residue, with x carbons and with y double bonds
PC ae Cx:y	Phosphatidylcholine with acyl-alkyl residue, with x carbons and with y double bonds
PEA	Phenylethylamine
Phe	Phenylalanine
Pro	Proline
PSC	Pluripotent Stem Cells
SDMA	Symmetric dimethylarginine
Ser	Serine

SM Cx:y	Sphingomyelin with acyl residue, with x carbons and with y double bonds
SM (OH) C14:1	Hydroxysphingomyelin with acyl residue, with x carbons and with y double bonds
TCA	Tricarboxylic acid cycle
Thr	Threonine
t4-OH-Pro	trans-4-Hydroxyproline
Trp	Tryptophan
Tyr	Tyrosine
Val	Valine

1

Introduction

Section 5 of this chapter was adapted from:

Sá J.V., Duarte T.M., Carrondo M.J.T., Alves P.M., Teixeira A.P. (2015) Metabolic Flux Analysis: A Powerful Tool in Animal Cell Culture. In: Al-Rubeai M. (eds) Animal Cell Culture. Cell Engineering, vol 9. Springer, Cham.

Author contributions to this chapter:

João Sá wrote this chapter based on the referred bibliography.

Table of Contents

1. Stem Cells' Industry

Stem cells have unlimited capacity for self-renewal while being capable for the generation of different types of cells (Herberts et al., 2011). Human pluripotent stem cells (hPSC) have the ability to differentiate into cells of the three germ layers (Robinton and Daley, 2012) thus opening up opportunities to improve human health and disease. hPSC-derived cells can be used for cell therapy (Pigeau et al., 2018), disease modeling, drug screening and drug toxicity testing (Drawnel et al., 2014; Skelton et al., 2017).

A recent example of the potential of stem cell-based bioproducts, part of a new medicine category called advanced therapy medicinal products (ATMPs), is a Phase 1 clinical trial comprising two people with age-related macular degeneration (AMD). Patients received a bioengineered patch containing retinal cells produced from embryonic stem cells and reported an improvement of visual acuity of 15 letters or more (da Cruz et al., 2018). Knowledge gained from differentiation of hPSC and disease modeling can be used to identify new targets and approaches for pharmaceuticals (Fonoudi et al., 2014).

Regarding drug screening and drug toxicity testing, considering the high attrition rate in drug development (Scannell et al., 2012), drug testing performed in stem cell derivatives represent a promising solution to tackle the efficacy and safety issues responsible for clinical phase failures (Hay et al., 2014; Ko and Gelb, 2014), prompting the attractive phenomena of failing fast and cheap. For instance, stem cell derived *in vitro* organoids have been shown to be predictive of the patient outcome (Berkers et al., 2019; Saini, 2016), helping patients to have best treatment possible with minimal side effects.

However, stem cell's industry faces serious problems. Cell bioprocesses are challenging, mainly because of their highly complex

product, cells themselves. Even by employing concepts and technologies from other biotechnological industries such as antibody industry, the process of achieving clinical doses of at least 10^9 cells (Jenkins and Farid, 2015) for cell therapy applications is demanding. In autologous applications, the financial burden is a special concern given the clinical doses required in allogenic applications the safety concern becomes more relevant. Indeed, it is revealing of the complexity of stem cell bioprocessing that at the moment, few cell therapy products have succeeded in Phase III clinical trials (Goldman and Gouon-Evans, 2016). Moreover, many of those that succeeded to transit to the market present a high cost-to-efficacy ratio, leading to some disappointing sales such as Chondrocelect.

This difficulty in entering the pharmaceutical market happens in part because current protocols for reliable differentiation of hPSC are still ineffective, expensive, and time-consuming in obtaining developmental lineages with mature phenotypes, resulting in cell products with functionality features distant from those reported for adult cells. Moreover, the presence of immature cells means that there is a higher probability of finding residual stem cells in the bulk, representing a safety hazard (Herberts et al., 2011). These problems are not specific to applications in cell therapy, and also affect other applications such as drug toxicity and testing, and disease modelling.

Essentially, there is a need for adequate methods for quantitative and rapid cell characterization, and tools capable of optimizing differentiation yield, cost and time.

2. Metabolism and Cell Fate

The optimization of stem cell bioprocesses requires knowledge of the factors that modulate stem cell fate. Stem cells usually reside in niche environments where stem cells sense different types of cues: extracellular matrix, secreted factors, physical forces, chemical gradients, pH, oxygen concentration, and metabolites (Figure 1.1). There is extensive literature on the influence of extracellular metabolic composition in cell fate and behavior (Keisuke Ito and Suda Toshio, 2014; Lane et al., 2014; Serra et al., 2012; Shyh-Chang et al., 2013; Tatapudy et al., 2017). Reciprocally, cells also exert an effect on their environment.

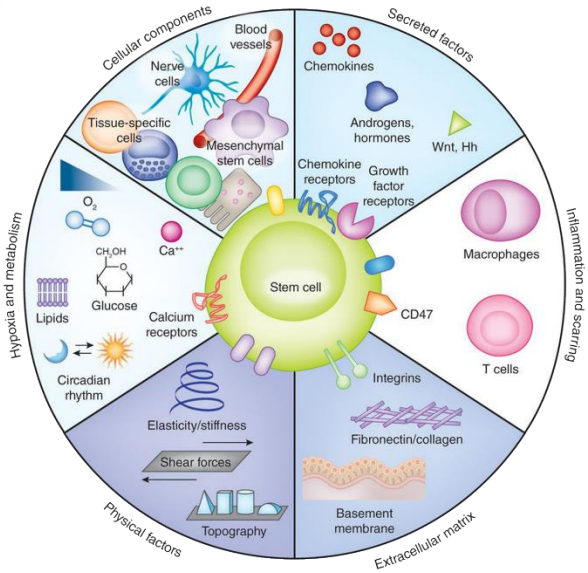

Figure 1.1 – Composition of stem cell niches with their varied cues for cell fate. From (Lane et al., 2014).

The classical paradigm states that most cell decisions are defined during mRNA transcription which leads to protein synthesis and, for enzymatic proteins, to metabolic reactions. To maintain a stable and consistent intracellular protein and metabolic environment, control

mechanisms need to be in place (Hansen et al., 2018). Cell types usually present metabolic-related functions that need to be tightly controlled. For instance, astrocytes provide metabolic support to neurons, neurons release neurotransmitters and hepatocytes synthesize cholesterol. Therefore, in principle, metabolism should also exerts feedback control on other molecular levels (Figure 1.2) to assure a good control of metabolic-related functions. Homeostasis is a fundamental characteristic of an ordered system.

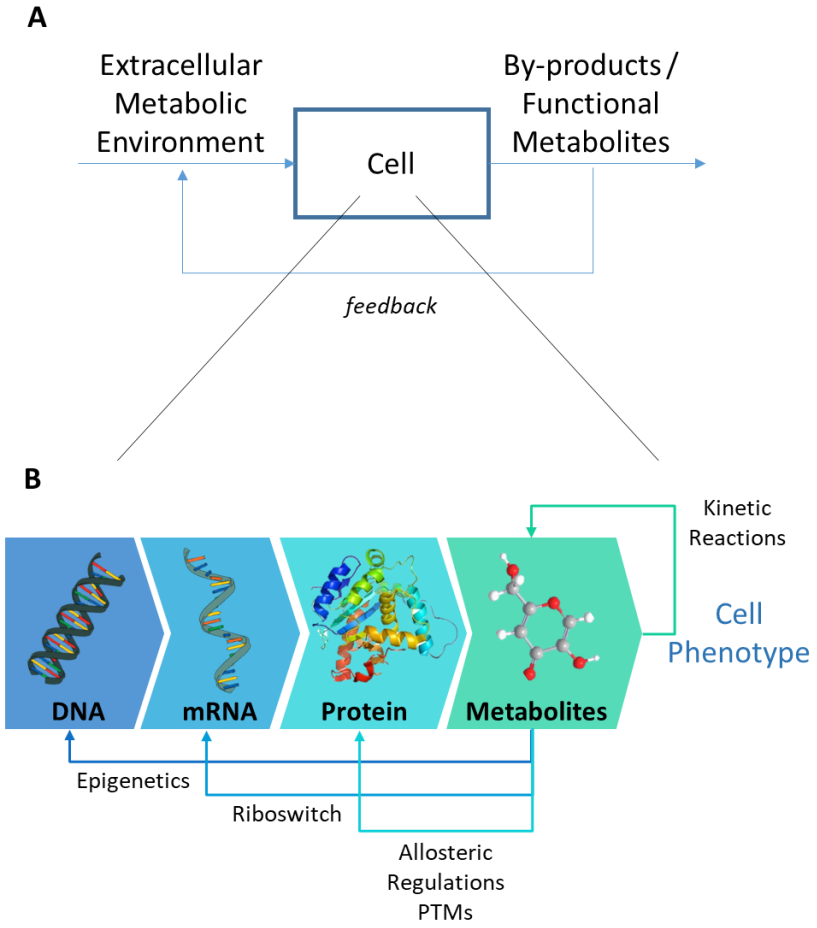

Figure 1.2 – Metabolic relations and controls with A) extracellular environment and with B) intracellular molecular levels. The metabolic function

of many cells hints at controlled regulation of metabolism and other molecular levels inside the cell due to natural noise. Image was improved and permitted to be used here by Daniel Simão.

2.1. Mechanisms of Intracellular Regulation by Metabolism

Metabolites regulate all other intracellular molecular levels and through diverse mechanisms – Table 1.1 and Figure 1.2. It ranges from downstream molecular phenomena such as post-translation modifications of proteins (PTMs) (Geiger et al., 2016) to upstream molecular phenomena such as methylations of histones (Shiraki et al., 2014).

Metabolic flux regulation is perhaps the most immediate regulatory role performed by metabolites, either by activating or inhibiting the enzymatic activity and thus adjusting the metabolic fluxes maintaining homeostasis in bioenergetics and redox state. For example, the glycolytic enzyme phosphofructokinase-1 is allosterically activated by fructose 2,6 biphosphate (Mor et al., 2011) thereby increasing the overall glycolytic flux (Figure 1.3).

Besides allosteric regulation, metabolic donors can also affect metabolic fluxes through PTMs of proteins, such as acetylation (Zhao et al., 2011) and phosphorylation (Humphrey et al., 2015). PTMs are also responsible for another paramount role of metabolic regulation: modulation of gene expression. PTMs can activate transcription factors, for instance by phosphorylation (Gao et al., 2012), or can translocate proteins to the nucleus where they can locally influence the genetic program (Hara et al., 2005; Tristan et al., 2011). Interestingly, proteins that are not post-translationally modified, mostly metabolic enzymes, can also translocate to the nucleus (Figure 1.3). In fact, practically all glycolytic enzymes and many TCA cycle enzymes have now been observed in the nucleus (Kim and Dang, 2005). Boukouris and his co-workers extensively reviewed the

Table 1.1 – Types of interactions that metabolism performs on other cell constituents, and how these interactions works as regulating force on cell phenotype. Despite histones being proteins, the actions of metabolites over histones were separated from all other proteins as a way to make clear the relevance of metabolism regulation in epigenetics.

Targets	Mechanisms / Action Modes	Effects	References
Protein	Allosteric regulation: activators and inhibitors	Increases or decreases of enzymatic activity and, consequently, of metabolic fluxes	(Mor et al., 2011)
	Donors for Phosphorylation	Activates transcription factors	(Gao et al., 2012)
	Acetylation of lysine residues by Acetyl-CoA	Increases or decreases of enzymatic activity and, consequently, of metabolic fluxes	(Zhao et al., 2011)
	S-nitrosylation caused by oxidative stress	Induces nuclear translocation	(Hara et al., 2005) (Tristan et al., 2011)
	Occupies the enzyme for its enzymatic activity diminishing its moonlight function	Avoids Nuclear translocation	(Chang et al., 2013)
DNA	Methylation	Guarantees stable long-term repression Decreases the expression of differentiation genes	(Bird, 2002)
	Demethylation by α-Ketoglutarate	Removes methyl groups	(TeSlaa et al., 2016)
	Inhibition of Demethylation by Succinate	Inhibits of histone demethylation activities	(TeSlaa et al., 2016)
Histone	Acetylation by Acetyl-CoA	Promotes gene transcription, especially genes associated with cell-cycle progression and cell growth	(Peng et al., 2016) (Moussaieff et al., 2015) (Madiraju et al., 2009) (Sutendra et al., 2014)
	Methylation	Regulates local formation of heterochromatin Decreases the expression of differentiation genes	(Wang et al., 2004)
	Demethylation by α-Ketoglutarate	Removes methyl groups	(TeSlaa et al., 2016)
	Inhibition of Demethylation by Succinate	Inhibits of histone demethylation activities	(Jiang et al., 2015; Yogev et al., 2010) (TeSlaa et al., 2016)
	Phosphorylation by PEP	Changes gene expression	(Yang et al., 2012)

non-canonical functions, termed moonlight functions, of those metabolic enzymes which translocate to the nucleus to influence gene transcription (Boukouris et al., 2016).The high predominance of metabolic enzymes in the known universe of moonlight proteins leads one to hypothesize that metabolism indirectly regulates such moonlight activity. Chang and his co-workers demonstrated how, in T cells, aerobic glycolysis regulates the translocation of the glycolytic enzyme GAPDH to the nucleus where it binds to the untranslated region of IFN-γ mRNA. This binding reduces protein translation leading to production decrease of IFN-γ (Chang et al., 2013).

Besides the indirect modulation of gene expression by protein nuclear translocation, metabolites can directly imprint chemical alterations in histones and DNA through acetylation and methylation (Bird, 2002; Huang et al., 2014; Kaelin and McKnight, 2013; Klose and Zhang, 2007) (Table 1.1 and Figure 1.3). Indeed, demethylation of DNA and histones has been shown to help the differentiation of primed pluripotent stem cells, and this process could be induced by α-ketoglutarate and inhibited by succinate (TeSlaa et al., 2016). The epigenetic regulation of pluripotent stem cells by metabolites is multivariable as histone acetylation by acetyl-CoA also causes the delay of differentiation of hPSC (Moussaieff et al., 2015). The authors show that aerobic glycolysis is fundamental in hPSC for the production of acetyl-CoA, a function that is lost during differentiation. However, glycolysis is not the sole metabolic way for producing acetyl-CoA (Madiraju et al., 2009), further increasing the complexity of metabolic regulation of epigenetics. Moreover, acetyl-CoA can act in over 60 histone acetylation sites; acetylation can not only provoke large and general genetic expression programs but also be performed in a spatially controlled manner thus eliciting the expression of specific genes. In fact, the expression of specific genes through epigenetics is critical for the

prenatal development and postnatal maturation of cardiomyocytes (Gilsbach et al., 2018; Martinez et al., 2015).

Overall, metabolism significantly influences cell phenotype through allosteric regulation, protein translocation, PTMs and epigenetic regulation. From this varied and simultaneous metabolic regulations happening intracellularly, it can be hypothesized that there are consequently systemic properties of metabolism that need to be conserved so that cell identity can be maintained. In other words, metabolic systems may constitute a phenotypic feature of a cell.

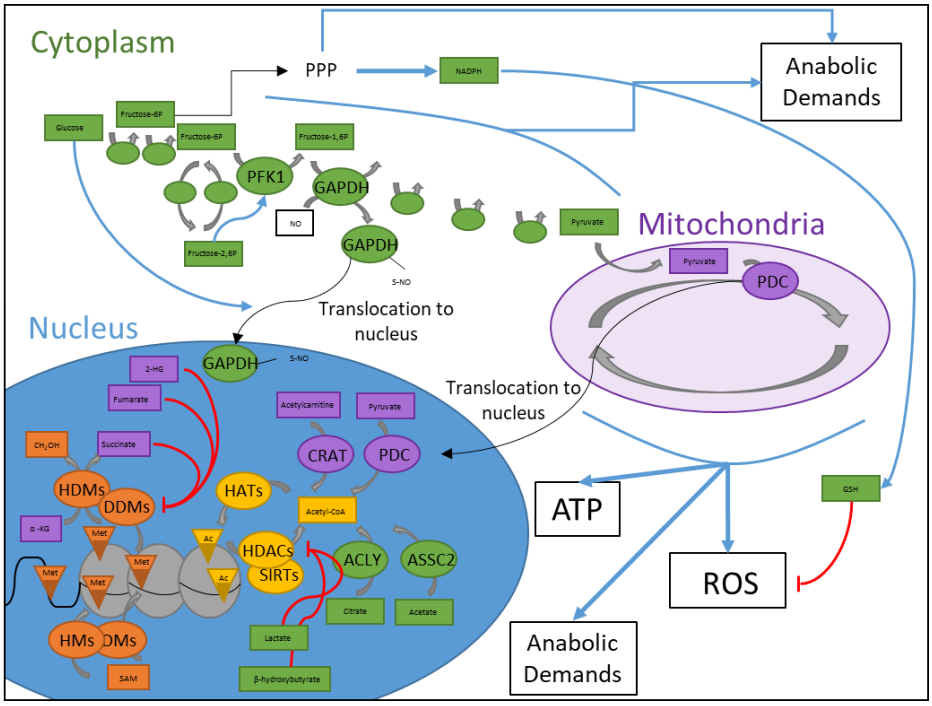

Figure 1.3 – Examples of Intracellular Regulation by Metabolism. Rectangles and circles represent metabolites and enzymes, respectively. In green background, metabolites and enzymes that are usually located in the cytoplasm. In purple background, metabolites and enzymes that are usually located in the mitochondria. In orange background, metabolites

and enzymes involved in methylation or demethylation of histones and DNA. In yellow background, metabolites and enzymes involved in acetylation or deacetylation of histones.

3. Contributions of Metabolism for Stem Cell Bioprocesses

3.1. Manufacturing Process and Costs

Process workflow of stem cells involves several operation steps (Figure 1.4), those concerning expansion and differentiation being the most critical for defining the quality, safety and cost (quantity) of the product (Pigeau et al., 2018). Several operational factors contribute to this: one being the costly matrices and other supports needed for cell culture such as the Synthemax matrix in PSC expansion, other is culture media high costs as protein factors are needed to maintain stem cell pluripotency or promote differentiation. In addition, these costs are multiplied by the long operation time required, especially for differentiation. For instance, in order to obtain glutamatergic and GABAergic neurons with some degree of maturation, at least 20 days are needed after obtaining the neuronal progenitor (Simão et al., 2016). For cardiomyocytes at least 30 days (Robertson et al., 2013) and for rod photoreceptors as many as 20 weeks are needed (Gonzalez-Cordero et al., 2017). For some processes which are not scaled-up such as autologous cell treatments, these costs of goods do not go down with higher volume productions. So, even with the advent of automation, expansion and differentiation operations need to be profoundly improved in order to make stem cell-based products more cost-effective and accessible to patients. For instance, Spherox for cartilage defects treatment is being sold from 9 500 $ (Hildreth, 2018) and for

autologous CAR-T cell therapy, Kymriah is sold at 475 000 $ (Bach et al., 2017).

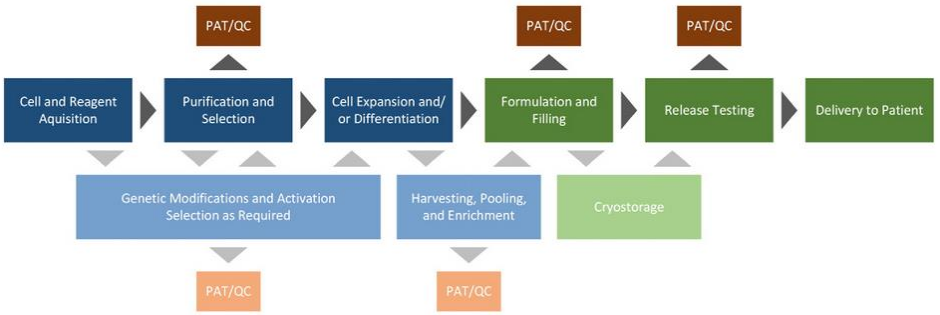

Figure 1.4 – General overview of current state-of-the-art cell manufacturing processes. Bold colors on the top half indicate processing steps common to most cell types; watershed colors on the bottom half indicate process steps that may be added depending on application. Upstream and downstream processing are indicated by blue and green, respectively. Orange boxes indicate desired QC and PAT for key process steps. Abbreviations: QC, quality control; PAT, process analytical technologies. Figure and legend from Dwarshuis et al., 2017.

3.2. In-Process/Quality Control and Final Efficacy

Assessment of cell product quality is highly dependent on knowledge of which are the main identity and functional attributes. In the stem cell bioprocess industry, this is most difficult because current biomarkers are non-unique. This happens as most of biomarkers used are based on surface protein markers which can span through several cell identities in a given cell differentiation course. For instance, a 99% “pure” population of CD4 positive cells, can comprise a heterogeneous mix of monocytes, T regulatory and T lymphocyte subsets at different developmental stages

(Tomlinson et al., 2013). Moreover, sometimes inaccurate protein markers are attributed to stem cells as it has happened to c-kit+ marker for cardiac stem cells (Sultana et al., 2015). This means that is difficult to use proteins markers as accurate critical quality attributes (CQA). For most cases, these CQA, properties of cells that can be measured to assure functional quality and ensure reproducibility, are largely unknown (Dwarshuis et al., 2017).

Metabolism can be a helpful complement to the current quality control (Klontzas et al., 2017). By being accurate and quantifiable, metabolic studies can be used as a complementary quality control tool. Indeed, vast literature has shown how different cells are metabolically distinct, even between supposedly close relatives such as naïve pluripotent stem cells and primed pluripotent stem cells (Chandrasekaran et al., 2017; Zhang et al., 2016). Thus, metabolic characterization of cells could be used during the stem cell bioprocess as an in-process control, this is, as monitoring tool of changes during the stem cell bioprocess. In complementation of using observations of cell morphology or surface markers as requirements for moving to the next stem cell differentiation step, metabolic characterization could, at least, complement surface markers and thus help providing more decision confidence to start the next operation.

Currently, in order to get the desired quality, bioprocess optimization of conditions such as culture media, temperature, agitation, pH, osmolarity are usually performed, at least in a later stage, by screening approaches, though secreted lineage specifiers (growth factors and cytokines) revealed from developmental biology were initially used (Kempf and Zweigerdt, 2018; Spiering et al., 2015). Despite this methodology being feasible nowadays with the advent of miniaturization of cell culture plates and of robotics making process optimization almost a high-throughput process, the use of cell surface markers as optimization output may not be

completely correlated with cell functionality (Rutten et al., 2015; Salmikangas et al., 2015). For instance, Lo Surdo et al., (2013) have shown that while MSC cell surface markers were the same among different cell lines and passages, their functionality was distinct. An incomplete correlation between markers and functionality results in poor or difficult definition of the critical process parameters (CPP), that are necessary to maintain and ensure cell quality and consistency across batches and facilities, such as culture conditions, durations, media compositions, and transition from 2D to 3D cultures (Dwarshuis et al., 2017). This means the bioprocess products will have limited efficacy. If cells during differentiation were metabolically monitored, the quality and therapeutic potential of resulting cell products could be probably increased. The improvement in efficacy would also have an important effect on bioprocess products destined for cell therapy: the reduction of cell quantity for a treatment dose, reducing sizes of processes batches.

3.3. Safety

Allogeneic cell therapy that uses differentiated cells derived from stem cells faces a serious risk still today: the tumorigenic properties of residual stem cells (Ben-David and Benvenisty, 2011). So, either persistent progenitors are physically separated from the cell products or those need to be eliminated during culture. In the separation approach, techniques based on adherence and density are not very specific (Tomlinson et al., 2013), and techniques based on cell sorting through cell-surface markers use fluorescent probes and antibodies that might represent a clinical complication (Tohyama et al., 2013). In cell sorting, only magnetic-activated cell sorting (MACS) are currently used, as in fluorescent-activated cell sorting (FACS) there is great difficulty in developing single-

use sterile fluidics (Tomlinson et al., 2013). Moreover, some stem cells-based products might not have unique surface markers (or suffer from weak expression) or contain a unique intracellular marker that requires cell membrane permeabilisation which can lead to cell death (Tomlinson et al., 2013).

In the approach where undesired cells are eliminated during cell culture, metabolism-based strategies have been used. Tohyama and his co-workers have described that culturing PSC derivatives with glucose-depleted culture medium containing 4 mM lactate resulted in cardiomyocytes populations with 99 % purity that did not form tumors after transplantation into mice (Tohyama et al., 2013). On top of that, the same group has also reported that both glucose and glutamine depleted conditions with supplementation of lactate further enriched hPSC-derived cardiomyocytes (hPSC-CM) by decreasing impurities to levels lower than 0.001 % (Tohyama et al., 2016), obtaining thus a clinical-grade purity (Kamao et al., 2014). Under those conditions, hPSCs cannot utilize pyruvate efficiently because of low ACO2 and IDH2/3 expression. In contrast, CMs can utilize pyruvate or lactate efficiently for oxidative phosphorylation. These conditions were very effective at eliminating cell types other than CM, since any hPSC-derived non-cardiac cells that remain after differentiation also depend on glucose and/or glutamine. Similarly, it has been described that prolonged methionine deprivation can also lead to hPSC apoptosis (Shiraki et al., 2014). These metabolic purification approaches are less expensive and more suitable for large-scale bioprocesses (Tohyama et al., 2013). For defining the design of those metabolism-based purification steps, the characterization of cell metabolism during the different cell stages from stem cell to final cell product is needed so that metabolic vulnerabilities of unwanted cells can be identified and exploited.

3.4. Economics of Using Metabolites as Cell Modulators

In addition to the efficacy and safety challenges affecting stem cell bioprocesses, these bioprocesses present a high cost of production. Indeed, CAR-T cells currently marketed for curing several types of cancers are being sold at 475 000 dollars per patient (Hagen, 2017). A key contributor to the bioprocessing cost comes from the use of culture media with cytokines and other soluble factors. For that reason, stem cell differentiation processes have been progressively transitioning to the use of small molecules, as replacements for those more expensive molecules (Chen et al., 2014; Lin et al., 2017). Moreover, as the differentiation takes a long time, the total cost of the process is increased several fold by the cost of hPSC expansion for the same final cell number. Through a deeper understanding of metabolism, metabolites in culture media could be used as complement or alternative to expensive secreted factors as modulators of cell fate, and thus reduce overall costs.

3.5. Metabolism toolbox for Improved Bioprocesses

In the past sections, arguments have been presented that picture metabolism as a substantial contribution for many problems affecting cell therapy, either by using it for cell characterization or even by using as a bioprocess strategy to differentiate stem cells and purify the final product. In the former case, there is large evidence that intracellular metabolomics provide a strong tool to identify cells (McNamara et al., 2012). This constitutes a promising strategy for complementing the lack of specific characterization of final cell products which usually leads to low efficacy. Moreover, the proposed “one-to-one” relation between metabolic status

and cell fate could also provide a prediction of hPSC-derivatives potency as cell products, thus providing the possibility for bioprocess developments and in-process adjustments of final cell product. In the latter case, the demonstration that metabolism also constitutes an effector of cell fate raises the exciting hypothesis that specific metabolic targets can be identified to make stem cell niches supportive of tissue self-repair. Overall, the gaining of metabolic understanding of cells through the study of mammalian development and stem cell differentiation have the potential to create new strategies for more efficient protocols for differentiation, purification, and maturation of different hPSC-derivatives.

Overall, metabolism can be a driving force for transforming stem cell bioprocesses by allowing the design of rational protocols improving cell functionality and, in a cell therapy application, yielding products with clinically relevant quality, quantity and safety (Figure 1.5). From the analytical point of view, metabolic analytical tools are in accelerated development and acquiring greater quantification capabilities. From the production point of view, using metabolism for manipulation of stem cell bioprocesses is very attractive as it usually requires strategies that are scalable and cheap.

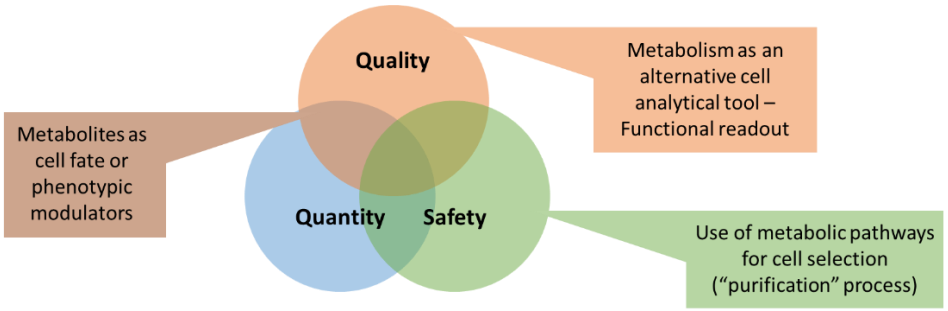

Figure 1.5 – Needed attributes for commercial success of stem cell based bioproducts and potential metabolism-based solutions.

4. Tools for Inspecting Metabolism

The bioengineering challenge to improve the differentiation of PSC, in terms of quality, quantity and safety, requires a reasonable understanding of the metabolism of the PSC, of the desired differentiated cell and of all the cell states in-between. With that goal in mind, metabolism of a given cell type can be studied in terms of its interaction with the environment or in terms of intracellular metabolic features. Moreover, the knowledge gained can vary from a reductionist sense (component-level) to an integrative sense (see section 6. and 7.) regarding Metabolic Systems Biology. For both types of metabolic characterization and knowledge level, several analytical methods are available.

The simplest approach to characterize cells is by looking at the footprint cells leave in the extracellular environment, i.e. by analyzing what cells are consuming and secreting – the exometabolome. This footprint sometimes represents characteristic features of a cell phenotype. For example, the secretion of citrate is a metabolic characteristic of astrocytes (Westergaard et al., 1994), while neurons that release dopamine need to be dopaminergic neurons (Brito et al., 2012).

A richer cell characterization is performed in intracellular metabolomics due to the number of metabolites identified and/or quantified. Specific metabolites might have very high or very low pool concentrations in comparison with other cell types which could then be considered cell biomarkers. Moreover, identification of higher or lower levels of metabolic pools provides potential targets relevant for manipulation of stem cell differentiation. For instance, through LC-MS and GC-MS untargeted analysis, Sperber and his co-workers identified stearic acid and cholesterol metabolic levels as critical for the distinction between naïve and primed PSC. Based on this finding, the authors later proved that lipidic pathways

were indeed changed during the switch from naïve to primed PSC (Sperber et al., 2015). Fluorescence resonance energy transfer (FRET)-based metabolite sensors (Okumoto et al., 2008) are a recent and promising method that will allow to follow the dynamic changes of metabolites during stem cell differentiation.

There are also analysis of metabolites and of another parameters (pH, oxygen) without involving complex mathematical methods or dynamic experimental data (section 6. and 7.) yielding some knowledge on certain metabolic pathways. The pathways may add to a list of metabolic features helping to characterize a given cell. Glycolysis and oxidative phosphorylation, which are a reflection of a cell's bioenergetics state, are an example of pathways that can be indirectly studied. The most straightforward method is by calculating the ratio of glucose consumption to lactate production. If the ratio comes close to 2, it means that every glucose is converted to lactate and thus the cell is highly glycolytic. A second, more reliable method, is through the use of glycolytic assay kits and equipment (e.g. Agilent's SeaHorse), where multiple measurements of pH and oxygen consumption are performed upon addition of different mitochondrial inhibitors, thus providing more detailed information on glycolytic and oxidative phosphorylation capacities of the cell.

When looking for metabolic characteristics at component-level, it is difficult to uniquely identify cells. After all, some of the cell characteristics are emergent properties that arise from the combination of elements. As the structure of metabolism is a complex metabolic network, metabolism of a given cell can only be comprehensively and accurately understood if its systemic behavior is known. In this case, methods inserted in the field of systems biology, are preferred for describing metabolic phenotypes. These methods of systems biology are usually characterized by quantitative reasoning, computational models and high-throughput

experimental technologies (Tavassoly et al., 2018). Results from metabolic systems biology can range from metabolic characterization to elucidations of control of cell, tissue, organ and organismal level functions. The aim of the field of metabolic systems biology is to retrieve systems-level insights to understand interactions and dynamics at various scales, within cells, tissues, organs and organisms. This is, metabolic systems biology is not a impermeable field and comprises different quantitative experimental and computational methodologies that give different types of information. In the next two sections, different approaches to metabolic systems biology will be introduced, one focusing in providing a view of the system on material flows while the other focusing on unveiling information about the control of the system.

5. Metabolic Flux Analysis *

5.1. Introduction

Framed in a systems biology view, the fluxome (the collection of metabolic fluxes inside the cell) reflects the integrated response of molecular interactions at the genome, transcriptome, proteome and metabolome levels, including their inter-regulatory mechanisms (Sauer, 2006) (Figure 1.6). Such comprehensive studies of metabolism can provide valuable information to effectively optimize the next generation of stem cell-based processes. Likewise, differences of cell metabolism observed under pathological conditions or under drug administration can provide important insights for biomedical research and toxicology. Studies of disease phenotypes have traditionally focused on different “omic” layers independently of each other, but current trends show a more integrated view of disease, which can be best reported by a study of the cell fluxome. As for the toxicology area, the substantial amount of resources and time

**Note: This section is adapted from the manuscript: Sá J.V., Duarte T.M., Carrondo M.J.T., Alves P.M., Teixeira A.P. (2015) Metabolic Flux Analysis: A Powerful Tool in Animal Cell Culture. In: Al-Rubeai M. (eds) Animal Cell Culture. Cell Engineering, vol 9. Springer, Cham.*

spent on drug development before reliable results are obtained could be obviated by the direct inspection of the response of the cell fluxome to a given drug, expediting the process of drug development.

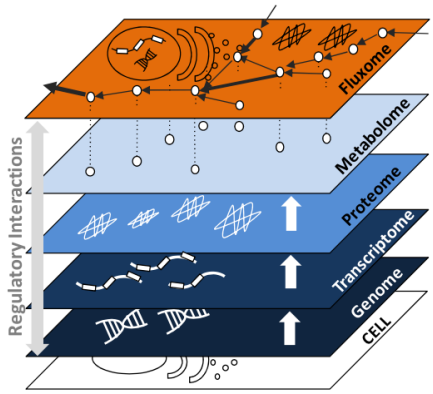

Figure 1.6 – The fluxome, being the layer closer to the cell phenotype, integrates information from interactions between all other layers of cellular components. Adapted from (Sauer, 2006).

Determining *in vivo* fluxes provides a quantitative description on the degree of engagement of various metabolic pathways in the overall cellular metabolism (Bonarius and Schmid, 1997; Crown et al., 2011; Moxley et al., 2009). During the past two decades, metabolic flux analysis (MFA) has become the preferred technique for obtaining quantitative information on *in vivo* fluxes (Ahn and Antoniewicz, 2013), in particular to validate metabolic pathways and uncover its regulation (Crown et al., 2011; Moxley et al., 2009), to identify bottlenecks in product formation and gain fundamental understanding of the balance between catabolic and anabolic processes, and homeostasis in general (Wiechert, 2001). Overall, a solid systems understanding gained by MFA will assist in rewiring metabolic fluxes towards increased product yields and better quality attributes in production of stem cell derivatives.

5.2. Metabolic Network Setup

A key step in MFA studies is the assembling of the metabolic network representing the metabolism of the cells under study. The main focus is generally on central metabolism, comprising glycolysis, pentose phosphate pathway, TCA cycle, as well as amino acid and fatty acid metabolism (Figure 1.7). Additional intracellular reactions and transport rates can be included upon reconciliation of all available experimental measurements. Concerning cofactors that contribute to energy balancing (e.g. ATP) or redox balancing (e.g. NADH and NADPH), they can be omitted from the model to ensure that their difficult-to-quantify balancing does not unduly bias the overall flux estimation (Zamboni et al., 2009).

The stoichiometry of biochemical reactions can be retrieved from online databases such as the Kyoto Encyclopedia of Genes and Genomes pathway database (KEGG; http://www.genome.jp/kegg/), BioCyc (http://biocyc.org/), ENZYME (http://enzyme.expasy.org/) or BRENDA (http://www.brenda-enzymes.info/), each cataloguing the metabolisms of several species. Animal cells are compartmentalized in different organelles (mitochondrion, nucleus, Golgi apparatus, etc.) and there is metabolite flow between the different compartments (Niklas et al., 2010). For the analysis of central metabolism, the two compartments cytosol and mitochondrion are normally considered, with metabolite pools of the cytosol distinguished from those residing in mitochondria (Figure 1.7).

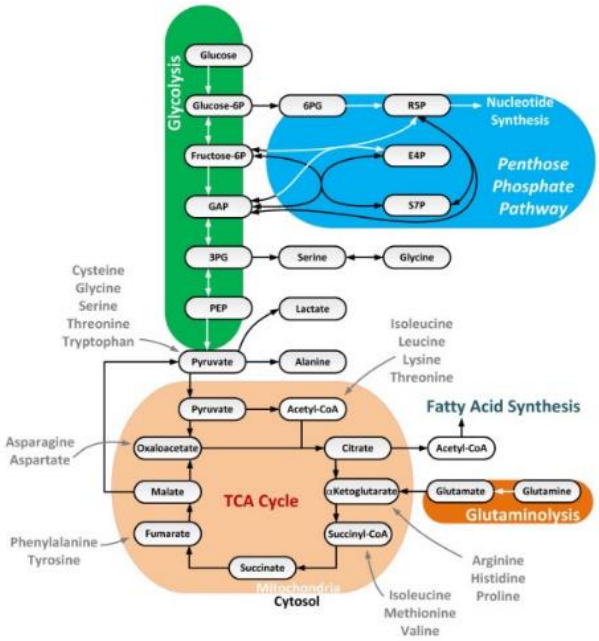

Figure 1.7 – Overview of a typical metabolic network for metabolic flux analysis in animal cell cultures.

5.3. MFA Methods

As opposed to metabolite concentrations, the intracellular reaction rates or fluxes are not directly measurable; *in vitro*, the rate of a reaction is determined by monitoring the concentration profiles of both substrates and products through time. This method can be extended to sequential reactions in a network of metabolites; mass balances are written for each metabolite of the network, resulting in the following matricial equation: $\frac{dX}{dt} = S.v$, where *X* is the vector of metabolite concentrations, *S* is the stoichiometric matrix (with dimensions of *m* x *n*, *m* metabolites and *n* reactions) and *v* is the vector of reaction fluxes. The stoichiometric matrix is mainly sparse, meaning that most of their coefficients are zero, since

most metabolites participate in just a small number of reactions. Assuming the pseudo-steady state hypothesis, which is normally valid during the exponential growth phase, the pools of intracellular compounds are constant for the time interval under study and a homogenous system of linear equations is obtained: $S.v = 0$. This system has f = $n - m$ degrees of freedom, meaning that f fluxes have to be measured so that all the remaining can be estimated. If the system is overdetermined (number of flux measurements higher than f), a complete set of fluxes can be estimated representing a least squares solution of the system. When this occurs, it also allows verifying if experimental measurements are consistent with the network stoichiometry if allowing accurate balancing of each metabolite.

The original and most simple method of MFA uses only measured metabolite transport rates in and out of the cells as experimental data, which are then balanced in the reaction network to provide estimates of intracellular fluxes. Despite its simplicity, it is still the most applied method for the analysis of metabolism in animal cells (Quek et al., 2010), with recent applications to hepatocytes (Nault et al., 2013), Chinese Hamster Ovary (CHO) (Carinhas et al., 2013), and human neural AGE1.HN cells (Niklas et al., 2013). A key limitation of this classical MFA method is that it cannot elucidate fluxes of parallel pathways (e.g. glycolysis vs. pentose phosphate pathway) and cyclic pathways (e.g. pyruvate cycling) (Goudar et al., 2010).

To address this limitation, isotopic tracer-studies, usually using ^{13}C substrates, have been applied to complement extracellular data with isotopic labeling information obtained by nuclear magnetic resonance (NMR) spectroscopy and mass spectrometry (MS) (Choi and Antoniewicz, 2011; Choi et al., 2012; Jeffrey et al., 2002; Szyperski, 1995; Wittmann, 2007). When ^{13}C containing nutrients are added to cell cultures, the label

propagates through the network as a function of metabolic activity, producing labeling patterns in the backbone of metabolic intermediates over time. Mathematical models describing label propagation are then used to calculate the *in vivo* fluxes from measured isotopic patterns and extracellular transport rates. A more realistic representation of the cell metabolism is attained and more subtle differences in flux phenotypes can be identified (Niklas and Heinzle, 2012). Recent studies applying ^{13}C substrates revealed that several assumptions used in previous metabolite balancing MFA studies may not be valid, especially regarding the activities of the oxidative pentose-phosphate pathway and anaplerosis at the pyruvate node (Ahn and Antoniewicz, 2011; Goudar et al., 2010; Sengupta et al., 2011). Thus, future studies on animal cells should use isotope tracers to better constrain flux solutions and validate other modeling assumptions (Ahn and Antoniewicz, 2012).

The simpler version of ^{13}C-based flux analysis is the isotopic stationary ^{13}C-MFA method, which assumes an isotopic steady-state that is reached when all intracellular isotopomer species are constant over time; this can be checked by plotting the label incorporation of each metabolite throughout time and verifying if label incorporation reaches a plateau (Figure 1.). The major advantage of this method is that it simplifies the experimental design and saves computational power. However, in some cases the ^{13}C- labeling incorporation in intracellular metabolites of animal cells is slow due to: i) utilization of multiple non-enriched carbon sources that dilute labeling of intracellular metabolites, ii) existence of large intracellular metabolite pools that act as buffers for labeling incorporation, and iii) metabolism compartmentalization. Moreover, different intermediates show distinct isotopic dynamics depending on their concentration, fluxes and pathway positioning in relation to the source of label. As a result, the requirement for isotopic steady-state imposes severe

limitations on the minimum duration of a labeling experiment, with implications on the feasibility of maintaining metabolic steady-state until isotopic steady-state is reached. For example, Sengupta et al. (2011) did not detect any significant labeling in the tricarboxylic acid cycle (TCA) metabolites of CHO cells, 6 h after administration of ^{13}C-glucose, and Ahn and Antoniewicz, (2011) reported that at least 24 h were needed to accumulate ~10% labeling in TCA cycle metabolites in a fed-batch culture of CHO cells. This means that the fluxes will have poor temporal resolution, and therefore the pseudo-steady state assumption may not be valid for long labeling times (Ahn and Antoniewicz, 2013).

In case of slow labelling dynamics, isotopically nonstationary MFA (INST-MFA) is preferentially applied to estimate the fluxes, using data from the transient period of label incorporation into intracellular pools (Nöh and Wiechert, 2006; Nöh et al., 2006) (Figure 1.8). Then, an iterative optimization procedure fits the mass balance equations describing the labeling of each isotopomer species to the measured time profiles, by adjusting the flux values (Amaral et al., 2011a; Maier et al., 2008). However, the application of INST- MFA implies higher experimental effort as well as higher computational power to solve the system of differential equations, which becomes prohibitive for larger scale network models.

As hinted before, the issue of metabolic compartmentalization poses a significant limitation to the ability of accurately resolve metabolic fluxes. While some metabolic pathways are restricted to a single compartment, e.g., pentose-phosphate pathway in the cytosol, other pathways span multiple compartments. However, the analytical procedures available today only allow measuring the combined mitochondrial and cytosolic pools (Zamboni, 2011). Experimental data suggest that some of these pools are differently labeled and have different labeling time scales *in vivo*. For example, Munger et al. (2008) showed differential labeling patterns for

metabolically related metabolites using uniformly labeled glucose and glutamine tracers, providing strong evidence of compartmentalized metabolism in fibroblast cells. Lu et al. (2002) also suggested the existence of two pyruvate pools based on ^{13}C NMR measurements in INS-1 β cells.

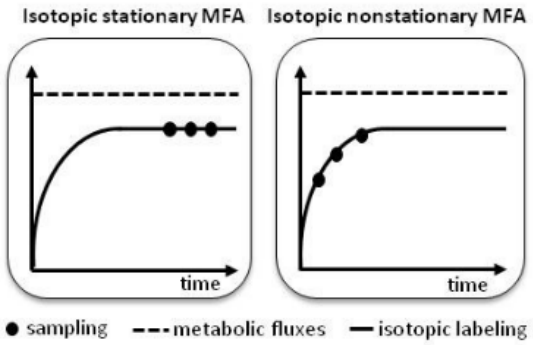

Figure 1.8 – Isotopic stationary versus nonstationary metabolic flux analysis. When isotopic steady-state is reached during the metabolic steady-state under study, the former methodology is preferentially applied due to the lower experimental and computational burden.

To address the resolution of fluxes between compartments, a technique based on fluorescence resonance energy transfer (FRET) has been proposed to measure conformation changes in certain protein sensors upon metabolite binding (Niittylae et al., 2009). FRET sensors permit the analysis of dynamic animal cell cultures with high temporal and subcellular resolution, by calculating intracellular fluxes for the sensed metabolite (Okumoto et al., 2008). Several sensors are available, from carbohydrates to amino acids (Wiechert et al., 2007). For example, Kaper et al. (2007) detected the accumulation of tryptophan in the cytosol of mammalian cells, and the amino acid was trapped inside the cell even after

removal of tryptophan from the perfusion medium. Furthermore, the authors observed that tryptophan effluxed from the cells only after addition of an exchange substrate, such as histidine or kynurenines (the degradation products of tryptophan). Another example of FRET ability for compartment resolution was shown by Takanaga et al. (2008), where the authors found that the kinetics of import and export rate across the endoplasmatic reticulum membrane are asymmetric at lower intracellular glucose concentrations. Thus, combining this method with ^{13}C-MFA can be very promising for tackling the compartmentalization issues that affect the current MFA methods, as it will help to differentiate compartment pools of some metabolites.

Finally, all MFA methods described before are based on the assumption of metabolic pseudo-steady state. In reality, a true steady state may not ever be reached in animal cells due to constant fluctuations in media components and the adapting response of cellular metabolism to varying substrate concentrations (Sanfeliu et al., 1997). During the past years, metabolic flux dynamics in batch and fed-batch cultures of animal cells was described in several studies using a combination of stationary MFA with a kinetic model (Goudar et al., 2006; Naderi et al., 2011; Nolan and Lee, 2011; Provost and Bastin, 2004; Provost et al., 2006; Teixeira et al., 2007; Zamorano et al., 2010). For instance, Nolan and Lee, (2011) used a kinetic modeling approach to trace changes in intracellular and extracellular metabolic fluxes in fed-batch cultures of CHO cells. With this in mind, it is expected in coming years the appearance of more research in animal cells where MFA is used in dynamic culture states, as well as an evolution of those methods which are still underdeveloped.

5.4. Experimental Design of ^{13}C Studies

The precision of estimated fluxes is heavily dependent on experimental conditions: the isotopic tracer(s) applied, the timing of the measurements

(for transient isotopic methods), and the metabolites that are measured. For the latter, the predominant philosophy is to measure as many metabolites as possible that are relevant to the pathways of interest. Caution should be taken when measuring certain metabolites that are prone to natural degradation, or more generally consider the increase in metabolite concentrations due to evaporation. Ideally, experiments without cells should be performed in parallel to estimate the natural decomposition rates of compounds in the culture medium, such as glutamine (Ozturk and Palsson, 1991), and to estimate the increase of metabolite concentrations due to evaporation (Ahn and Antoniewicz, 2011). Additionally, in some animal cell processes, the medium is supplemented with protein hydrolysates that contain amino acids used as substrates by cells; these must be accounted for to provide accurate metabolic flux estimates (Nyberg et al., 1999).

The choice of labeled tracers determines which metabolic pathways are resolved. Multiple tracers may be chosen in order to amplify the scope of observed metabolic pathways, especially relevant for the complex networks of animal cells. These pathways are disclosed through analysis of mass isotope distributions (MID) for each labeled metabolite. The sensitivity of each MID to changes in metabolic fluxes becomes as important as the flux itself since it unveils specific pathways. Thus, it is essential to wisely evaluate the choice of tracer(s) as well as optimizing measurements for flux determination (Antoniewicz, 2013; Metallo et al., 2009). Efficient algorithms have been developed for this purpose combining different tracers, namely glucose and glutamine, aiming at a more detailed view of metabolism in cancer cells (Walther et al., 2012). Furthermore, a recent open source software for assisting the choice of tracers is available – IsoDesign (Millard et al., 2013). In order to fully exploit the use of multiple tracers, parallel experiments using different labeled

substrates or multiple isotope types of the same substrate can be particularly beneficial. This has already started to be tested in animal cells (Ahn and Antoniewicz, 2013), with a thorough description of the advantages and disadvantages of this approach exposed in Crown and Antoniewicz (2013). Parallel experiments can better clarify the structure and function of metabolic pathways, eliminating inconsistencies in a hypothesized network. Inherent to parallel experiments is, however, the increase of time and resources spent for its completion and for data analysis (Crown and Antoniewicz, 2013).

The impact of the timing of measurements on the accuracy of flux estimation is particularly relevant for INST-MFA. Instead of collecting a single sample at isotopic steady state, multiple samples must be collected over time to obtain accurate profiles of ^{13}C-labeling dynamics. A careful selection of sampling time points is required, for which several computational tools have been developed, including parameterized sampling and a posteriori ranking of measurement time points (Nöh and Wiechert, 2006; Nöh et al., 2006).

Another important aspect of the design of ^{13}C experiments is that the standard culture media should be replaced by customized media with reduced concentrations of the metabolites which will be added as tracers, so that their total concentrations remain identical to the standard media. Furthermore, replicate experiments without tracers should always be performed in parallel to i) accurately determine metabolite uptake/secretion rates, which normally require longer time courses than isotope incorporation (Jazmin and Young, 2013), and ii) validate natural isotope abundances of measured intracellular metabolites to determine the real label incorporation from the added tracer (Ahn and Antoniewicz, 2013). As an option, the open source software IsoCor (Millard et al., 2012) is able to correct mass isotopomer data for the contribution of all naturally

abundant isotopes based on the tracer applied in the experiment and the derivatization reagents used for MS analytics.

5.5. Metabolomics Techniques

The quantification of metabolite levels in the supernatants of animal cell cultures and/or intracellularly is essential for estimation of flux models of cell metabolism. For classical MFA, monitoring extracellular metabolite concentrations is required to determine macroscopic fluxes of substrate uptake and product formation. The most used techniques are automated biochemistry analyzers (e.g. YSI and BioProfile) and High Performance Liquid Chromatography (HPLC), which are sufficient to measure the essential carbon and nitrogen sources in animal cells and their by-products, providing an overall snapshot of metabolic activity. For more comprehensive profiling, MS (Dettmer et al., 2007) and NMR spectroscopy, mainly ^{1}H-NMR and ^{13}C-NMR (Duarte et al., 2014; Khoo and Al-Rubeai, 2009) should be used, allowing the identification of larger metabolic networks.

When resorting to isotope tracer methods, the analysis of intracellular metabolites is crucial for their full exploitation to resolve metabolic fluxes that cannot be discriminated otherwise. While monitoring isotopic fractions of each metabolite, it is necessary to determine flux distributions in both types of ^{13}C-MFA methods, the quantification of absolute intracellular metabolite levels is crucial only for flux estimation in transient isotopic studies. In either case, since intracellular metabolites are usually present in very small quantities and have short turnover rates, quenching of metabolism should be done immediately after sampling. Isotopic labeling analysis can be performed through NMR and/or MS, the latter coupled with gas chromatography (GC) or liquid chromatography (LC) for peak separation (Choi and Antoniewicz, 2011; Goudar et al., 2010). Despite the lower sensitivity of NMR for absolute metabolite quantification, it provides

complete information on the labeling pattern for each detectable metabolite. MS, on the other hand, is a highly sensitive method but gives limited information on the position of carbon-labeled atoms. To tackle this limitation, tandem MS is starting to be used to obtain additional labeling information on key metabolites (Choi and Antoniewicz, 2011; Choi et al., 2012).

As the number and precision of the measured metabolites determines the quality of the estimated metabolic fluxes, the choice of the technique and metabolites to be measured should be carefully chosen during experimental design. Ideally, the goal is to measure all metabolite concentrations and isotopic fractions of the chosen metabolic network; but the incurred cost, time-consuming procedures and the unfeasibility of effectively measuring some metabolites, ensures approximate solutions are used.

5.6. Flux Estimation Algorithms for Isotope Models

The first proposed model for deriving material balances in carbon labeled experiments was based on atom-mapping matrices (AMM) (Zupke and Stephanopoulos, 1994). This approach allowed following the label in each atom through the entire metabolic network. The AMM was built on the notion of a metabolite vector containing all fractional enrichments at individual carbon atom positions and considering all possible enzymatic reactions for each metabolite. This framework was later generalized by Schmidt et al. (1997), constructing a new model considering the possibility of each carbon atom to be in a labeled (^{13}C) or unlabeled state, enabling its representation as a binary code of zeros and ones. The conversion to decimal numbers provided a unique way of ordering labeling patterns. Thus, in a similar way to AMMs, this model defines isotopomer mapping matrices (IMM) where each vector is based on the isotopomer distribution for each metabolite in the network (Schmidt et al., 1997). Here the need

for powerful computation to solve the isotopomer balance equations analytically became evident due to their nonlinear structure and high dimensionality. In this respect, the concept of cumulative isotopomers (cumomers) was introduced, representing a variable transformation which allows to explicitly solving isotopomer balances (Wiechert et al., 1999). More recently, the concept of elementary metabolite units (EMUs) allowed reducing the total number of the balanced equations in a typical ^{13}C-labeling system by one order-of-magnitude, while significantly reducing the computation time required for flux estimation without loss of information. This approach uses an algorithm that allows identifying the minimum amount of information needed to simulate the measured isotopomer species within a metabolic network based on the knowledge of atomic transitions (Antoniewicz et al., 2007a). A number of user-friendly software for flux estimation based on carbon labeling experiments is currently available, such as ^{13}CFlux (Wiechert et al., 2001), Metran (Yoo et al., 2008), OpenFlux (Quek et al., 2009) and INCA (Young, 2014).

5.7. Past Uses of MFA in Animal Cell Cultures

MFA can be instrumental in providing a deeper understanding of the physiology of stem cells and derivatives at a global metabolic level. In order to show what can be achieved in stem cell bioprocesses, this section will describe past uses of MFA in the areas of recombinant protein production, viral production, cancer biology, brain biology and drug toxicology.

CHO cells are the preferred animal host for production of protein biopharmaceuticals. MFA studies allowed for improved medium designs and fed-batch strategies, published in (Altamirano et al., 2001, 2004, 2006). A vast amount of studies have been also performed in hybridoma cell lines which are used for antibody production. Multiple steady states were observed in hybridoma continuous cultures by applying MFA, which

indicates cell performance could be improved by inducing specific metabolic shifts leading to favourable flux distributions (Follstad et al., 1999). In a study comparing three different physiological states of hybridoma cells (Gambhir et al., 2003), amino acid metabolism was found to be very important for reducing lactate production. More recently, Omasa et al. (2010) used metabolic flux estimations to design supplementation schemes of the intermediates pyruvate, malate and citrate leading to increased ATP and antibody production.

The impact of viral infection on cellular metabolism has also been assessed in recent years by MFA methods, in order to optimize viral vector or vaccine production processes. The aim is to compare infected vs. non-infected cells, infection at different cell concentrations, early vs. late stages of infection or even infection of different cell lines with the same virus, ultimately to increase understanding of the host-virus relationship and enable targeted optimization. For example, Wahl et al. (2008) investigated an influenza vaccine production process in MDCK cells using a segregated growth model for distinct growth phases. The observed metabolic fluxes were compared with theoretical minimum requirements and revealed large optimisation potential for this process. Using HEK-293 cells, Henry et al. (2005) showed that MFA can provide a basis to develop a feeding strategy for a perfusion process for adenovirus vectors production. In the same biological system, Martinez et al. (2010) separated HEK-293 cell growth from adenovirus production and compared its metabolic states in order to optimise the medium according to cellular demand, achieving increased cell densities and adenovirus production. Finally, a Sf9 insect cell line producing baculovirus was also analyzed by an hybrid MFA, which involved a combination of stoichiometric and statistical constraints (Carinhas et al., 2011). Through this hybrid approach, the authors found a strong association between TCA cycle and mitochondrial respiration with

virus replication. This new approach might serve in the near future as a valuable complement to metabolic studies pairing metabolic state with improved cell culture performance.

Overall, these studies related to industrial applications of animal cell cultures have been contributing to the progress in understanding the causes and consequences of metabolic shifts and inefficiencies in animal cell cultures. The quantitative information given by MFA studies will eventually allow a finer control and better manipulation of animal cell culture needed to optimize biopharmaceutical processes.

The ability to quantify metabolic fluxes in animal cells, in particular mammalian cells, has also opened the door to elucidate the dynamics of health and disease at the level of metabolic network operation (Sauer and Zamboni, 2008). In principle, diseases or genetic alterations generating certain physiological responses should be reflected on specific flux patterns. In the area of cancer metabolism, Forbes et al. (2006) observed through MFA that breast cancer cells are dependent on PPP activity and glutamine consumption for estradiol-stimulated biosynthesis, concluding that these pathways may be possible targets for estrogen-independent breast cancer therapy. Furthermore, in breast cancers with amplified phosphoglycerate dehydrogenase activity, MFA allowed to estimate that 8 to 9% of the glycolytic flux was directed towards serine biosynthesis (Possemato et al., 2011), confirming previous suppositions that functionality of the serine biosynthesis pathway is required for breast cancer proliferation (Keibler et al., 2012). In order to globally understand cancer metabolic phenotypes, Gaglio et al. (2011) applied ^{13}C-MFA in mouse fibroblasts and human carcinoma cell lines to analyse the metabolic alterations induced by the oncogene K-ras. An enhanced glycolytic flux, decreased TCA cycle activity and increased glutamine utilization for anabolic synthesis was observed, providing evidence for a

role of that oncogene in the metabolic reprogramming of cancer cells. ^{13}C-MFA proved also valuable in elucidating a novel oncogenic metabolic phenotype by confirming the reductive carboxylation of α-ketoglutarate to isocitrate under conditions of mitochondria stress (Metallo et al., 2012). A metabolic characterization of the effect of cancer cell detachment from the extracellular matrix, required for metastatic tumor invasion, was investigated by Grassian et al. (2011) showing decreased glycolytic, TCA cycle and PPP fluxes due to a substantial decrease in pyruvate dehydrogenase (PDH) activity. Interestingly, the authors assessed the influence of ErbB2 overexpression (which is amplified in about one quarter of breast tumors) and found that the PDH flux was partially rescued in breast cancer cell lines.

As another application in biomedical research, MFA has also been used to identify metabolic targets for antiviral therapy (Munger et al., 2008). The impact of human cytomegalovirus infection on mammalian fibroblasts was assessed by ^{13}C-MFA, and a significant increase in TCA cycle activity and fatty acid biosynthesis was observed. The latter pathway was then pharmacologically inhibited, successfully suppressing virus replication. As well, brain function and particularly the physiological and pathophysiological regulation of neural metabolism were also investigated using MFA methods. Teixeira et al. (2008) investigated the metabolism of primary cultures of astrocytes, integrating ^{13}C NMR data from secreted glutamine with transport rates in and out of the cells. In a following study, metabolic alterations induced by ischaemia in astrocytes were analysed, identifying a significant enhancement in branched-chain amino acids catabolism (Amaral et al., 2010). Neurons subjected to hypoglycemia were also studied by MFA, indicating glutamine as an important energy substrate and a significant activation of the pyruvate recycling pathway during recovery (Amaral et al., 2011b).

The analysis of drug effects on cellular metabolism is another very promising application of MFA highly relevant for toxicological research. Drug toxicity is one of the leading causes of attrition at all stages of drug development (Kramer et al., 2007) and is often detected late in the process implying larger economic costs (Kola and Landis, 2004). Earlier identification of drug toxicity by assessing global metabolic alterations would save money and expedite the drug development process. In Niklas et al. (2009), subtoxic drug effects of three hepatotoxic compounds were analysed in Hep G2 cells. Several changes in metabolism could be detected upon exposure to subtoxic drug levels, in particular an increase in TCA cycle activity. Also applying MFA to Hep G2 cells, Srivastava and Chan (2008) observed that free fatty acid toxicity is associated with the limitation of cysteine import causing reduced glutathione synthesis. In primary rat hepatocytes, the effect on hepatic cholesterol synthesis of therapeutic doses of atorvastatin, a hypolipidemic drug, was studied by transient ^{13}C-MFA by Maier et al. (2009). Despite the potential of these studies in toxicology research, larger scale toxicity screening usually requires a high-throughput format which was not yet been implemented for MFA studies. Moreover, improved analytical methods are needed to facilitate more detailed fluxome resolutions.

5.8. Conclusions and Perspectives

During the past two decades, MFA has emerged as a powerful and convenient tool to characterize the metabolism in living cells (Antoniewicz et al., 2006, 2007b, 2007a, 2011; Boghigian et al., 2010; Choi and Antoniewicz, 2011). The application of MFA in animal cells allows the identification of intracellular metabolic bottlenecks at specific stages of culture and eventually lead to novel strategies for improving cell performance towards optimized biopharmaceutical processes (Niklas et al., 2010). These process optimization strategies can be implemented

either by medium engineering (Niklas and Heinzle, 2012; Xing et al., 2011) or genetic manipulation of identified cellular pathways (Henry and Durocher, 2011; Niklas and Heinzle, 2012). Furthermore, in the field of process control, MFA was successfully integrated with kinetic models to predict fed-batch culture profiles (Naderi et al., 2011; Nolan and Lee, 2011; Teixeira et al., 2007).

Moreover, MFA can be combined with transcriptome and proteome profiling to provide an enlarged systems view of cell states. Nonetheless, MFA methods and associated experimental constraints are still evolving with refined techniques for flux estimation at the same time as solutions to important bottlenecks are being pursued. For example, Goudar et al. (2009) described a procedure for determining error propagation in flux analysis from extracellular metabolite measurements. To allow estimation of fluxes in underdetermined systems, Llaneras and Picó (2007) and Zamorano et al. (2010) proposed an extension to classical MFA for calculating upper and lower bounds of unresolved fluxes. Concerning intracellular compartmentalization, however, current extraction techniques are still not well suited to separate different intracellular metabolite pools without significant leakage. Advances in metabolite extraction techniques would greatly increase the potential of using ^{13}C-MFA to resolve compartment specific fluxes in animal cells.

Overall, promising new mathematical approaches as well as new experimental designs have been established during the past years. These are on the way to enable broad application and in-depth insights into the function and control of metabolic networks in animal cells in the near future.

6. Dynamic Metabolomics

Despite the referred potential of metabolic flux analysis for improving stem cell bioprocesses by giving a snapshot of what is happening in the metabolic system, it does not provide profound insights into the functioning and regulation of the system. Moreover, metabolic networks are intricate and not fully known making conclusions difficult. So, even when additional mathematical methods are added on top of MFA to model metabolic adaptations following environmental transitions, problems of incomplete topology or parameter uncertainty still arise (Gerosa et al. 2015). As an alternative to top-down approaches, identification of metabolic phenotypes and even of potential metabolic players can be done by dynamic metabolomics, a bottom-up approach. This is a recent field where the mathematical tools to analyze and incorporate dynamic experimental data into a model predicting systemic behaviour are still being developed. To probe for dynamic intracellular metabolic profiles over time, extracellular metabolic pulses are usually applied (Taymaz-Nikerel et al., 2011, 2013), but any other environmental change can be performed. In Krycer et al. (2017), dynamic metabolomics was performed on adipocytes upon insulin stimulation and the authors showed these cells respond with specific metabolic rearrangements in central carbon metabolism. Christodoulou et al. (2018) followed a similar approach by applying a sudden reactive oxygen species stress to E.coli. By employing dynamic metabolomics and modelling, the authors found novel allosteric regulations in glycolysis and in pentose phosphate pathway (PPP). Studies of dynamic metabolomics can be combined with experimental data of other molecular components (promoters, RNA, proteins) to help understand global intracellular control (Buescher et al., 2012).

7. Metabolism of Pluripotent Stem Cells, Neural Stem Cells and Astrocytes

Neural differentiation is attractive to research increasingly prevalent neurological disorders, such as Alzheimer's and Parkinson's disease (Maurer and Kuschinsky, 2006). As recently discovered, neural stem cells (NSC) reside in two regions in the brain and seem to lose their self-renewal and neurogenesis potential with aging (Hamilton et al., 2015; Wang et al., 2016). Thus, researching how to trigger their *in vivo* is ongoing (Hamilton et al., 2015). NSC are also being considered for cell therapy even if it is unclear how these could graft effectively into the highly complex neural network in the brain (Tang et al., 2017). More immediate applications are disease modelling and drug testing (Edri et al., 2015). For Alzheimer's and Parkinson's, understanding molecular mechanisms is essential for finding drug targets whereas for drug testing, NSC are differentiated into specific neural cells and co-cultured for screening new therapies. And for drug toxicity testing, as nearly one-quarter of attrition in drug discovery and development is due to central nervous system toxicity (Walker et al., 2018).

NSC can be obtained *in vitro* by differentiation of pluripotent stem cells (Figure 1.9), either embryonic stem cells or induced pluripotent stem cells (Hu et al., 2010). However, achieving a final a highly pure cell culture usually requires a long time and is accompanied by safety issues which complicate the application of these cells as a cell therapy (Tang et al., 2017). Neural differentiation of NSC into neurons, astrocyte and oligodendrocytes (Figure 1.9) is also problematic as a bioprocesses. Firstly, differentiated neural cells do not present a mature phenotype. Secondly, protein biomarkers used for evaluating neural cell phenotype do not correlate well with their functionality (Walker et al., 2018). Additionally,

the presence of two stem cell type stages during neural differentiation, pluripotent and neural stem cells, represents a safety risk as residual stem cells have tumorigenic potential (Kamao et al., 2014; Liu et al., 2010). Finally, neural differentiation uses expensive media and presents low yields of differentiation, especially in oligodendrocytes (Rodrigues et al., 2017).

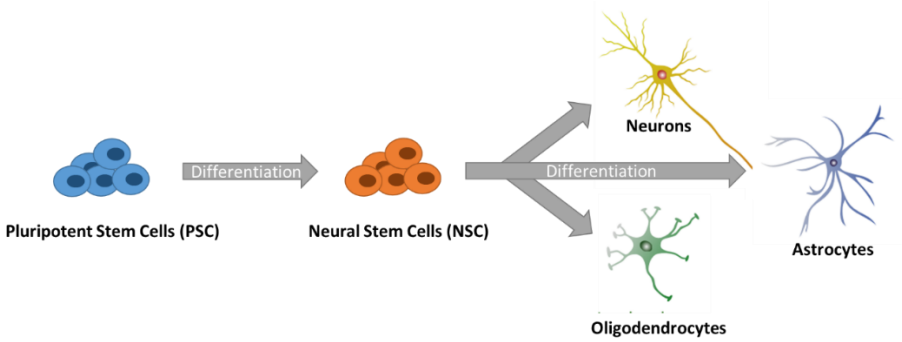

Figure 1.9 – Schematic representation of a neural differentiation process: from pluripotent stem cells to neural stem cells, and from these to neurons, astrocytes and oligodendrocytes. Adapted from (Cavallucci et al., 2016).

7.1. Metabolism of Pluripotent Stem Cells

Pluripotent stem cells are usually categorized in naïve-state and primed-sate. Naïve-state PSCs functionally resemble the pre-implantation blastocyst inner cell mass and possess the differentiation potential for all three germ layers and primordial germ cells. Primed-state resemble post-implantation epiblast cells PSCs (Brons et al., 2007; Tesar et al., 2007), have a low capacity to contribute to embryonic chimeras and a relatively low competence for germline differentiation (Weinberger et al., 2016). Both types of PSCs exhibit a high glycolytic flux to support high energy and biosynthetic demands during rapid proliferation (Folmes et al., 2011;

Zhang et al., 2011). These metabolic features are also reacquired during somatic reprogramming to iPSCs, and prior to the induction of pluripotency gene expression (Folmes et al., 2011; Kida et al., 2015). Beyond energetic and biosynthetic needs, there is important metabolic production for epigenome modifications, such as the production of acetyl-CoA by glycolysis that maintains histone acetylation and pluripotency (Moussaieff et al., 2015).

Metabolic differences exist between naïve-state and primed-state PSCs. Primed-state PSCs, the PSC state most used *in vitro* experiments, exhibit higher activation of the entire one-carbon metabolic pathway, including upstream serine production from glucose and downstream S-adenosyl-methionine (SAM) and nucleotide production through folate cycle and methionine cycle (Chandrasekaran et al., 2017). The increase of SAM levels leads to histone methylation (Sperber et al., 2015), a state in contrast with the hypomethylation characteristic of the naïve state (Marks et al., 2012). During priming of PSCs, glycolytic flux is reduced (Gu et al., 2016), despite maintaining higher levels than in somatic cells (Prigione et al., 2010). Interestingly, primed-state PSC also show lower respiration than naïve-state (Carbognin et al., 2016; Takashima et al., 2014).

7.2. Metabolism of Neural Stem Cells

Neural stem cells (NSC) reside in the subventricular zone and subgranular zone in the dentate gyrus where spontaneous production of new neurons from the resident NSCs have been observed (Jin et al., 2001). NSCs possess predominantly a glycolytic metabolism despite containing functional respiratory complexes, ready to produce ATP through oxidative phosphorylation quickly when neurogenesis is boosted (Khacho et al., 2016). Furthermore, single-cell transcriptomic analysis of NSCs isolated from the subependymal zone and dentate gyrus identified

a set of dormant NSCs with higher expression of glycolytic genes and lipid intermediates (Llorens-Bobadilla et al., 2015; Shin et al., 2015). Indeed, a metabolic switch from a higher glycolytic metabolism towards an increased oxidative phosphorylation state, occurs in neuronal differentiation of NSCs *in vivo* and *in vitro* (Agostini et al., 2016; Candelario et al., 2013; Fang et al., 2016; Khacho et al., 2016; Zheng et al., 2016). These changes include the downregulation of key glycolytic enzymes such as hexokinase II (HKII), lactate dehydrogenase (LDHA) and pyruvate dehydrogenase kinase 1 (PDK1), alternative splicing from pyruvate kinase isozymes M2 (PKM2) to M1 (PKM1), and increased mitochondrial biogenesis (Gascón et al., 2017).

7.3. Metabolism of Differentiated Astrocytes

Astrocytes play a fundamental role in numerous functions of the central nervous system, such as glutamate, ion and water homeostasis, defense against oxidative stress, energy storage in the form of glycogen, scar formation, tissue repair, modulation of synaptic activity via the release of gliotransmitters, and synapse formation and remodeling (Bélanger and Magistretti, 2009; Volterra and Meldolesi, 2005). With all these supporting functions, it is unsurprising that astrocytes outnumber neurons in the human brain (Nedergaard et al., 2003) and establish intricate and numerous metabolic interactions with spatially nearby neurons and endothelial cells (Bélanger et al., 2011).

One of these metabolic interactions is the lactate shuttle. Astrocytes avidly take up glucose and a large fraction of it is released as lactate in the extracellular space (Bouzier-Sore et al., 2006; Itoh et al., 2003; Lovatt et al., 2007; Pellerin and Magistretti, 1994; Serres et al., 2005). This lactate is then used by neurons for their metabolic needs, constituting what is called the astrocyte-neuron lactate shuttle (ANLS) model (Pellerin and Magistretti, 1994), a model still under intensive debate (Bélanger et al., 2011).

Another important function of astrocytes is the removal of neurotransmitters released into the synapses, an essential process for stopping synaptic transmission and maintaining neuronal excitability (Bélanger et al., 2011). The primary excitatory neurotransmitter in the brain, glutamate, has to be removed as overstimulation of glutamate receptors is highly toxic to neurons. Astrocytes uptake glutamate via high-affinity transporters (Bak et al., 2006) and convert it into glutamine which is then transferred to neurons. Neurons use then this glutamine to synthesize glutamate for neurotransmission, completing a process called glutamate-glutamine cycle (Bak et al., 2006; McKenna, 2007).

Astrocytes are also responsible for the largest energy reserve of the brain by storing glycogen (Brown, 2004; Magistretti et al., 1993). Glycogen represents an advantageous form of glucose storage, as it can be rapidly metabolized without requirements for ATP, and, unlike fatty acids, it can yield ATP under anaerobic conditions. Astrocytes use up this glycogen to support the activity of the more energy-requiring neurons. Glycogen functions as an emergency energy reserve by being converted to lactate for neuronal use during aglycemic conditions (Brown et al., 2005; Tekkök et al., 2005).

The metabolic features of astrocytes are not unique *per se*. For instance, the cell-cell lactate shuttle exists in several other biological systems (Brooks, 2009), for instance in the intestinal crypt (Roper and Yilmaz, 2017). Therefore, the metabolic characterization of astrocytes has to be performed by grouping several of its metabolic features, to ensure higher accuracy.

8. Aims and Scope of Thesis

The relevance of metabolism as regulator for stem cell fate and its consequent value for stem cell bioprocesses define the scope of this

thesis. Two major axis, each with a biological and an application question, were considered: the metabolism as a characterization tool and as a process development tool – Figure 1.10. In the first axis, the biological question concerns the relationship between cell identity and metabolism, in particular if those attributes can be described as variables of a one-to-one function. If so, metabolic characterization could be complementary used as in-process control or supporting quality control of a stem cell bioprocess. The second biological question kept in mind in this thesis was whether this strong link between cell fate and metabolism could guide to new bioprocess tools for manipulation of stem cells' fate, specifically in optimizing expansion and differentiation of stem cells by employing metabolic modulators.

With these questions in mind, a neural differentiation process was metabolically characterized (Figure 1.10). In Chapter 2, ^{13}C-metabolic flux analysis was employed to identify a set of features putatively specific of neural stem cells and astrocytes. In Chapter 3, a novel strategy, involving dynamic characterization of metabolic pools, was used to characterize pluripotent stem cells and neural stem cells. Chapter 2 and 3 are two different approaches for attempting a metabolic characterization of cells which, due to their output data, give origin to possible metabolic strategies for optimization of stem cell bioprocesses. These results and consequent proposals were discussed in more detail and together in chapter 4, and contextualized with the available literature and state-of-the-art for the fields addressed throughout the previous chapters.

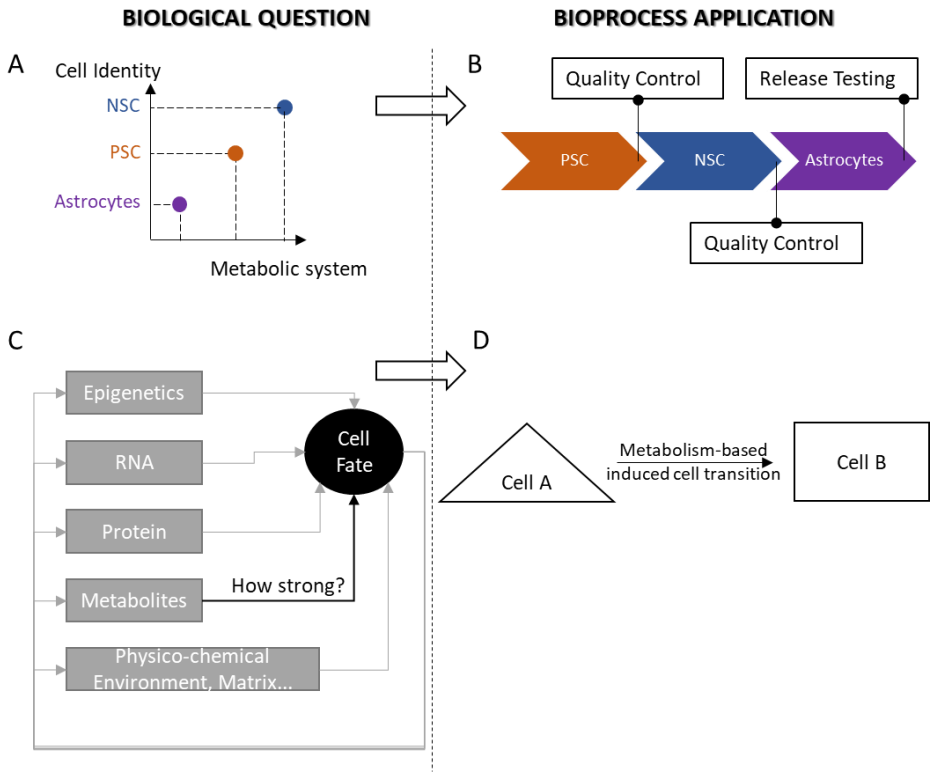

Figure 1.10 – Biological questions and applications in bioprocesses pursued in this thesis. A) Is cell identity and metabolism an one-to-one function? B) If so, can metabolism be used for quality control during process and after obtaining final product? C) How strong is the influence of metabolism in cell fate? D) Can it be used for designing differentiation protocols based on metabolism-based approaches?

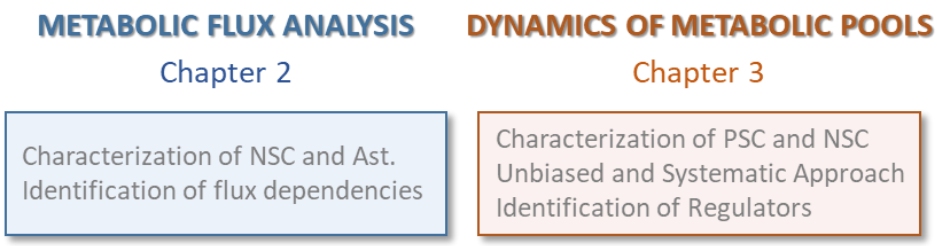

Figure 1.11 – Thesis aims and its discrimination by chapter. NSC – Neural Stem Cells; Ast – Astrocytes; TCA – tricarboxylic acid cycle; PSC – pluripotent stem cells; Gln – Glutamine.

9. References

Agostini, M., Romeo, F., Inoue, S., Niklison-Chirou, M., Elia, A., Dinsdale, D., Morone, N., Knight, R., Mak, T., and Melino, G. (2016). Metabolic reprogramming during neuronal differentiation. Cell Death Differ. *23*, 1502–1514.

Ahn, W.S., and Antoniewicz, M.R. (2011). Metabolic flux analysis of CHO cells at growth and non-growth phases using isotopic tracers and mass spectrometry. Metab. Eng. *13*, 598–609.

Ahn, W.S., and Antoniewicz, M.R. (2012). Towards dynamic metabolic flux analysis in CHO cell cultures. Biotechnol. J. *7*, 61–74.

Ahn, W.S., and Antoniewicz, M.R. (2013). Parallel labeling experiments with [1,2-(13)C]glucose and [U-(13)C]glutamine provide new insights into CHO cell metabolism. Metab. Eng. *15*, 34–47.

Altamirano, C., Illanes, a, Casablancas, a, Gámez, X., Cairó, J.J., and Gòdia, C. (2001). Analysis of CHO cells metabolic redistribution in a glutamate-based defined medium in continuous culture. Biotechnol. Prog. *17*, 1032–1041.

Altamirano, C., Paredes, C., Illanes, a, Cairó, J.J., and Gòdia, F. (2004). Strategies for fed-batch cultivation of t-PA producing CHO cells: substitution of glucose and glutamine and rational design of culture medium. J. Biotechnol. *110*, 171–179.

Altamirano, C., Illanes, A., Becerra, S., Cairó, J.J., and Gòdia, F. (2006). Considerations on the lactate consumption by CHO cells in the presence of galactose. J. Biotechnol. *125*, 547–556.

Amaral, A.I., Teixeira, A.P., Martens, S., Bernal, V., Sousa, M.F.Q., and Alves, P.M. (2010). Metabolic alterations induced by ischemia in primary cultures of astrocytes: merging 13C NMR spectroscopy and metabolic flux analysis. J. Neurochem. *113*, 735–748.

Amaral, A.I., Teixeira, A.P., Håkonsen, B.I., Sonnewald, U., and Alves, P.M. (2011a). A comprehensive metabolic profile of cultured astrocytes using isotopic transient metabolic flux analysis and C-labeled glucose. Front. Neuroenergetics *3*, 1–5.

Amaral, A.I., Teixeira, A.P., Sonnewald, U., and Alves, P.M. (2011b). Estimation of intracellular fluxes in cerebellar neurons after hypoglycemia: importance of the pyruvate recycling pathway and glutamine oxidation. J. Neurosci. Res. *89*, 700–710.

Antoniewicz, M.R. (2013). (13)C metabolic flux analysis: optimal design of isotopic labeling experiments. Curr. Opin. Biotechnol. *24*, 1–6.

Antoniewicz, M.R., Kelleher, J.K., and Stephanopoulos, G. (2006). Determination of confidence intervals of metabolic fluxes estimated from stable isotope measurements. Metab. Eng. *8*, 324–337.

Antoniewicz, M.R., Kelleher, J.K., and Stephanopoulos, G. (2007a). Elementary Metabolite Units (EMU): a novel framework for modeling isotopic distributions. Metab. Eng. *9*, 68–86.

Antoniewicz, M.R., Kelleher, J.K., and Stephanopoulos, G. (2007b). Accurate assessment of amino acid mass isotopomer distributions for metabolic flux analysis. Anal. Chem. *79*, 7554–7559.

Antoniewicz, M.R., Kelleher, J.K., and Stephanopoulos, G. (2011). Measuring deuterium enrichment of glucose hydrogen atoms by gas chromatography mass spectrometry. Anal. Chem. *83*, 3211–3216.

Bach, P.B., Giralt, S.A., and Saltz, L.B. (2017). FDA Approval of Tisagenlecleucel: Promise and Complexities of a $475 000 Cancer Drug. JAMA *318*, 1861–1862.

Bak, L.K., Schousboe, A., and Waagepetersen, H.S. (2006). The glutamate/GABA-glutamine cycle: Aspects of transport, neurotransmitter homeostasis and ammonia transfer. J. Neurochem. *98*, 641–653.

Bélanger, M., and Magistretti, P.J. (2009). The role of astroglia in neuroprotection. Dialogues Clin. Neurosci. *11*, 281–295.

Bélanger, M., Allaman, I., and Magistretti, P.J. (2011). Brain energy metabolism: focus on astrocyte-neuron metabolic cooperation. Cell Metab. *14*, 724–738.

Ben-David, U., and Benvenisty, N. (2011). The tumorigenicity of human embryonic and induced pluripotent stem cells. Nat. Rev. Cancer *11*, 268–277.

Berkers, G., van Mourik, P., Vonk, A.M., Kruisselbrink, E., Dekkers, J.F., de Winter-de Groot, K.M., Arets, H.G.M., Marck-van der Wilt, R.E.P., Dijkema, J.S., Vanderschuren, M.M., et al. (2019). Rectal Organoids Enable Personalized Treatment of Cystic Fibrosis. Cell Rep. *26*, 1701–1708.

Bird, A. (2002). DNA methylation patterns and epigenetic memory.

Genes Dev. *16*, 6–21.

Boghigian, B. a, Seth, G., Kiss, R., and Pfeifer, B. a (2010). Metabolic flux analysis and pharmaceutical production. Metab. Eng. *12*, 81–95.

Bonarius, H.P.J., and Schmid, G. (1997). Flux analysis of underdetermined metabolic networks: the quest for the missing constraints. Trends Biotechnol. *15*, 308–314.

Boukouris, A.E., Zervopoulos, S.D., and Michelakis, E.D. (2016). Metabolic Enzymes Moonlighting in the Nucleus : Metabolic Regulation of Gene Transcription. Trends Biochem. Sci. *41*, 712–730.

Bouzier-Sore, A.-K., Voisin, P., Bouchaud, V., Bezancon, E., Franconi, J.-M., and Pellerin, L. (2006). Competition between glucose and lactate as oxidative energy substrates in both neurons and astrocytes: a comparative NMR study. Eur. J. Neurosci. *24*, 1687–1694.

Brito, C., Simão, D., Costa, I., Malpique, R., Pereira, C.I., Fernandes, P., Serra, M., Schwarz, S.C., Schwarz, J., Kremer, E.J., et al. (2012). Generation and genetic modification of 3D cultures of human dopaminergic neurons derived from neural progenitor cells. Methods *56*, 452–460.

Brons, I.G.M., Smithers, L.E., Trotter, M.W.B., Rugg-Gunn, P., Sun, B., Chuva de Sousa Lopes, S.M., Howlett, S.K., Clarkson, A., Ahrlund-Richter, L., Pedersen, R.A., et al. (2007). Derivation of pluripotent epiblast stem cells from mammalian embryos. Nature *448*, 191–195.

Brooks, G.A. (2009). Cell-cell and intracellular lactate shuttles. J. Physiol. *587*, 5591–5600.

Brown, A.M. (2004). Brain glycogen re-awakened. J. Neurochem. *89*, 537–552.

Brown, A.M., Sickmann, H.M., Fosgerau, K., Lund, T.M., Schousboe, A., Waagepetersen, H.S., and Ransom, B.R. (2005). Astrocyte glycogen metabolism is required for neural activity during aglycemia or intense stimulation in mouse white matter. J. Neurosci. Res. *79*, 74–80.

Buescher, J.M., Liebermeister, W., Jules, M., Uhr, M., Muntel, J., Botella, E., Hessling, B., Kleijn, R.J., Le Chat, L., Lecointe, F., et al. (2012). Global Network Reorganization During Dynamic Adaptations of Bacillus subtilis Metabolism. Science (80-.). *335*, 1099–1103.

Candelario, K.M., Shuttleworth, C.W., and Cunningham, L.A. (2013). Neural stem/progenitor cells display a low requirement for oxidative metabolism independent of hypoxia inducible factor-1 alpha expression. J. Neurochem. *125*, 420–429.

Carbognin, E., Betto, R.M., Soriano, M.E., Smith, A.G., and Martello, G. (2016). Stat3 promotes mitochondrial transcription and oxidative respiration during maintenance and induction of naive pluripotency. EMBO J. *35*, 618–634.

Carinhas, N., Bernal, V., Teixeira, A.P., Carrondo, M.J., Alves, P.M., and Oliveira, R. (2011). Hybrid metabolic flux analysis: combining stoichiometric and statistical constraints to model the formation of complex recombinant products. BMC Syst. Biol. *5*, 1–13.

Carinhas, N., Duarte, T.M., Barreiro, L.C., Carrondo, M.J.T., Alves, P.M., and Teixeira, A.P. (2013). Metabolic signatures of GS-CHO cell clones associated with butyrate treatment and culture phase transition. Biotechnol. Bioeng. *110*, 3244–3257.

Cavallucci, V., Fidaleo, M., and Pani, G. (2016). Neural Stem Cells and Nutrients: Poised Between Quiescence and Exhaustion. Trends Endocrinol. Metab. *27*, 756–769.

Chandrasekaran, S., Zhang, J., Sun, Z., Zhang, L., Ross, C.A., Huang, Y.-C., Li, H., Daley, G.Q., and Collins, J.J. (2017). Comprehensive Mapping of Pluripotent Stem Cell Metabolism Using Dynamic Genome-Scale Network Modeling. Cell Rep. *21*, 2965–2977.

Chang, C., Curtis, J.D., Maggi, L.B., Faubert, B., Villarino, A. V, Sullivan, D.O., Huang, S.C., Windt, G.J.W. Van Der, Blagih, J., Qiu, J., et al. (2013). Posttranscriptional Control of T Cell Effector Function by Aerobic Glycolysis. Cell *153*, 1239–1251.

Chen, A., Ting, S., Seow, J., Reuveny, S., and Oh, S. (2014). Considerations in designing systems for large scale production of human cardiomyocytes from pluripotent stem cells. Stem Cell Res. Ther. *5*, 1–13.

Choi, J., and Antoniewicz, M.R. (2011). Tandem mass spectrometry: a novel approach for metabolic flux analysis. Metab. Eng. *13*, 225–233.

Choi, J., Grossbach, M.T., and Antoniewicz, M.R. (2012). Measuring complete isotopomer distribution of aspartate using gas chromatography/tandem mass spectrometry. Anal. Chem. *84*, 4628–4632.

Crown, S.B., and Antoniewicz, M.R. (2013). Parallel labeling experiments and metabolic flux analysis: Past, present and future methodologies. Metab. Eng. *16*, 21–32.

Crown, S.B., Indurthi, D.C., Ahn, W.S., Choi, J., Papoutsakis, E.T., and Antoniewicz, M.R. (2011). Resolving the TCA cycle and pentose-phosphate pathway of Clostridium acetobutylicum ATCC 824: Isotopomer analysis, in vitro activities and expression analysis. Biotechnol. J. *6*, 300–305.

da Cruz, L., Fynes, K., Georgiadis, O., Kerby, J., Luo, Y.H., Ahmado, A.,

Vernon, A., Daniels, J.T., Nommiste, B., Hasan, S.M., et al. (2018). Phase 1 clinical study of an embryonic stem cell–derived retinal pigment epithelium patch in age-related macular degeneration. Nat. Biotechnol. *36*, 328–337.

Dettmer, K., Aronov, P.A., and Hammock, B.D. (2007). Mass spectrometry-based metabolomics. Mass Spectrom. Rev. *26*, 51–78.

Drawnel, F.M., Boccardo, S., Prummer, M., Delobel, F., Graff, A., Weber, M., Gérard, R., Badi, L., Kam-Thong, T., Bu, L., et al. (2014). Disease modeling and phenotypic drug screening for diabetic cardiomyopathy using human induced pluripotent stem cells. Cell Rep. *9*, 810–820.

Duarte, T.M., Carinhas, N., Silva, A.C., Alves, P.M., and Teixeira, A.P. (2014). ^{1}H-NMR protocol for exometabolome analysis of cultured mammalian cells. Methods Mol. Biol. *1104*, 237–247.

Dwarshuis, N.J., Parratt, K., Santiago-Miranda, A., and Roy, K. (2017). Cells as advanced therapeutics: State-of-the-art, challenges, and opportunities in large scale biomanufacturing of high-quality cells for adoptive immunotherapies. Adv. Drug Deliv. Rev. *114*, 222–239.

Edri, R., Yaffe, Y., Ziller, M.J., Mutukula, N., Volkman, R., David, E., Jacob-Hirsch, J., Malcov, H., Levy, C., Rechavi, G., et al. (2015). Analysing human neural stem cell ontogeny by consecutive isolation of Notch active neural progenitors. Nat. Commun. *6*, 1–15.

Fang, D., Qing, Y., Yan, S., Chen, D., and Yan, S.S. Du (2016). Development and Dynamic Regulation of Mitochondrial Network in Human Midbrain Dopaminergic Neurons Differentiated from iPSCs. Stem Cell Reports *7*, 678–692.

Follstad, B.D., Balcarcel, R.R., Stephanopoulos, G., and Wang, D.I. (1999). Metabolic flux analysis of hybridoma continuous culture steady

state multiplicity. Biotechnol. Bioeng. *63*, 675–683.

Folmes, C.D.L., Nelson, T.J., Martinez-Fernandez, A., Arrell, D.K., Lindor, J.Z., Dzeja, P.P., Ikeda, Y., Perez-Terzic, C., and Terzic, A. (2011). Somatic oxidative bioenergetics transitions into pluripotency-dependent glycolysis to facilitate nuclear reprogramming. Cell Metab. *14*, 264–271.

Fonoudi, H., Ansari, H., Abbasalizadeh, S., Larijani, M.R., Kiani, S., Hashemizadeh, S., Zarchi, A.S., Bosman, A., Blue, G.M., Pahlavan, S., et al. (2014). A Universal and Robust Integrated Platform for the Scalable Production of Human Cardiomyocytes From Pluripotent Stem Cells. Stem Cells Transl. Med. *4*, 1482–1494.

Forbes, N.S., Meadows, A.L., Clark, D.S., and Blanch, H.W. (2006). Estradiol stimulates the biosynthetic pathways of breast cancer cells: detection by metabolic flux analysis. Metab. Eng. *8*, 639–652.

Gaglio, D., Metallo, C.M., Gameiro, P. a, Hiller, K., Danna, L.S., Balestrieri, C., Alberghina, L., Stephanopoulos, G., and Chiaradonna, F. (2011). Oncogenic K-Ras decouples glucose and glutamine metabolism to support cancer cell growth. Mol. Syst. Biol. *7*, 1–15.

Gambhir, A., Korke, R., Lee, J., Fu, P., Europa, A., and Hu, W. (2003). Analysis of Cellular Metabolism of Hybridoma Cells at Distinct Physiological States. J. Biosci. Bioeng. *95*, 317–327.

Gao, X., Wang, H., Yang, J.J., Liu, X., and Liu, Z. (2012). Pyruvate Kinase M2 Regulates Gene Transcription by Acting as a Protein Kinase. Mol. Cell *45*, 598–609.

Gascón, S., Masserdotti, G., Russo, G.L., and Götz, M. (2017). Direct Neuronal Reprogramming: Achievements, Hurdles, and New Roads to Success. Cell Stem Cell *21*, 18–34.

Geiger, R., Rieckmann, J.C., Wolf, T., Zamboni, N., Sallusto, F., Lanzavecchia, A., Geiger, R., Rieckmann, J.C., Wolf, T., Basso, C., et al. (2016). L-Arginine Modulates T Cell Metabolism and Enhances Survival and Anti-tumor Activity. Cell *167*, 829–842.

Gilsbach, R., Schwaderer, M., Preissl, S., Grüning, B.A., Kranzhöfer, D., Schneider, P., Nührenberg, T.G., Mulero-Navarro, S., Weichenhan, D., Braun, C., et al. (2018). Distinct epigenetic programs regulate cardiac myocyte development and disease in the human heart in vivo. Nat. Commun. *9*, 1–14.

Goldman, O., and Gouon-Evans, V. (2016). Human Pluripotent Stem Cells: Myths and Future Realities for Liver Cell Therapy. Cell Stem Cell *18*, 703–706.

Gonzalez-Cordero, A., Kruczek, K., Naeem, A., Fernando, M., Kloc, M., Ribeiro, J., Goh, D., Duran, Y., Blackford, S.J.I., Abelleira-Hervas, L., et al. (2017). Recapitulation of Human Retinal Development from Human Pluripotent Stem Cells Generates Transplantable Populations of Cone Photoreceptors. Stem Cell Reports *9*, 820–837.

Goudar, C., Biener, R., Zhang, C., Michaels, J., Piret, J., and Konstantinov, K. (2006). Towards industrial application of quasi real-time metabolic flux analysis for mammalian cell culture. Adv. Biochem. Eng. Biotechnol. *101*, 99–118.

Goudar, C., Biener, R., Boisart, C., Heidemann, R., Piret, J., de Graaf, A., and Konstantinov, K. (2010). Metabolic flux analysis of CHO cells in perfusion culture by metabolite balancing and 2D [13C, 1H] COSY NMR spectroscopy. Metab. Eng. *12*, 138–149.

Goudar, C.T., Biener, R., Konstantinov, K.B., and Piret, J.M. (2009). Error Propagation from Prime Variables into Specific Rates and

Metabolic Fluxes for Mammalian Cells in Perfusion Culture. Am. Inst. Chem. Eng. *25*, 986–998.

Grassian, A.R., Metallo, C.M., Coloff, J.L., Stephanopoulos, G., and Brugge, J.S. (2011). Erk regulation of pyruvate dehydrogenase flux through PDK4 modulates cell proliferation. Genes Dev. *25*, 1716–1733.

Gu, W., Gaeta, X., Sahakyan, A., Chan, A.B., Hong, C.S., Kim, R., Braas, D., Plath, K., Lowry, W.E., and Christofk, H.R. (2016). Glycolytic Metabolism Plays a Functional Role in Regulating Human Pluripotent Stem Cell State. Stem Cell *19*, 476–490.

Hagen, T. (2017). Novartis Sets a Price of $475,000 for CAR T-Cell Therapy.

Hamilton, L.K., Dufresne, M., Joppé, S.E., Petryszyn, S., Aumont, A., Calon, F., Barnabé-Heider, F., Furtos, A., Parent, M., Chaurand, P., et al. (2015). Aberrant Lipid Metabolism in the Forebrain Niche Suppresses Adult Neural Stem Cell Proliferation in an Animal Model of Alzheimer's Disease. Cell Stem Cell *17*, 397–411.

Hansen, M.M.K., Wen, W.Y., Ingerman, E., Razooky, B.S., Thompson, C.E., Dar, R.D., Chin, C.W., Simpson, M.L., and Weinberger, L.S. (2018). A Post-Transcriptional Feedback Mechanism for Noise Suppression and Fate Stabilization. Cell *173*, 1609–1621.

Hara, M.R., Agrawal, N., Kim, S.F., Cascio, M.B., Fujimuro, M., Ozeki, Y., Takahashi, M., Cheah, J.H., Tankou, S.K., Hester, L.D., et al. (2005). S-nitrosylated GAPDH initiates apoptotic cell death by nuclear translocation following Siah1 binding. Nat. Cell Biol. *7*, 665–674.

Hay, M., Thomas, D.W., Craighead, J.L., Economides, C., and Rosenthal, J. (2014). Clinical development success rates for investigational drugs. Nat. Biotechnol. *32*, 40–51.

Henry, O., and Durocher, Y. (2011). Enhanced glycoprotein production in HEK-293 cells expressing pyruvate carboxylase. Metab. Eng. *13*, 499–507.

Henry, O., Perrier, M., and Kamen, A. (2005). Metabolic flux analysis of HEK-293 cells in perfusion cultures for the production of adenoviral vectors. Metab. Eng. *7*, 467–476.

Herberts, C.A., Kwa, M.S.G., and Hermsen, H.P.H. (2011). Risk factors in the development of stem cell therapy. J. Transl. Med. *9*, 1–14.

Hildreth, C. (2018). Pricing of Approved Cell Therapy Products (BioInformant).

Hu, B.-Y., Weick, J.P., Yu, J., Ma, L.-X., Zhang, X.-Q., Thomson, J. a, and Zhang, S.-C. (2010). Neural differentiation of human induced pluripotent stem cells follows developmental principles but with variable potency. Proc. Natl. Acad. Sci. U. S. A. *107*, 4335–4340.

Huang, H., Sabari, B.R., Garcia, B.A., Allis, C.D., and Zhao, Y. (2014). SnapShot: Histone Modifications. Cell *159*, 458–458.

Humphrey, S.J., James, D.E., and Mann, M. (2015). Protein Phosphorylation : A Major Switch Mechanism for Metabolic Regulation. Trends Endocrinol. Metab. *26*, 676–687.

Itoh, Y., Esaki, T., Shimoji, K., Cook, M., Law, M.J., Kaufman, E., and Sokoloff, L. (2003). Dichloroacetate effects on glucose and lactate oxidation by neurons and astroglia in vitro and on glucose utilization by brain in vivo. Proc. Natl. Acad. Sci. U. S. A. *100*, 4879–4884.

Jazmin, L.J., and Young, J.D. (2013). Isotopically Nonstationary 13C Metabolic Flux Analysis. In Systems Metabolic Engineering: Methods and Protocols, H.S. Alper, ed. (Totowa, NJ: Humana Press), pp. 367–390.

Jeffrey, F.M.H., Roach, J.S., Storey, C.J., Sherry, a D., and Malloy, C.R. (2002). 13C isotopomer analysis of glutamate by tandem mass spectrometry. Anal. Biochem. *300*, 192–205.

Jenkins, M.J., and Farid, S.S. (2015). Human pluripotent stem cell-derived products: Advances towards robust, scalable and cost-effective manufacturing strategies. Biotechnol. J. *10*, 83–95.

Jiang, Y., Qian, X., Shen, J., Wang, Y., Li, X., Liu, R., Xia, Y., Chen, Q., Peng, G., Lin, S., et al. (2015). Local generation of fumarate promotes DNA repair through inhibition of histone H3 demethylation. Nat. Cell Biol. *17*, 1158–1170.

Jin, K., Minami, M., Lan, J.Q., Mao, X.O., Batteur, S., Simon, R.P., and Greenberg, D.A. (2001). Neurogenesis in dentate subgranular zone and rostral subventricular zone after focal cerebral ischemia in the rat. Proc. Natl. Acad. Sci. *98*, 4710–4715.

Kaelin, W.G., and McKnight, S.L. (2013). Influence of Metabolism on Epigenetics and Disease. Cell *153*, 56–69.

Kamao, H., Mandai, M., Okamoto, S., Sakai, N., Suga, A., Sugita, S., Kiryu, J., and Takahashi, M. (2014). Characterization of human induced pluripotent stem cell-derived retinal pigment epithelium cell sheets aiming for clinical application. Stem Cell Reports *2*, 205–218.

Kaper, T., Looger, L.L., Takanaga, H., Platten, M., Steinman, L., and Frommer, W.B. (2007). Nanosensor detection of an immunoregulatory tryptophan influx/kynurenine efflux cycle. PLoS Biol. *5*, 2201–2210.

Keibler, M.A., Fendt, S., and Stephanopoulos, G. (2012). Expanding the Concepts and Tools of Metabolic Engineering to Elucidate Cancer Metabolism. Biotechnol. Prog. *28*, 1409–1418.

Keisuke Ito, and Suda Toshio (2014). Metabolic requirements for the maintenance of self-renewing stem cells. Nat. Rev. Mol. Cell Biol. *15*, 243–256.

Kempf, H., and Zweigerdt, R. (2018). Scalable Cardiac Differentiation of Pluripotent Stem Cells Using Specific Growth Factors and Small Molecules BT - Engineering and Application of Pluripotent Stem Cells. In Engineering and Application of Pluripotent Stem Cells, U. Martin, R. Zweigerdt, and I. Gruh, eds. (Cham: Springer International Publishing), pp. 39–69.

Khacho, M., Clark, A., Svoboda, D.S., Azzi, J., MacLaurin, J.G., Meghaizel, C., Sesaki, H., Lagace, D.C., Germain, M., Harper, M.E., et al. (2016). Mitochondrial Dynamics Impacts Stem Cell Identity and Fate Decisions by Regulating a Nuclear Transcriptional Program. Cell Stem Cell *19*, 232–247.

Khoo, S.H.G., and Al-Rubeai, M. (2009). Metabolic characterization of a hyper-productive state in an antibody producing NS0 myeloma cell line. Metab. Eng. *11*, 199–211.

Kida, Y.S., Kawamura, T., Wei, Z., Sogo, T., Jacinto, S., Shigeno, A., Kushige, H., Yoshihara, E., Liddle, C., Ecker, J.R., et al. (2015). ERRs mediate a metabolic switch required for somatic cell reprogramming to pluripotency. Cell Stem Cell *16*, 547–555.

Kim, J., and Dang, C. V (2005). Multifaceted roles of glycolytic enzymes. Trends Biochem. Sci. *30*, 142–150.

Klontzas, M.E., Vernardis, S.I., Heliotis, M., Tsiridis, E., and Mantalaris, A. (2017). Metabolomics Analysis of the Osteogenic Differentiation of Umbilical Cord Blood Mesenchymal Stem Cells Reveals Differential Sensitivity to Osteogenic Agents. Stem Cells Dev. *26*, 723–733.

Klose, R.J., and Zhang, Y. (2007). Regulation of histone methylation by demethylimination and demethylation. Nat. Mol. Cell Biol. *8*, 307–318.

Ko, H.C., and Gelb, B.D. (2014). Concise Review: Drug Discovery in the Age of the Induced Pluripotent Stem Cell. Stem Cells Transl. Med. *3*, 500–509.

Kola, I., and Landis, J. (2004). Can the pharmaceutical industry reduce attrition rates? Nat. Rev. Drug Discov. *3*, 711–716.

Kramer, J.A., Sagartz, J.E., and Morris, D.L. (2007). The application of discovery toxicology and pathology towards the design of safer pharmaceutical lead candidates. Nat. Rev. Drug Discov. *6*, 636–649.

Lane, S.W., Williams, D.A., and Watt, F.M. (2014). Modulating the stem cell niche for tissue regeneration. Nat. Biotechnol. *32*, 795–803.

Lin, Y., Linask, K.L., Mallon, B., Johnson, K., Klein, M., Beers, J., Xie, W., Du, Y., Liu, C., Lai, Y., et al. (2017). Heparin Promotes Cardiac Differentiation of Human Pluripotent Stem Cells in Chemically Defined Albumin-Free Medium, Enabling Consistent Manufacture of Cardiomyocytes. Stem Cells Transl. Med. *6*, 527–538.

Liu, H.K., Wang, Y., Beiz, T., Bock, D., Takacs, A., Radlwimmer, B., Barbus, S., Reifenberger, G., Lichter, P., and Schütz, G. (2010). The nuclear receptor tailless induces long-term neural stem cell expansion and brain tumor initiation. Genes Dev. *24*, 683–695.

Llaneras, F., and Picó, J. (2007). A procedure for the estimation over time of metabolic fluxes in scenarios where measurements are uncertain and/or insufficient. BMC Bioinformatics *8*, 1–25.

Llorens-Bobadilla, E., Zhao, S., Baser, A., Saiz-castro, G., and Martin-Villalba, A. (2015). Single-Cell Transcriptomics Reveals a Population of

Dormant Neural Stem Cells that Become Activated upon Brain Injury. Cell Stem Cell *17*, 329–340.

Lovatt, D., Sonnewald, U., Waagepetersen, H.S., Schousboe, A., He, W., Lin, J.H.-C., Han, X., Takano, T., Wang, S., Sim, F.J., et al. (2007). The transcriptome and metabolic gene signature of protoplasmic astrocytes in the adult murine cortex. J. Neurosci. *27*, 12255–12266.

Lu, D., Mulder, H., Zhao, P., Burgess, S.C., Jensen, M. V, Kamzolova, S., Newgard, C.B., and Sherry, a D. (2002). 13C NMR isotopomer analysis reveals a connection between pyruvate cycling and glucose-stimulated insulin secretion (GSIS). Proc. Natl. Acad. Sci. U. S. A. *99*, 2708–2713.

Madiraju, P., Pande, S. V, Prentki, M., and Madiraju, S.R.M. (2009). Mitochondrial acetylcarnitine provides acetyl groups for nuclear histone acetylation. Epigenetics *4*, 399–403.

Magistretti, P.J., Sorg, O., and Martin, J.-L. (1993). Regulation of glycogen metabolism in astrocytes: physiological, pharmacological and pathological aspects. In Astrocytes: Pharmacology and Function, S. Murphy, ed. (Academic Press PP - San Diego), pp. 243–265.

Maier, K., Hofmann, U., Reuss, M., and Mauch, K. (2008). Identification of metabolic fluxes in hepatic cells from transient 13C-labeling experiments: Part II. Flux estimation. Biotechnol. Bioeng. *100*, 355–370.

Maier, K., Hofmann, U., Bauer, A., Niebel, A., Vacun, G., Reuss, M., and Mauch, K. (2009). Quantification of statin effects on hepatic cholesterol synthesis by transient (13)C-flux analysis. Metab. Eng. *11*, 292–309.

Marks, H., Kalkan, T., Menafra, R., Denissov, S., Jones, K., Hofemeister, H., Nichols, J., Kranz, A., Francis Stewart, A., Smith, A., et al. (2012). The transcriptional and epigenomic foundations of ground state

pluripotency. Cell *149*, 590–604.

Martinez, S.R., Gay, M.S., and Zhang, L. (2015). Epigenetic mechanisms in heart development and disease. Drug Discov. Today *20*, 799–811.

Martinez, V., Gerdtzen, Z.P., Andrews, B. a, and Asenjo, J. a (2010). Viral vectors for the treatment of alcoholism: use of metabolic flux analysis for cell cultivation and vector production. Metab. Eng. *12*, 129–137.

Maurer, M.H., and Kuschinsky, W. (2006). Screening the brain: molecular fingerprints of neural stem cells. Curr. Stem Cell Res. Ther. *1*, 65–77.

McKenna, M.C. (2007). The Glutamate-Glutamine Cycle Is Not Stoichiometric: Fates of Glutamate in Brain. J. Neurosci. Res. *85*, 2352–2359.

McNamara, L.E., Sjöström, T., Meek, R.M.D., Oreffo, R.O.C., Su, B., Dalby, M.J., and Burgess, K.E.V. (2012). Metabolomics: A valuable tool for stem cell monitoring in regenerative medicine. J. R. Soc. Interface *9*, 1713–1724.

Metallo, C.M., Walther, J.L., and Stephanopoulos, G. (2009). Evaluation of 13C isotopic tracers for metabolic flux analysis in mammalian cells. J. Biotechnol. *144*, 167–174.

Metallo, C.M., Gameiro, P.A., Bell, E.L., Mattaini, K.R., Yang, J., Hiller, K., Jewell, C.M., Johnson, Z.R., Irvine, D.J., Guarente, L., et al. (2012). Reductive glutamine metabolism by IDH1 mediates lipogenesis under hypoxia. Nature *481*, 380–384.

Millard, P., Letisse, F., Sokol, S., and Portais, J.-C. (2012). IsoCor: correcting MS data in isotope labeling experiments. Bioinformatics *28*, 1294–1296.

Millard, P., Sokol, S., Letisse, F., and Portais, J.-C. (2013). IsoDesign: A software for optimizing the design of (13) C-metabolic flux analysis experiments. Biotechnol. Bioeng. *111*, 1–19.

Mor, I., Cheung, E.C., and Vousden, K.H. (2011). Control of Glycolysis through Regulation of PFK1: Old Friends and Recent Additions. Cold Spring Harb. Symp. Quant. Biol. *76*, 211–216.

Moussaieff, A., Rouleau, M., Kitsberg, D., Cohen, M., Levy, G., Barasch, D., Nemirovski, A., Shen-Orr, S., Laevsky, I., Amit, M., et al. (2015). Glycolysis-Mediated Changes in Acetyl-CoA and Histone Acetylation Control the Early Differentiation of Embryonic Stem Cells. Cell Metab. *21*, 392–402.

Moxley, J.F., Jewett, M.C., Antoniewicz, M.R., Villas-boas, S.G., Alper, H., Wheeler, R.T., Tong, L., Hinnebusch, A.G., Ideker, T., Nielsen, J., et al. (2009). Linking high-resolution metabolic flux phenotypes and transcriptional regulation in yeast modulated by the global regulator Gcn4p. Proc. Natl. Acad. Sci. U. S. A. *106*, 6477–6482.

Munger, J., Bennett, B.D., Parikh, A., Feng, X., Rabitz, H.A., Shenk, T., and Rabinowitz, J.D. (2008). Systems-level metabolic flux profiling identifies fatty acid synthesis as a target for antiviral therapy. Nat Biotechnol *26*, 1179–1186.

Naderi, S., Meshram, M., Wei, C., McConkey, B., Ingalls, B., Budman, H., and Scharer, J. (2011). Development of a mathematical model for evaluating the dynamics of normal and apoptotic Chinese hamster ovary cells. Biotechnol. Prog. *27*, 1197–1205.

Nault, R., Abdul-Fattah, H., Mironov, G.G., Berezovski, M. V, and Moon, T.W. (2013). Assessment of energetic costs of AhR activation by β-naphthoflavone in rainbow trout (Oncorhynchus mykiss) hepatocytes

using metabolic flux analysis. Toxicol. Appl. Pharmacol. *271*, 86–94.

Nedergaard, M., Ransom, B., and Goldman, S. a. (2003). New roles for astrocytes: Redefining the functional architecture of the brain. Trends Neurosci. *26*, 523–530.

Niittylae, T., Chaudhuri, B., Sauer, U., and Frommer, W.B. (2009). Comparison of Quantitative Metabolite Imaging Tools and Carbon-13 Techniques for Fluxomics. In Methods in Molecular Biology, D.A. Belostotsky, ed. (Clifton, NJ: Humana Press), pp. 1–15.

Niklas, J., and Heinzle, E. (2012). Metabolic Flux Analysis in Systems Biology of Mammalian Cells. Adv. Biochem. Eng. Biotechnol. *127*, 109–132.

Niklas, J., Noor, F., and Heinzle, E. (2009). Effects of drugs in subtoxic concentrations on the metabolic fluxes in human hepatoma cell line Hep G2. Toxicol. Appl. Pharmacol. *240*, 327–336.

Niklas, J., Schneider, K., and Heinzle, E. (2010). Metabolic flux analysis in eukaryotes. Curr. Opin. Biotechnol. *21*, 63–69.

Niklas, J., Priesnitz, C., Rose, T., Sandig, V., and Heinzle, E. (2013). Metabolism and metabolic burden by α1-antitrypsin production in human AGE1.HN cells Table S1. Metab. Eng. *16*, 103–114.

Nöh, K., and Wiechert, W. (2006). Experimental Design Principles for Isotopically Instationary C Labeling Experiments. Biotechnol. Bioeng. *94*, 234–251.

Nöh, K., Wahl, A., and Wiechert, W. (2006). Computational tools for isotopically instationary 13C labeling experiments under metabolic steady state conditions. Metab. Eng. *8*, 554–577.

Nolan, R.P., and Lee, K. (2011). Dynamic model of CHO cell metabolism.

Metab. Eng. *13*, 108–124.

Nyberg, G.B., Balcarcel, R.R., Follstad, B.D., Stephanopoulos, G., and Wang, D.I. (1999). Metabolism of peptide amino acids by Chinese hamster ovary cells grown in a complex medium. Biotechnol. Bioeng. *62*, 324–335.

Okumoto, S., Takanaga, H., and Frommer, W.B. (2008). Quantitative imaging for discovery and assembly of the metabo-regulome. New Phytol. *180*, 271–295.

Omasa, T., Furuichi, K., Iemura, T., Katakura, Y., Kishimoto, M., and Suga, K.-I. (2010). Enhanced antibody production following intermediate addition based on flux analysis in mammalian cell continuous culture. Bioprocess Biosyst. Eng. *33*, 117–125.

Ozturk, S.S., and Palsson, B.O. (1991). Effect of Medium Osmolarity on Hybridoma Growth, Metabolism, and Antibody Production. Biotechnol. Bioeng. *37*, 989–993.

Pellerin, L., and Magistretti, P.J. (1994). Glutamate uptake into astrocytes stimulates aerobic glycolysis: a mechanism coupling neuronal activity to glucose utilization. Proc. Natl. Acad. Sci. U. S. A. *91*, 10625–10629.

Peng, M., In, N., Chhangawala, S., Xu, K., Leslie, C.S., and Li, M.O. (2016). Aerobic glycolysis promotes T helper 1 cell differentiation through an epigenetic mechanism. Science (80-.). *354*, 481–484.

Pigeau, G.M., Csaszar, E., and Dulgar-Tulloch, A. (2018). Commercial Scale Manufacturing of Allogeneic Cell Therapy. Front. Med. *5*, 1–8.

Possemato, R., Marks, K.M., Shaul, Y.D., Pacold, M.E., Kim, D., Birsoy, K., Sethumadhavan, S., Woo, H.-K., Jang, H.G., Jha, A.K., et al. (2011). Functional genomics reveal that the serine synthesis pathway is essential

in breast cancer. Nature *476*, 346–350.

Prigione, A., Fauler, B., Lurz, R., Lehrach, H., and Adjaye, J. (2010). The senescence-related mitochondrial/oxidative stress pathway is repressed in human induced pluripotent stem cells. Stem Cells *28*, 721–733.

Provost, a., and Bastin, G. (2004). Dynamic metabolic modelling under the balanced growth condition. J. Process Control *14*, 717–728.

Provost, a, Bastin, G., Agathos, S.N., and Schneider, Y.-J. (2006). Metabolic design of macroscopic bioreaction models: application to Chinese hamster ovary cells. Bioprocess Biosyst. Eng. *29*, 349–366.

Quek, L.-E., Wittmann, C., Nielsen, L.K., and Krömer, J.O. (2009). OpenFLUX: efficient modelling software for 13C-based metabolic flux analysis. Microb. Cell Fact. *8*, 1–15.

Quek, L.-E., Dietmair, S., Krömer, J.O., and Nielsen, L.K. (2010). Metabolic flux analysis in mammalian cell culture. Metab. Eng. *12*, 161–171.

Robertson, C., Tran, D.D., and George, S.C. (2013). Concise Review: Maturation Phases of Human Puripotent Stem Cell-Derived Cardiomyocytes. Stem Cells *31*, 1–17.

Robinton, D.A., and Daley, G.Q. (2012). The promise of induced pluripotent stem cells in research and therapy. Nature *481*, 295–305.

Rodrigues, G.M.C., Gaj, T., Adil, M.M., Wahba, J., Rao, A.T., Lorbeer, F.K., Kulkarni, R.U., Diogo, M.M., Cabral, J.M.S., Miller, E.W., et al. (2017). Defined and Scalable Differentiation of Human Oligodendrocyte Precursors from Pluripotent Stem Cells in a 3D Culture System. Stem Cell Reports *8*, 1770–1783.

Roper, J., and Yilmaz, Ö.H. (2017). Metabolic Teamwork in the Stem Cell

Niche. Cell Metab. *25*, 993–994.

Rutten, M.J., Laraway, B., Gregory, C.R., Xie, H., Renken, C., Keese, C., and Gregory, K.W. (2015). Rapid assay of stem cell functionality and potency using electric cell-substrate impedance sensing. Stem Cell Res. Ther. *6*, 1–11.

Saini, A. (2016). Cystic Fibrosis Patients Benefit from Mini Guts. Cell Stem Cell *19*, 425–427.

Salmikangas, P., Menezes-Ferreira, M., Reischl, I., Tsiftsoglou, A., Kyselovic, J., Borg, J.J., Ruiz, S., Flory, E., Trouvin, J.H., Celis, P., et al. (2015). Manufacturing, characterization and control of cell-based medicinal products: Challenging paradigms toward commercial use. Regen. Med. *10*, 65–78.

Sanfeliu, A., Paredes, C., Cair, J.J., and Gbdia, F. (1997). Identification of key patterns in the metabolism of hybridoma cells in culture. Enzyme Microb. Technol. *21*, 421–428.

Sauer, U. (2006). Metabolic networks in motion: 13C-based flux analysis. Mol. Syst. Biol. *2*, 1–10.

Sauer, U., and Zamboni, N. (2008). From biomarkers to integrated network responses. Nat. Biotechnol. *26*, 1090–1092.

Scannell, J.W., Blanckley, A., Boldon, H., and Warrington, B. (2012). Diagnosing the decline in pharmaceutical R&D efficiency. Nat. Rev. Drug Discov. *11*, 191–200.

Schmidt, K., Carlsen, M., Nielsen, J., and Villadsen, J. (1997). Modeling isotopomer distributions in biochemical networks using isotopomer mapping matrices. Biotechnol. Bioeng. *55*, 831–840.

Sengupta, N., Rose, S.T., and Morgan, J. a (2011). Metabolic flux

analysis of CHO cell metabolism in the late non-growth phase. Biotechnol. Bioeng. *108*, 82–92.

Serra, M., Brito, C., Correia, C., and Alves, P.M. (2012). Process engineering of human pluripotent stem cells for clinical application. Trends Biotechnol. *30*, 350–359.

Serres, S., Bezancon, E., Franconi, J.M., and Merle, M. (2005). Ex vivo NMR study of lactate metabolism in rat brain under various depressed states. J. Neurosci. Res. *79*, 19–25.

Shin, J., Berg, D.A., Christian, K.M., Shin, J., Berg, D.A., Zhu, Y., Shin, J.Y., Song, J., and Bonaguidi, M.A. (2015). Single-Cell RNA-Seq with Waterfall Reveals Molecular Cascades underlying Adult Neurogenesis. Stem Cell *17*, 360–372.

Shiraki, N., Shiraki, Y., Tsuyama, T., Obata, F., Miura, M., Nagae, G., Aburatani, H., Kume, K., Endo, F., and Kume, S. (2014). Methionine Metabolism Regulates Maintenance and Differentiation of Human Pluripotent Stem Cells. Cell Metab. *19*, 780–794.

Shyh-Chang, N., Daley, G.Q., and Cantley, L.C. (2013). Stem cell metabolism in tissue development and aging. Development *140*, 2535–2547.

Simão, D., Terrasso, A., Teixeira, A., Brito, C., Sonnewald, U., and Alves, P.M. (2016). Functional metabolic interactions of human neuron-astrocyte 3D in vitro networks. Sci. Rep. *6*, 1–12.

Skelton, R.J.P., Kamp, T.J., Elliott, D.A., and Ardehali, R. (2017). Biomarkers of Human Pluripotent Stem Cell-Derived Cardiac Lineages. Trends Mol. Med. *23*, 651–668.

Sperber, H., Mathieu, J., Wang, Y., Ferreccio, A., Hesson, J., Xu, Z.,

Fischer, K.A., Devi, A., Detraux, D., Gu, H., et al. (2015). The metabolome regulates the epigenetic landscape during naive-to-primed human embryonic stem cell transition. Nat. Cell Biol. *17*, 1523–1535.

Spiering, S., Davidovics, H., Bushway, P.J., Mercola, M., and Willems, E. (2015). High Content Screening for Modulators of Cardiac Differentiation in Human Pluripotent Stem Cells. Methods Mol. Biol. *1263*, 43–61.

Srivastava, S., and Chan, C. (2008). Application of Metabolic Flux Analysis to Identify the Mechanisms of Free Fatty Acid Toxicity to Human Hepatoma Cell Line. Biotechnol. Bioeng. *99*, 399–410.

Sultana, N., Zhang, L., Yan, J., Chen, J., Cai, W., Razzaque, S., Jeong, D., Sheng, W., Bu, L., Xu, M., et al. (2015). Resident c-kit + cells in the heart are not cardiac stem cells. Nat. Commun. *6*, 1–10.

Lo Surdo, J.L., Millis, B., and Bauer, S.R. (2013). Automated Microscopy as a Quantitative Method to Measure Differences in Adipogenic Differentiation in Preparations of Human Mesenchymal Stem Cells. Cytotherapy *15*, 152–150.

Sutendra, G., Kinnaird, A., Dromparis, P., Paulin, R., Stenson, T.H., Haromy, A., Hashimoto, K., Zhang, N., Flaim, E., and Michelakis, E.D. (2014). A Nuclear Pyruvate Dehydrogenase Complex Is Important for the Generation of Acetyl-CoA and Histone Acetylation. Cell *158*, 84–97.

Szyperski, T. (1995). Biosynthetically directed fractional 13C-labeling of proteinogenic amino acids. An efficient analytical tool to investigate intermediary metabolism. Eur. J. Biochem. *232*, 433–448.

Takanaga, H., Chaudhuri, B., and Frommer, W.B. (2008). GLUT1 and GLUT9 as major contributors to glucose influx in HepG2 cells identified by a high sensitivity intramolecular FRET glucose sensor. Biochim. Biophys. Acta *1778*, 1091–1099.

Takashima, Y., Guo, G., Loos, R., Nichols, J., Ficz, G., Krueger, F., Oxley, D., Santos, F., Clarke, J., Mansfield, W., et al. (2014). Resetting Transcription Factor Control Circuitry toward Ground-State Pluripotency in Human. Cell *158*, 1254–1269.

Tang, Y., Yu, P., and Cheng, L. (2017). Current progress in the derivation & therapeutic application of neural stem cells. Cell Death Dis. *8*, 1–12.

Tatapudy, S., Aloisio, F., Barber, D., and Nystul, T. (2017). Cell fate decisions: emerging roles for metabolic signals and cell morphology. EMBO Rep. *18*, 2105–2118.

Tavassoly, I., Goldfarb, J., and Iyengar, R. (2018). Systems biology primer: the basic methods and approaches. Essays Biochem. *62*, 487–500.

Taymaz-Nikerel, H., van Gulik, W.M., and Heijnen, J.J. (2011). Escherichia coli responds with a rapid and large change in growth rate upon a shift from glucose-limited to glucose-excess conditions. Metab. Eng. *13*, 307–318.

Taymaz-Nikerel, H., Mey, M. De, Baart, G., Maertens, J., Heijnen, J.J., and van Gulik, W. (2013). Changes in substrate availability in Escherichia coli lead to rapid metabolite, flux and growth rate responses. Metab. Eng. *16*, 115–129.

Teixeira, A.P., Alves, C., Alves, P.M., Carrondo, M.J.T., and Oliveira, R. (2007). Hybrid elementary flux analysis/nonparametric modeling: application for bioprocess control. BMC Bioinformatics *8*, 1–15.

Teixeira, A.P., Santos, S.S., Carinhas, N., Oliveira, R., and Alves, P.M. (2008). Combining metabolic flux analysis tools and 13C NMR to estimate intracellular fluxes of cultured astrocytes. Neurochem. Int. *52*, 478–486.

Tekkök, S.B., Brown, A.M., Westenbroek, R., Pellerin, L., and Ransom, B.R. (2005). Transfer of glycogen-derived lactate from astrocytes to axons via specific monocarboxylate transporters supports mouse optic nerve activity. J. Neurosci. Res. *81*, 644–652.

Tesar, P.J., Chenoweth, J.G., Brook, F.A., Davies, T.J., Evans, E.P., Mack, D.L., Gardner, R.L., and McKay, R.D.G. (2007). New cell lines from mouse epiblast share defining features with human embryonic stem cells. Nature *448*, 196–199.

TeSlaa, T., Chaikovsky, A.C., Lipchina, I., Escobar, S.L., Hochedlinger, K., Huang, J., Graeber, T.G., Braas, D., Teitell, M.A., Birsoy, K., et al. (2016). α-Ketoglutarate Accelerates the Initial Differentiation of Primed Human Pluripotent Stem Cells. Cell Metab. *24*, 485–493.

Tohyama, S., Hattori, F., Sano, M., Hishiki, T., Nagahata, Y., Matsuura, T., Hashimoto, H., Suzuki, T., Yamashita, H., Satoh, Y., et al. (2013). Distinct metabolic flow enables large-scale purification of mouse and human pluripotent stem cell-derived cardiomyocytes. Cell Stem Cell *12*, 127–137.

Tohyama, S., Fujita, J., Hishiki, T., Matsuura, T., Hattori, F., Ohno, R., Kanazawa, H., Seki, T., Nakajima, K., Kishino, Y., et al. (2016). Glutamine Oxidation Is Indispensable for Survival of Human Pluripotent Stem Cells. Cell Metab. *23*, 663–674.

Tomlinson, M.J., Tomlinson, S., Yang, X.B., and Kirkham, J. (2013). Cell separation: Terminology and practical considerations. J. Tissue Eng. *4*, 1–14.

Tristan, C., Shahani, N., Sedlak, T.W., and Sawa, A. (2011). The diverse functions of GAPDH : Views from different subcellular compartments. Cell. Signal. *23*, 317–323.

Volterra, A., and Meldolesi, J. (2005). Astrocytes, from brain glue to communication elements: the revolution continues. Nat. Rev. Neurosci. *6*, 620–640.

Wahl, A., Sidorenko, Y., Dauner, M., Genzel, Y., and Reichl, U. (2008). Metabolic flux model for an anchorage-dependent MDCK cell line: characteristic growth phases and minimum substrate consumption flux distribution. Biotechnol. Bioeng. *101*, 135–152.

Walker, A.L., Imam, S.Z., and Roberts, R.A. (2018). Drug discovery and development: Biomarkers of neurotoxicity and neurodegeneration. Exp. Biol. Med. *243*, 1037–1045.

Walther, J.L., Metallo, C.M., Zhang, J., and Stephanopoulos, G. (2012). Optimization of 13C isotopic tracers for metabolic flux analysis in mammalian cells. Metab. Eng. *14*, 162–171.

Wang, X., Dong, C., Sun, L., Zhu, L., Sun, C., and Ma, R. (2016). Quantitative proteomic analysis of age-related subventricular zone proteins associated with neurodegenerative disease. Sci. Rep. *6*, 1–11.

Wang, Y., Wysocka, J., Sayegh, J., Lee, Y., Perlin, J.R., Leonelli, L., Sonbuchner, L.S., Mcdonald, C.H., Cook, R.G., Stallcup, M.R., et al. (2004). Human PAD4 Regulates Histone Arginine Methylation Levels via Demethylimination. Science (80-.). *306*, 279–284.

Weinberger, L., Ayyash, M., Novershtern, N., and Hanna, J.H. (2016). Dynamic stem cell states: naive to primed pluripotency in rodents and humans. Nat. Rev. Mol. Cell Biol. *17*, 155–169.

Westergaard, N., Sonnewald, U., Unsgård, G., Peng, L., Hertz, L., and Schousboe, a (1994). Uptake, release, and metabolism of citrate in neurons and astrocytes in primary cultures. J. Neurochem. *62*, 1727–1733.

Wiechert, W. (2001). 13C metabolic flux analysis. Metab. Eng. *3*, 195–206.

Wiechert, W., Möllney, M., Isermann, N., Wurzel, M., and de Graaf, a a (1999). Bidirectional reaction steps in metabolic networks: III. Explicit solution and analysis of isotopomer labeling systems. Biotechnol. Bioeng. *66*, 69–85.

Wiechert, W., Möllney, M., Petersen, S., and de Graaf, a a (2001). A universal framework for 13C metabolic flux analysis. Metab. Eng. *3*, 265–283.

Wiechert, W., Schweissgut, O., Takanaga, H., and Frommer, W.B. (2007). Fluxomics: mass spectrometry versus quantitative imaging. Curr. Opin. Plant Biol. *10*, 323–330.

Wittmann, C. (2007). Fluxome analysis using GC-MS. Microb. Cell Fact. *6*, 1–17.

Xing, Z., Kenty, B., Koyrakh, I., Borys, M., Pan, S.-H., and Li, Z.J. (2011). Optimizing amino acid composition of CHO cell culture media for a fusion protein production. Process Biochem. *46*, 1423–1429.

Yang, W., Xia, Y., Hawke, D., Li, X., Liang, J., Xing, D., Aldape, K., Hunter, T., Yung, W.K.A., and Lu, Z. (2012). PKM2 Phosphorylates Histone H3 and Promotes Gene Transcription and Tumorigenesis. Cell *150*, 685–696.

Yogev, O., Yogev, O., Singer, E., Shaulian, E., Goldberg, M., and Fox, T.D. (2010). Fumarase: A Mitochondrial Metabolic Enzyme and a Cytosolic / Nuclear Component of the DNA Damage Response. PLoS Biol. *8*, 1–13.

Yoo, H., Antoniewicz, M.R., Stephanopoulos, G., and Kelleher, J.K.

(2008). Quantifying reductive carboxylation flux of glutamine to lipid in a brown adipocyte cell line. J. Biol. Chem. *283*, 20621–20627.

Young, J.D. (2014). INCA: A computational platform for isotopically nonstationary metabolic flux analysis. Bioinformatics *30*, 11–13.

Zamboni, N. (2011). 13C metabolic flux analysis in complex systems. Curr. Opin. Biotechnol. *22*, 103–108.

Zamboni, N., Fendt, S.-M., Rühl, M., and Sauer, U. (2009). (13)C-based metabolic flux analysis. Nat. Protoc. *4*, 878–892.

Zamorano, F., Wouwer, a Vande, and Bastin, G. (2010). A detailed metabolic flux analysis of an underdetermined network of CHO cells. J. Biotechnol. *150*, 497–508.

Zhang, J., Khvorostov, I., Hong, J.S., Oktay, Y., Vergnes, L., Nuebel, E., Wahjudi, P.N., Setoguchi, K., Wang, G., Do, A., et al. (2011). UCP2 regulates energy metabolism and differentiation potential of human pluripotent stem cells. EMBO J. *30*, 4860–4873.

Zhang, J., Ratanasirintrawoot, S., Chandrasekaran, S., Wu, Z., Ficarro, S.B., Yu, C., Ross, C.A., Cacchiarelli, D., Xia, Q., Selugson, M., et al. (2016). LIN28 Regulates Stem Cell Metabolism and Conversion to Primed Pluripotency. Cell Stem Cell *19*, 66–80.

Zhao, S., Xu, W., Jiang, W., Yu, W., Lin, Y., Zhang, T., Zhou, L., Zeng, Y., Li, H., Li, Y., et al. (2011). Regulation of Cellular Metabolism by Protein Lysine Acetylation. Science (80-.). *327*, 1000–1004.

Zheng, X., Boyer, L., Jin, M., Mertens, J., Kim, Y., Ma, L., Ma, L., Hamm, M., Gage, F.H., and Hunter, T. (2016). Metabolic reprogramming during neuronal differentiation from aerobic glycolysis to neuronal oxidative phosphorylation. Elife *5*, 1–25.

Zupke, C., and Stephanopoulos, G. (1994). Modeling of Isotope Distributions and Intracellular Fluxes in Metabolic Networks Using Atom Mapping Matrices. Biotechnol. Prog. *10*, 489–498.

2

Metabolic rearrangements during neural stem cell differentiation into astrocytes

This chapter was adapted from:

Sá,JV; Kleiderman, S; Brito, C; Sonnewald, U; Leist, M; Teixeira, AP; Alves, PM. (2017) Quantification of metabolic rearrangements during neural stem cells differentiation into astrocytes by metabolic flux analysis. Neurochemical Research 42(1): 244-253.

Author contributions to this chapter:

João Sá participated in the experimental setup and design, participated in the analytical measurements, performed the computational analyses and wrote this chapter.

Table of Contents

Abstract

Proliferation and differentiation of neural stem cells (NSCs) have a crucial role to ensure neurogenesis and gliogenesis in the mammalian brain throughout life. As there is growing evidence for the significance of metabolism in regulating cell fate, knowledge on the metabolic programs in NSCs and how they evolve during differentiation into somatic cells may provide novel therapeutic approaches to address brain diseases. In this work, we applied a quantitative analysis to assess how the central carbon metabolism evolves upon differentiation of NSCs into astrocytes. Murine embryonic stem cell (mESC)-derived NSCs and astrocytes were incubated with labelled [1-^{13}C]glucose and the label incorporation into intracellular metabolites was followed by GC-MS. The obtained ^{13}C labelling patterns, together with uptake/secretion rates determined from supernatant analysis, were integrated into an isotopic non-stationary metabolic flux analysis (^{13}C-MFA) model to estimate intracellular flux maps. Significant metabolic differences between NSCs and astrocytes were identified, with a general downregulation of central carbon metabolism during astrocytic differentiation. While glucose uptake was 1.7-fold higher in NSCs (on a per cell basis), a high lactate-secreting phenotype was common to both cell types. Furthermore, NSCs consumed glutamine from the medium; the highly active reductive carboxylation of alpha-ketoglutarate indicates that this was converted to citrate and used for biosynthetic purposes. In astrocytes, pyruvate entered the TCA cycle mostly through pyruvate carboxylase (81%). This pathway supported glutamine and citrate secretion, recapitulating well described metabolic features of these cells *in vivo*. Overall, this fluxomics study allowed us to quantify the metabolic rewiring accompanying astrocytic lineage specification from NSCs.

1. Introduction

Neural stem cells (NSCs) are multipotent cells present in the developing brain that persist in restricted regions of postnatal and adult brains, where they continue to produce the three neural lineages: neurons, astrocytes and oligodendrocytes (Kriegstein and Alvarez-Buylla, 2009). Astrocytes are the most abundant brain cells (Nedergaard et al, 2003), being involved in virtually every function of the central nervous system, including energy metabolism (Rouach et al., 2008), ionic homeostasis (Simard and Nedergaard, 2004) and synaptic transmission (Ullian et al., 2001; Johnson et al., 2007). Importantly, glutamatergic and GABAergic neurotransmission processes are dependent on astrocytic metabolism for neurotransmitter replenishment (Bak et al., 2006). Furthermore, astrocytes store brain energy currency in the form of glycogen (Brown, 2004), and release substrates for neuronal oxidative phosphorylation (Pellerin et al., 2007). Moreover, astrocytes have been suggested as contributors to neurodegenerative disorders by various mechanisms, including via metabolic dysfunction (Phatnani and Maniatis, 2015), making them potential targets for novel strategies to treat brain disorders. Given their importance for brain function, the generation of astrocytes from NSCs has attracted much attention recently. It is known that NSCs and astrocytes share several phenotypic and functional features (Doetsch et al, 1999; Seri et al, 2001), but their metabolic programs have not been compared at a global metabolic flux level yet.

In vivo intracellular metabolic fluxes have been estimated using several mathematical frameworks. When metabolic steady-state can be assumed (i.e all fluxes and intracellular concentrations are approximately constant over time), ^{13}C-Metabolic flux analysis (^{13}C-MFA) is the most useful tool to provide a metabolic snapshot of cells (Sauer, 2006; Wiechert, 2001; Sá et al., 2015). Nuclear magnetic resonance (NMR) spectroscopy and/or mass

spectrometry (MS) techniques are used to measure the incorporation of a ^{13}C label from medium nutrients into intracellular metabolites. A computational framework based on both metabolite and isotopomer balances is then used to integrate this data with experimentally determined uptake and secretion rates to estimate intracellular metabolic fluxes. This approach has been applied to study metabolic network operation and diagnosing of phenotypic perturbations in several biological systems (Munger et al., 2008; Metallo et al., 2012; Ahn and Antoniewicz, 2013; Carinhas et al., 2016), including primary astrocytic cultures (Amaral et al., 2011).

In this work, we present the first quantitative study of the metabolic programs during specification of astrocytes from NSCs. To obtain highly homogeneous non-proliferating astrocyte cultures, we have recently developed a protocol using pure and defined populations of mouse pluripotent stem cell-derived NSCs (Kleiderman et al., 2016). Exposure to BMP4 promoted astrocytic differentiation of these NSCs within 2 days. The resulting astrocytes expressed several positive astrocyte markers (GFAP, aquaporin-4, and GLT-1), showed negligible expression of the NSC marker nestin, and acquired innate immune functions (Kleiderman et al., 2016). Herein, NSCs and NSC-derived astrocytes were incubated with [1-^{13}C]glucose, and the transient ^{13}C labelling profiles of intracellular metabolites were modelled by isotopically non-stationary ^{13}C-MFA (Noh and Wiechert, 2006), identifying significantly different metabolic flux maps in each population.

2. Materials and Methods

2.1. Differentiation of NSCs and Astrocytes from murine embryonic stem cells

The murine embryonic stem cell (mESC) line CGR8 (07032901, Sigma) was used in this work for commitment to the neural lineage, as described in Kleiderman et al., (2016). Briefly, for differentiation into neural stem cells (NSCs), cultures of mESCs were harvested with 0.05% trypsin, pelleted, and replated in N2B27-medium (1:1 Neurobasal-A and Advanced DMEM/F12, containing N2 & B27 supplements, 100 µM β-mercaptoethanol, 7.5 µg/mL insulin, and 50 µg/mL bovine serum albumin). On day 7, the growth factors FGF2 (20 ng/mL) and EGF (20 ng/mL) were added. After about 8 to 12 passages of NSCs, homogeneous and aggregate-free cultures were obtained and used for differentiation into astrocytes using N2B27-medium supplemented with BMP4 (20 ng/mL). Cells were incubated at 37 °C with 5% CO_2.

2.2. Stable isotope cultures

For isotopic labelling, NSCs and astrocytes were cultured in 6-well plates with custom N2B27-medium without glucose and without glutamine, supplemented with 10 mM [1-^{13}C]glucose (Sigma-Aldrich, 297046) and 2 mM glutamine for NSCs, or without glutamine supplementation for astrocytes.

Sampling was performed immediately after label administration and then at 3 h, 12 h, and 24 h (Figure 2.1A). Replicate samples of culture supernatants were collected, clarified (200*xg* for 10 min) and stored at -20 °C for later extracellular metabolite analysis (see below). Upon removing the culture supernatants, cell monolayers were washed twice with ice-cold PBS to eliminate tracer amounts of extracellular metabolites, and the plates were placed on liquid nitrogen to rapidly stop metabolism. For intracellular metabolite extraction, 700 µl of ethanol 70% (v/v) were added

to each well and the cells were detached using a cell scraper, followed by clarification (15 min at 20,000*xg*) and storage of the supernatants at -80 °C until GC-MS analysis (see below). The pellets containing cellular material were stored at -20 °C for protein quantification (see below). Additional wells seeded with NSCs and astrocytes were used to profile cell concentration and viability along the same sampling schedule.

2.3. Analysis of extracellular metabolites

Glucose and lactate concentrations in culture supernatants were measured with an automated YSI 7100 Multiparameter Bioanalytical System (Dayton, OH, USA). Amino acid concentrations were analyzed by HPLC using the Waters AccQ.Tag Amino Acid Analysis Method (Waters, Milford, MA) as described elsewhere (Carinhas et al., 2010). The extracellular concentrations of citrate and pyruvate were determined by ^{1}H-NMR spectroscopy using a 500 MHz Avance spectrometer (Bruker, Billerica, MA) with a 5 mm QXI inversed probe. Spectra were recorded at 25 ºC using a NOESY-based pulse sequence with water pre-saturation, performing 256 scans with 4 s acquisition time, 2 s relaxation delay and 100 ms mixing time. DSS-d6 (Sigma Aldrich, St. Louis, MO; USA) was used as internal standard for metabolite quantification in all samples. In order to obtain a similar pH between samples, they were mixed with phosphate buffer (pH 7.4) prepared in D_2O at a 2:1 ratio. Before spectra acquisition, the spectrometer was calibrated by determining the 90º pulse and the water chemical shift centre of each sample. Each spectrum was phased, baseline corrected and integrated using the Chenomx NMR Suite 8.0 (Chenomx Inc., Edmonton, Alberta, Canada) software.

2.4. Cell concentration, viability and protein content measurements

Total cell concentration was determined after trypsinization using the haemocytometer counting method. Cell viability was measured by

quantification of resazurin reduction. Resazurin was added to the medium at 1 µg/ml for 30 min at 37 °C. Resazurin reduction (560 nm excitation, 590 nm emission) was measured as cell viability parameter using the Infinite® 200 PRO multimode reader (Tecan). The protein content was measured in cell pellets after metabolite extraction. The cell pellets were lysed in 2% sodium dodecyl sulfate (SDS) (in 125 mM Trizma, 10% glycerol) and the protein quantified with the Pierce™ BCA Protein Assay Kit (Thermo Scientific), according to the manufacturer's protocol.

2.5. Quantification of intracellular mass isotopomer distributions by GC-MS

For analysis of ^{13}C enrichment in lactate, amino acids (alanine, aspartate, glutamate, and glutamine), and TCA cycle intermediates (citrate, fumarate, succinate and malate), lyophilized metabolite extracts were dissolved in 0.01 M HCl followed by pH adjustment to pH < 2 with 6 M HCl. The samples were then dried under atmospheric air (50 °C), and the metabolites extracted in multiple steps into an organic phase of ethanol and benzene. Afterwards, the samples were lyophilized again and derivatized with N-Methyl-N-(t-Butyldimethylsilyl)trifluoroacetamide (MTBSTFA) + 1% t-butyldimethylchlorosilane (TBDMSCI). The glycolytic intermediates phosphoenolpyruvate (PEP) and 3-phosphoglycerate (3PG) were analyzed using a similar protocol to that described in (Hofmann et al., 2008). Briefly, lyophilized metabolite extracts were dissolved in methanol and dried under atmospheric air (50 °C). The metabolites were then extracted with toluene and dried again under atmospheric air (50 °C). Derivatization was performed using a mixture of N-Methyl-N-(trimethylsilyl)trifluoroacetamide (MSTFA) + 1% trimethylchlorosilane and acetonitrile.

The mass isotopomer distributions of the derivatized metabolites were analyzed on an Agilent 6890 gas chromatographer equipped with a

capillary column (WCOT fused silica 25 mm × 0.25 mm ID, 0.25 µm film thickness, VF-1ms, Varian), and connected to an Agilent 5975B mass spectrometer with electron impact ionization (Agilent Technologies, Palo Alto, CA, USA). All ions (M, M1, Mm, where M is the mass/charge ratio of the unlabelled derivatized fragment and m is the number of labelled carbons) were measured by spectra integration using the MassHunter software (Agilent Technologies, Palo Alto, CA, USA) and corrected for natural ^{13}C abundance using non-enriched standards (Walls et al., 2014).

2.6. Metabolic flux determination

Estimation of metabolic fluxes of NSCs and astrocytes was performed by isotopic non-stationary ^{13}C-MFA. Our experimental data was comprised of extracellular metabolite rates and corrected mass isotopomer distributions of intracellular metabolites. The extracellular rates were calculated by linear fitting of extracellular metabolite profiles (assuming metabolic steady state throughout the labeling experiment) and normalized to protein content per well. The reaction network used for flux estimation included the main pathways of central carbon metabolism: glycolysis, pentose phosphate pathway, tricarboxylic acid cycle and amino acids metabolism. Table 2.1 lists all metabolic reactions and carbon atom transitions (balanced and unbalanced metabolite pools are also identified). Since cell concentration and protein content were maintained during the labelling experiment, reactions for biomass formation were omitted in the network. Extracellular transport reactions were considered reversible to allow equilibration with extracellular pools, except for essential amino acids and glucose.

Non-stationary ^{13}C-MFA was performed using the publicly available software package INCA (Young, 2014), which implements the elementary metabolite units framework (Young et al., 2008). Briefly, fluxes are estimated by minimizing the variance-weighted sum of squared residuals

(SSR) between experimental measurements and model predictions using least-squares regression. At least 10 restarts with random initial values were performed to find a global optimum (Crown and Antoniewicz, 2013). At convergence, the obtained solution was subject to a qui-square statistical test to evaluate goodness-of-fit. 95% confidence intervals of estimated fluxes were calculated through the parameter continuation method described by Antoniewicz et al. (2006). The number of degrees of freedom (n-p) associated with each flux estimation solution is 86 and 73 for NSCs and astrocytes, respectively (see supplementary material, Supplementary Table 2.3). This means that in each case the number of independent measurements n (MIDs and extracellular fluxes) is superior to the number of free parameters p that were estimated (pools and unconstrained fluxes). A redundancy analysis is automatically performed during flux estimation by INCA, as described in Antoniewicz et al. (2006). Data overfitting was avoided by minimizing the number of metabolic reactions up to that necessary to accurately represent cellular carbon flow and satisfactorily simulate the data (i.e. intracellular compartmentation was considered only for pyruvate and no dilution fluxes or other pseudo-fluxes were used).

Table 2.1 - Metabolic network model used for isotopic non-stationary ^{13}C-MFA for NSCs and astrocytes, along with the carbon atom transitions.

	Glycolysis
R1	G6P (abcdef) ↔ F6P (abcdef)
R2	F6P (abcdef) → FBP (abcdef)
R3	FBP (abcdef) ↔ DHAP (cba) + GAP (def)
R4	DHAP (abc) ↔ GAP (abc)
R5	GAP (abc) ↔ 3PG (abc)
R6	3PG (abc) ↔ PEP (abc)

R7	PEP (abc) → Pyr.c (abc)
	Pentose-phosphate pathway
R8	G6P (abcdef) → P5P (bcdef) + CO_2 (a)
R9	P5P (abcde) + P5P (pqrst) ↔ GAP (rst) + S7P (pqabcde)
R10	S7P (abcdefg) + GAP (xyz) ↔ E4P (defg) + F6P (abcxyz)
R11	E4P (abcd) + P5P (pqrst) ↔ GAP (rst) + F6P (pqabcd)
	Lactate and alanine accumulation
R12	Pyr.c (abc) ↔ Lac (abc)
R13	Pyr.c (abc) ↔ Ala (abc)
	TCA cycle and pyruvate cycling
R14	Pyr.m (abc) → AcCoA.m (bc) + CO_2 (a)
R15	Pyr.m (abc) + CO_2 (d) → OAC (abcd)
R16	OAC (abcd) + AcCoA.m (ef) → Cit (dcbfea)
R17	Cit (abcdef) ↔ AKG (abcde) + CO_2 (f)
R18	AKG (abcde) → SucCoA (bcde) + CO_2 (a)
R19	SucCoA (abcd) ↔ Suc (abcd)
R20	Suc (abcd) ↔ Fum (abcd)
R21	Fum (abcd) ↔ Mal (abcd)
R22	OAC (abcd) ↔ Mal (abcd)
R23	Mal (abcd) → Pyr.m (abc) + CO_2 (d)
	Lipid precursor generation
R24	Cit (dcbfea) → OAC (abcd) + AcCoA.c (ef)
	Amino acids metabolism
R25	Gln (abcde) ↔ Glu (abcde)
R26	Glu (abcde) ↔ AKG (abcde)
R27	Asn (abcd) ↔ Asp (abcd)
R28	Asp (abcd) ↔ OAC (abcd)
R29	Ser (abc) → Pyr.c (abc)
R30	Ser (abc) ↔ Gly (ab) + C1 (c)
R31	Glu (abcde) ↔ Pro (abcde)
R32	Val (abcde) + CO_2 (f) → Suc (dcef) + CO_2 (a) + CO_2 (b)
R33	Ile (abcdef) + CO_2 (g) → Suc (bcdg) + AcCoA.m (ef) + CO_2 (a)
R34	Leu (abcdef) + CO_2 (g) → AcCoA.m (bc) + AcCoA.m (de) + AcCoA.m (gf) + CO_2 (a)

R35	Thr (abcd) → AcCoA.m (cd) + Gly (ab)
R36	Phe (abcdefghi) → Tyr (abcdefghi)
R37	Tyr (abcdefghi) → Fum (defg) + AcCoA.m (bc) + AcCoA.m (hi) + CO_2 (a)
R38	Met (abcde) + Ser (fgh) + CO_2 (i) → Suc (bcdi) + Cys.snk (fgh) + CO_2 (a) + C1 (e)
R39	Lys (abcdef) → CO_2 (a) + CO_2 (f) + AcCoA.m (bc) + AcCoA.m (de)
R40	His (abcdef) → Glu (edcba) + C1 (f)
R41	Arg (abcdef) → Glu (abcde) + Urea.snk (f)
R42	Glu (abcde) + CO_2 (f) → Arg (abcdef)
	Intracellular transport
R43	Pyr.c (abc) ↔ Pyr.m (abc)
	Extracellular transport
R44	CO_2 (a) ↔ CO_2.ext (a)
R45	Glc.ext (abcdef) → G6P (abcdef)
R46	Lac (abc) ↔ Lac.ext (abc)
R47	Ala (abc) ↔ Ala.ext (abc)
R48	Pyr.ext (abc) ↔ Pyr.c (abc)
R49	Cit (abcdef) → Cit.ext (abcdef)
R50	Gln (abcde) ↔ Gln.ext (abcde)
R51	Glu (abcde) ↔ Glu.ext (abcde)
R52	Asp (abcd) ↔ Asp.ext (abcd)
R53	Asn (abcd) ↔ Asn.ext (abcd)
R54	Ser.ext (abc) ↔ Ser (abc)
R55	Gly (ab) ↔ Gly.ext (ab)
R56	Pro.ext (abcde) ↔ Pro (abcde)
R57	Val.ext (abcde) → Val (abcde)
R58	Ile.ext (abcdef) → Ile (abcdef)
R59	Leu.ext (abcdef) → Leu (abcdef)
R60	Thr.ext (abcd) → Thr (abcd)
R61	Phe.ext (abcdefghi) → Phe (abcdefghi)
R62	Tyr.ext (abcdefghi) → Tyr (abcdefghi)
R63	Met.ext (abcde) → Met (abcde)
R64	Lys.ext (abcdef) → Lys (abcdef)
R65	His.ext (abcdef) → His (abcdef)
R66	Arg.ext (abcdef) ↔ Arg (abcdef)

Suffix abbreviations: mitochondrial (.m), cytosolic (.c), extracellular (.ext), sink (.snk). Sink pools were used for metabolites that could not be balanced (Cys, Urea).

Balanced metabolite pools: 3PG, AKG, AcCoA.m, Ala, Arg, Asn, Asp, CO_2, C1, Cit, Cys, DHAP, E4P, F6P, FBP, Fum, G6P, GAP, Gln, Glu, Gly, His, Ile, Lac, Leu, Lys, Mal, Met, OAC, P5P, PEP, Phe, Pro, Pyr.c, Pyr.m, S7P, Ser, Suc, SucCoA, Thr, Tyr, Val

Unbalanced metabolite pools: AcCoA.c, Ala.ext, Arg.ext, Asn.ext, Asp.ext, CO_2.ext, Cit.ext, Cys.snk, Gln.ext, Glu.ext, Glc.ext, Gly.ext, His.ext, Ile.ext, Lac.ext, Leu.ext, Lys.ext, Met.ext, Phe.ext, Pro.ext, Pyr.ext, Ser.ext, Thr.ext, Tyr.ext, Urea.snk, Val.ext.

3. Results and Discussion

To study the metabolic modulations occurring during differentiation of mESC-derived NSCs to astrocytes, adherent monolayers of either fully-differentiated astrocytes or of NSCs were incubated with [1-13C] glucose. Samples from the culture supernatant and cell extracts were collected during 24 h (Figure 2.1A). During this period, cell viability was always above 90%, and the exact protein amounts and cell number were determined for each individual dish used in the fluxomics study (data not shown). Astrocytes are larger in size when comparing to NSCs; they had on average a 1.7-fold higher protein content than their undifferentiated counterparts.

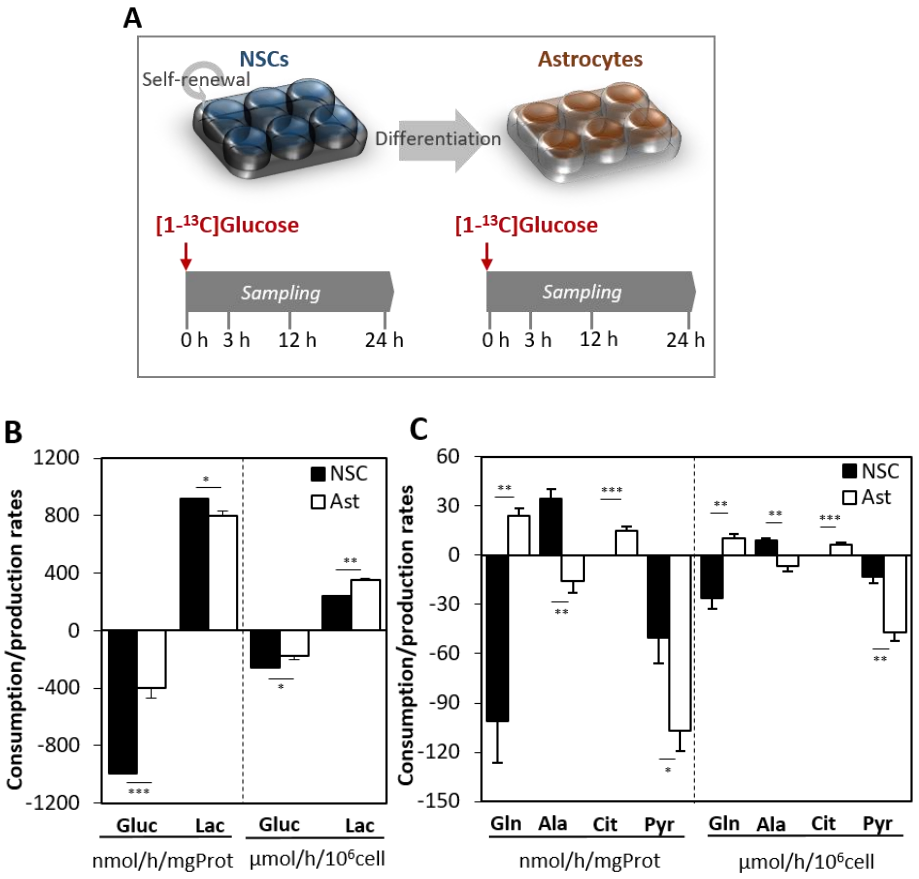

Figure 2.1 – Experimental design and consumption/secretion rates. A) Schematic representation of the experimental design, consisting in the incubation of NSCs and NSC-derived astrocytes with [1-^{13}C]glucose. Consumption/production rates of **B)** glucose and lactate, and **C)** glutamine, alanine, citrate and pyruvate for NSCs and astrocytes. Values represent average rates and error bars represent the standard deviation of biological replicates. Statistical significance was determined by performing a two-tailed Student t-test. Asterisks (*, ** and ***) denote statistically significant differences between conditions ($p \leq 0.1$, $p \leq 0.05$ and $p \leq 0.01$, respectively).

3.1. Modulation of consumption and production rates during astrocytic differentiation

Analysis of changes in supernatant composition of NSCs indicated a lactate production to glucose consumption ratio of approximately 1 (Figure 2.1B). Such high glycolytic metabolism in spite of oxygen availability is common to many stem cells (Folmes et al., 2011; Zhang et al., 2012) and has been reported in proliferating NSCs (Candelario et al., 2013). It allows more metabolic intermediates to be available for the biosynthesis of cellular building blocks, which are required for proliferation (Vander Heiden et al., 2009). Upon differentiation of NSCs into astrocytes, the glucose consumption decreased 1.5-fold on a per cell basis (2.5-fold on a per mg of protein basis; Figure 2.1B). We calculated the consumption/production rates on a per cell and on a per mg of protein basis (Figure 2.1B-C) because both data normalizations are commonly found in brain metabolic studies and/or differentiation studies. Owing to the differences in cell size between NSCs and astrocytes, data interpretation is affected by the normalization method; for instance, while lactate production slightly decreases (13%) on a per mg of protein basis, it is 1.5-fold upregulated on a per cell basis upon differentiation. Nevertheless, the downregulation of glucose consumption was not matched by a proportional decrease in lactate production upon astrocytic differentiation, resulting in an even higher lactate production to glucose consumption ratio (close to 2). This extremely high glycolytic metabolism has been previously reported in primary cultures of cortical astrocytes (e.g. Amaral et al., 2011; Bolanos et al., 1994).

Striking differences between NSCs and astrocytes were also observed in the specific transport rates of some amino and organic acids (Figure 2.1C, Supplementary Table 2.1). NSCs consumed glutamine at a high rate (10% of the glucose uptake rate) and, as opposed to astrocytes, cannot

survive in glutamine-free medium (data not shown). Yeo et al., (2013) had already demonstrated the importance of the glutaminolysis pathway for long-term maintenance of NSCs. Our comparative study showed that the NSC glutamine dependence is no longer present after its differentiation into astrocytes. NSC-derived astrocytes secreted glutamine (the rate was higher when cultured in glutamine-free medium), showing that even in the absence of neurons, these cells are able to recapitulate an important feature of the glutamate-glutamine cycle between neurons and astrocytes in the brain (Bélanger et al, 2011; McKenna et al, 2012). Noteworthy, astrocytes took up glutamate from the medium at a similar rate of glutamine secretion (Supplementary Table 2.1).

Another significant difference observed between these cell types was the upregulation of the pyruvate uptake rate upon astrocytic differentiation (3.6-fold on a per cell basis). Finally, astrocytes released citrate to the medium, while this metabolite was not detected in the medium of NSC cultures. Citrate secretion has been observed in primary cultures of astrocytes, but the reason is not entirely understood (Westergaard et al., 1994; Westergaard et al, 1995; Zwingmann and Leibfritz, 2003).

3.2. Intracellular ^{13}C-labelling in NSCs and Astrocytes

After label administration, the fraction of [1-^{13}C]glucose measured intracellularly by GC-MS was 87% in NSCs and 84% in astrocytes. In both cell populations, the label enrichment of the glycolytic intermediates 3PG and PEP reached values over 40%, showing conservation of the ^{13}C label coming from glucose (Figure 2.2). Since the first carbon of glucose is lost as CO_2 in the oxidative branch of the PPP, these results indicate that the non-oxidative PPP branch had low activity in both cell populations. Overall, the label enrichment in lactate, alanine, TCA cycle intermediates and related amino acids was lower than in glycolytic metabolites, indicating the contribution of other carbon sources (Figure 2.2).

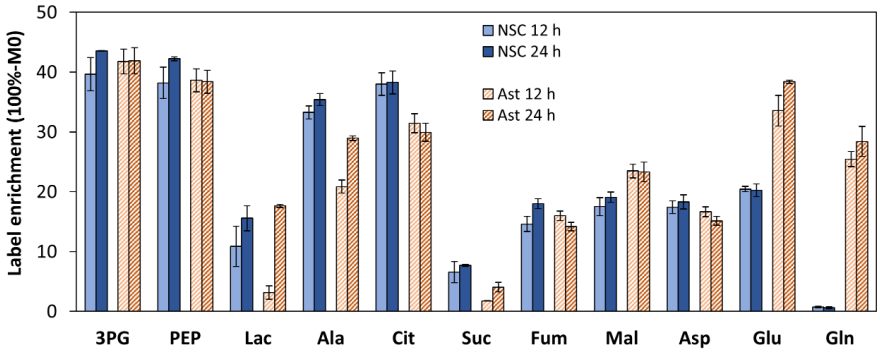

Figure 2.2 – Label enrichment of intracellular metabolites at 12 h and 24 h after [1-^{13}C]glucose addition to NSCs and astrocytes. The values correspond to the sum of all labeled isotopomers (100%-M0). Shown metabolites: 3-phosphoglyceric acid (3PG), phosphoenolpyruvate (PEP), lactate (Lac), alanine (Ala), citrate (Cit), succinate (Suc), fumarate (Fum), malate (Mal), aspartate (Asp), glutamate (Glu) and glutamine (Gln).

Despite the similarities, several differences emerged in the intracellular labelling patterns of NSCs and astrocytes. Firstly, isotopic steady-state was achieved for most metabolites in NSCs within 24 h, but not in astrocytes (Figures 2.3 and 2.4), in agreement with the downregulation of astrocytic glucose consumption. The largest difference in the rate of ^{13}C incorporation between both populations was observed for the lactate pool at 12 h post label addition. The M1 isotopomer abundance was 11% in NSCs while it was only 3% in astrocytes. The higher consumption of (unlabeled) pyruvate from the medium by astrocytes may have contributed to the slower labelling of the astrocytic lactate pool. Moreover, NSCs displayed higher labelling in the citrate (38% vs 30%) and succinate (8% vs 4%) pools compared with astrocytes, but this difference was not propagated throughout the TCA cycle. In fact, the opposite result was

observed for the malate pool, which was consistently more highly ^{13}C enriched in astrocytes at 12 h and 24 h after label addition. Moreover, succinate was less labeled than fumarate (57% less in NSCs and 71% less in astrocytic populations), which suggests additional routes of label entry into the TCA cycle, and at the same time suggests that succinate dehydrogenase (SucD) has limited reverse activity. Finally, significant enrichment in intracellular glutamine was observed in astrocytes but not in NSCs, consistent with the measured glutamine secretion and consumption rates, respectively. However, when cultured in glutamine-free media, NSCs also incorporated significant ^{13}C from glucose into glutamine despite the viability loss, indicating glutamine synthetase (GS) activity (data not shown).

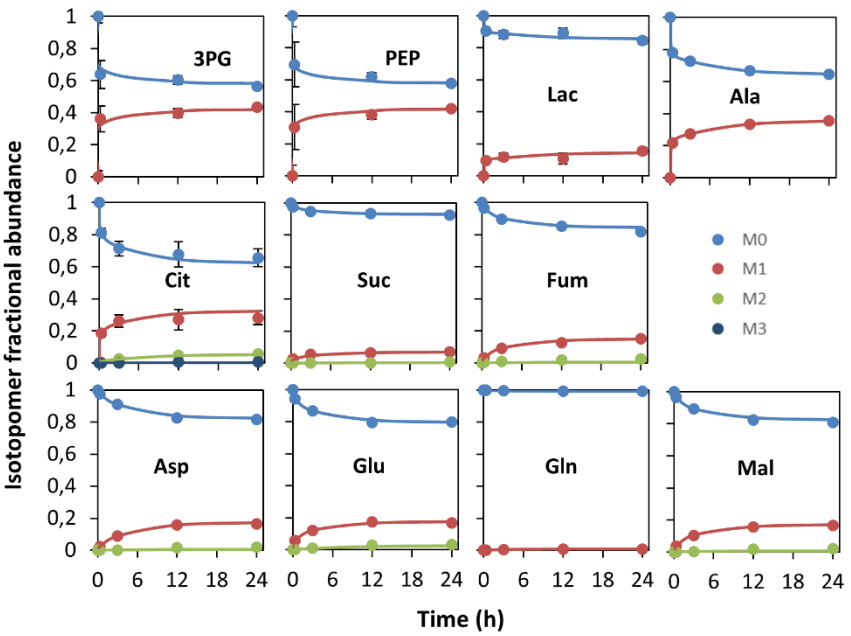

Figure 2.3 - Intracellular ^{13}C-labelling dynamics along 24 h culture of NSCs in the presence of [1-^{13}C]glucose. Symbols correspond to GC-MS measurements corrected for natural isotope abundance. Lines correspond to model fits obtained by non-stationary ^{13}C-MFA. M0 denotes the parent

fragment with a certain ion mass/charge ratio and Mm denotes the increased mass/charge ratio due to m labelled ^{13}C atoms. M0, M1, M2 and M3 measured values are provided in Supplementary Table 2.2.

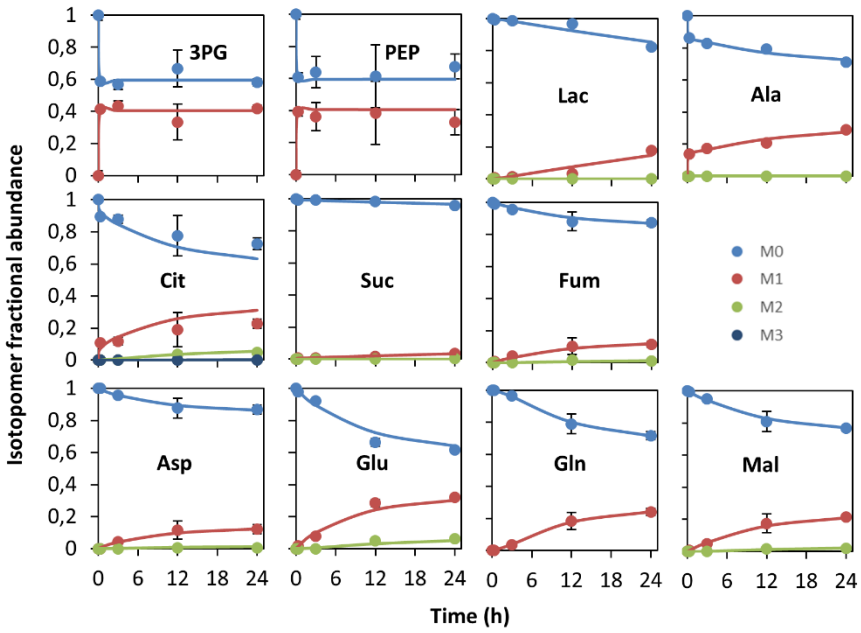

Figure 2.4 – Intracellular ^{13}C-labelling dynamics along 24 h culture of astrocytes in the presence of [1-^{13}C] glucose. Symbols correspond to GC-MS measurements corrected for natural isotope abundance. Lines correspond to model fits obtained by non-stationary ^{13}C-MFA flux estimation. M0 denotes the parent fragment with a certain ion mass/charge ratio and Mm denotes the increased mass/charge ratio due to m labelled ^{13}C atoms. M0, M1, M2 and M3 measured values are provided in Supplementary Table 2.2.

3.3. Fluxome rearrangements during astrocytic differentiation of NSCs

Using isotopic non-stationary ^{13}C-MFA, metabolic fluxes were estimated for each cell type by integrating the time-profiles of the mass isotopomer distributions (Figures 2.3 and 2.4) with extracellular transport rates (Supplementary Table 2.1) in a metabolic network model (Table 2.1). Reasonably good fits were obtained for all metabolites in both cultures (Figures 2.3 and 2.4). All estimated fluxes and associated 95% confidence intervals are provided as Supporting Information (Supplementary Table 2.3).

For a global comparison of metabolic differences between NSCs and astrocytes, metabolic flux ratios were calculated for fluxes with finite lower and upper confidence interval bounds which exclude the value zero (Figure 2.5A). Generally, NSCs displayed a higher metabolic flux in central carbon metabolism compared with astrocytes, including glycolysis (1.7-fold) and the TCA cycle (e.g. 19.4-fold higher citrate synthase flux). A detailed view of these differences can be observed in Figure 2.5B, where the thickness and color of arrows reflect absolute flux values. These flux maps show that the activity of the PPP remained lower than 6% of the corresponding glycolytic flux in both cell populations. Half of the cytosolic pyruvate was converted to mitochondrial pyruvate in NSCs, while in astrocytes most of the cytosolic pyruvate was diverted to lactate secretion, consistent with the measured extracellular rates. In mitochondria, the majority of pyruvate in NSCs entered the TCA cycle by conversion to Acetyl-CoA (AcCoA) through pyruvate dehydrogenase activity (PDH; 318.0 nmol/h/10^{6}cell), and the rest was carboxylated to oxaloacetate (OAC) (PC; 57.7 nmol/h/10^{6}cell), resulting in a PC/PDH ratio of 0.18. On the other hand, astrocytes metabolization of mitochondrial pyruvate through PC was 4.3-fold higher (39.3 nmol/h/10^{6}cell) than through PDH (9.1 nmol/h/10^{6}cell). This anaplerotic metabolization of pyruvate in

astrocytes contributed to support glutamine and citrate secretion. In contrast, glutamine was taken up from the medium by NSCs and metabolized to citrate via reductive carboxylation of alpha-ketoglutarate (AKG). The importance of this metabolic route was first identified in cancer cell cultures to support lipogenesis (Metallo et al., 2012), and a recent study suggests its activity also in human NSCs (Palm et al., 2015). Although not pointed out by the authors, the prominent abundance of citrate M5 isotopomer upon incubation with [U-^{13}C]glutamine is indicative of reductive carboxylation of glutamine-derived AKG. This reaction involves addition of an unlabelled carbon by isocitrate dehydrogenase (IDH) acting in reverse relative to the canonical oxidative TCA cycle, which produces citrate M4 from [U-^{13}C]glutamine. In line with these results, Knobloch et al., (2013) showed that *de novo* lipogenesis is important for NSCs proliferation. These cells have high enzymatic activity of fatty acid synthase (Fasn) and the inhibition of Fasn led to a significant reduction in proliferation.

Finally, a net flux of malate formation from OAC was estimated in both cell populations, which was then recycled back to pyruvate by malic enzyme (ME). Regardless of the total pyruvate flux that enters the TCA cycle, pyruvate cycling becomes rather important through the activity of ME and PC to balance TCA cycle activity and biosynthesis efflux in both NSCs and astrocytes.

4. Conclusion

A deeper understanding of the metabolic circuits in NSCs and how they evolve during differentiation may provide novel approaches for reactivating astrogenesis and neurogenesis to treat neurodegenerative diseases. Herein, we aimed at assessing the alterations in central carbon metabolism associated with the differentiation of NSCs into astrocytes

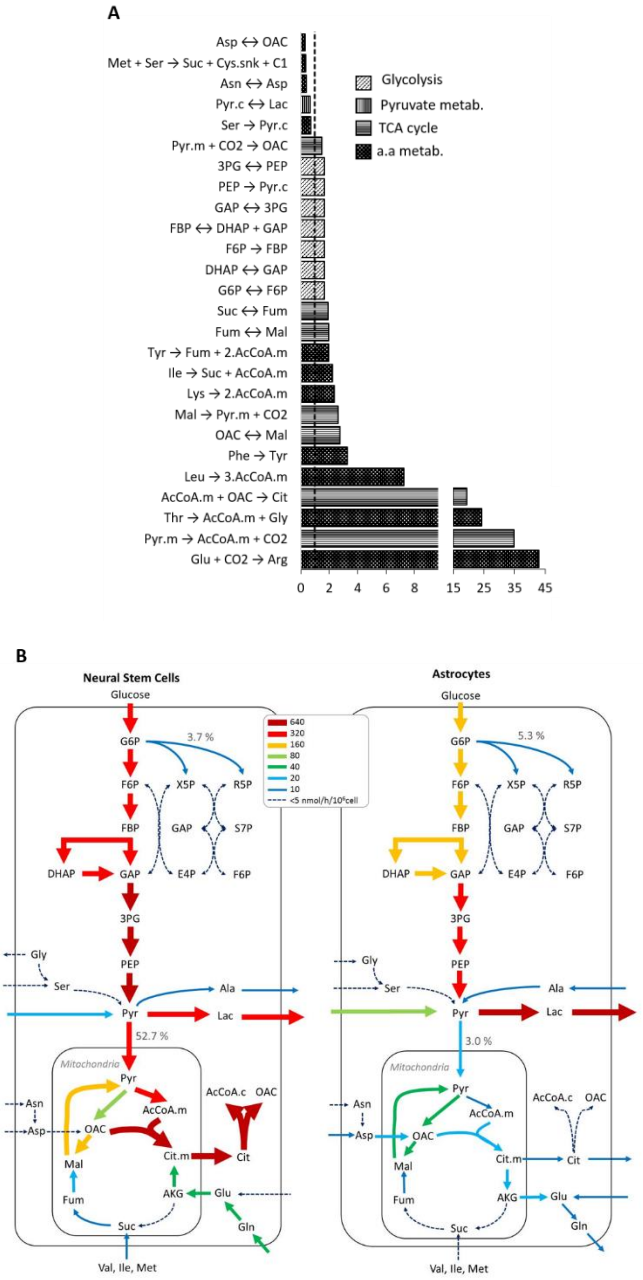

Figure 2.5 – Overview of metabolic flux distributions of NSCs and astrocytes. A) Metabolic flux ratios between cultures of NSCs and astrocytes. The estimated fluxes considered have finite lower and upper

95% confidence interval bounds that exclude zero. **B)** Metabolic flux maps for NSCs and astrocytes. Arrow thickness and colors reflect flux values in units of µmol/h/10^6cell (see Supplementary Table 2.3 for exact flux values and associated 95% confidence intervals).

using non-stationary ^{13}C-MFA. This is the first study in which a comparison of metabolic fluxes between these cell populations was performed, highlighting significant differences at the level of glycolysis, TCA cycle and amino acids metabolism. Specifically, astrocytic differentiation is followed by a downregulation of glucose consumption, but astrocytes keep an even higher lactate production to glucose consumption ratio than NSCs. Moreover, NSCs generated citrate by reductive carboxylation of AKG and channeled it towards cytosolic AcCoA formation, a precursor for fatty acid biosynthesis; in turn, the TCA cycle of astrocytes was rewired to support citrate and glutamine secretion, both metabolic features typically reported in primary astrocytic cultures. While the [1-^{13}C]glucose tracer used in this study provided a first overview of central carbon metabolism in this compelling biological setting, parallel experiments with other labeled substrates should be performed to specifically probe some of the identified metabolic features. For instance, [U-^{13}C]glutamine could be used to confirm the prominent reductive carboxylation flux in NSCs. Due to its power to resolve intracellular fluxes, we expect the multiplication of ^{13}C-MFA studies of neural metabolism in the future.

5. Acknowledgments

Support from iNOVA4Health - UID/Multi/04462/2013, a program funded by Fundação para a Ciência e a Tecnologia (FCT)/Ministério da Educação e Ciência and co-funded by FEDER under the PT2020 Partnership Agreement, is acknowledged. This research has also received

support from FCT through the project MITP-TB/ECE/0013/2013, from the German research foundation (RTG1331, KoRS-CB) and the German ministry for science (BMBF-DynaMeTox). JV Sá is a recipient of a PhD fellowship from FCT (PD/BD/52474/2014). The expert technical assistance of Lars Evje with GC-MS is gratefully acknowledged. We are also thankful to Nuno Carinhas for his help on fluxome analysis.

6. References

Ahn, W. S., and Antoniewicz, M. R. (2013). Parallel labeling experiments with [1,2-(13)C]glucose and [U-(13)C]glutamine provide new insights into CHO cell metabolism. *Metabolic Engineering*, *15*, 34–47.

Amaral, A. I., Teixeira, A. P., Håkonsen, B. I., Sonnewald, U., and Alves, P. M. (2011). A comprehensive metabolic profile of cultured astrocytes using isotopic transient metabolic flux analysis and C-labeled glucose. *Frontiers in Neuroenergetics*, *3*, 1–5.

Antoniewicz, M. R., Kelleher, J. K., and Stephanopoulos, G. (2006). Determination of confidence intervals of metabolic fluxes estimated from stable isotope measurements. *Metabolic Engineering*, *8*(4), 324–37.

Bak, L. K., Schousboe, A., and Waagepetersen, H. S. (2006). The glutamate/GABA-glutamine cycle: Aspects of transport, neurotransmitter homeostasis and ammonia transfer. *Journal of Neurochemistry*, *98*(3), 641–653.

Bélanger, M., Allaman, I., and Magistretti, P. J. (2011). Brain energy metabolism: focus on astrocyte-neuron metabolic cooperation. *Cell Metabolism*, *14*(6), 724–38.

Bolanos, J. P., S. Peuchen, S., Heales, S. J. R., Land, J. M., Clark, J. B. (1994). Nitric oxide-mediated inhibition of the mitochondrial respiratory chain in cultured astrocytes. *Journal of Neurochemistry,* 63, 910-916.

Brown, A. M. (2004). Brain glycogen re-awakened. *Journal of Neurochemistry*, *89*(3), 537–552.

Candelario, K. M., Shuttleworth, C. W., and Cunningham, L. A. (2013). Neural stem/progenitor cells display a low requirement for oxidative metabolism independent of hypoxia inducible factor-1 alpha expression. *Journal of Neurochemistry*, *125*(3), 420–429.

Carinhas, N., Bernal, V., Monteiro, F., Carrondo, M. J. T., Oliveira, R., and Alves, P. M. (2010). Improving baculovirus production at high cell density through manipulation of energy metabolism. *Metabolic Engineering*, *12*(1), 39–52.

Carinhas N, Pais DAM, Koshkin A, Fernandes P, Coroadinha A, Carrondo MJT, Alves PM, Teixeira AP (2016). Metabolic flux profiling of MDCK cells during growth and canine adenovirus vector production. *Scientific Reports, 6:* 23529.

Crown, S. B., and Antoniewicz, M. R. (2013). Publishing (13)C metabolic flux analysis studies: A review and future perspectives. *Metabolic Engineering*, *20*, 42–8.

Doetsch, F., Caille, I., Lim, D. A., Garcı, J. M., and Alvarez-buylla, A. (1999). Subventricular Zone Astrocytes Are Neural Stem Cells in the Adult Mammalian Brain. *Cell*, *97*, 703–716.

Folmes, C. D. L., Nelson, T. J., Martinez-Fernandez, A., Arrell, D. K., Lindor, J. Z., Dzeja, P. P., Ikeda, Y., Terzic, C. P. and Terzic, A. (2011). Somatic oxidative bioenergetics transitions into pluripotency-dependent glycolysis to facilitate nuclear reprogramming. *Cell Metabolism*, *14*(2), 264–71.

Hofmann, U., Maier, K., Niebel, A., Vacun, G., Reuss, M., and Mauch, K. (2008). Identification of metabolic fluxes in hepatic cells from transient 13C-labeling experiments: Part I. Experimental observations.

Biotechnology and Bioengineering, *100*(2), 344–54.

Johnson, M. A., Weick, J. P., Pearce, R. A., and Zhang, S.-C. (2007). Functional Neural Development from Human Embryonic Stem Cells: Accelerated Synaptic Activity Coculture. *Journal of Neuroscience*, *27*(12), 3069–3077.

Kleiderman, S. M., Sá, J. V, Teixeira, A. P., Brito, C., Gutbier, S., Evje, L. G., Hadera, M. G., Glaab, E., Henry, M., Sachinidis, A., Alves, P. M., Sonnewald, U. and Leist, M. (2016). Functional and phenotypic differences of pure populations of stem cell-derived astrocytes and neuronal precursor cells. *Glia*, 64(5): 695-715.

Knobloch, M., Braun, S. M. G., Zurkirchen, L., von Schoultz, C., Zamboni, N., Araúzo-Bravo, M. J., Kovacs, W. J., Karalay, Ö., Suter, U., Machado, R. A. C., Roccio, M., Lutolf, M. P., Semenkovich, C. F. and Jessberger, S. (2013). Metabolic control of adult neural stem cell activity by Fasn-dependent lipogenesis. *Nature*, *493*(7431), 226–30.

Kriegstein, A., and Alvarez-Buylla, A. (2009). The glial nature of embryonic and adult neural stem cells. *Annual Review of Neuroscience*, *32*, 149–184.

McKenna, M., Gruetter, R., Sonnewald, U., Waagepetersen, H., and Schousboe, A. (2012). Energy Metabolism of the Brain. In S. T. S. Brady, R. W. Albers, & D. L. Price (Eds.), *Basic Neurochemistry: Principles of Molecular, Cellular, and Medical Neurobiology* (8th ed., pp. 200–299). Oxford, UK: Elsevier Academic Press.

Metallo, C. M., Gameiro, P. A., Bell, E. L., Mattaini, K. R., Yang, J., Hiller, K., Jewell, C. M., Johnson, Z. R., Irvine, D. J., Guarente, L., Kelleher, J. K., Vander Heiden, M. G., Iliopoulos, O. and Stephanopoulos, G. (2012). Reductive glutamine metabolism by IDH1 mediates lipogenesis under hypoxia. *Nature*, *481*, 380–384.

Munger, J., Bennett, B. D., Parikh, A., Feng, X., Rabitz, H. A., Shenk, T.,

and Rabinowitz, J. D. (2008). Systems-level metabolic flux profiling identifies fatty acid synthesis as a target for antiviral therapy. *Nat Biotechnol*, *26*(10), 1179–1186.

Nedergaard, M., Ransom, B., and Goldman, S. A. (2003). New roles for astrocytes: Redefining the functional architecture of the brain. *Trends in Neurosciences*, *26*(10), 523–530.

Noh, K., and Wiechert, W. (2006). Experimental Design Principles for Isotopically Instationary C Labeling Experiments. *Biotechnology and Bioengineering*, *94*, 234–251.

Palm, T., Bolognin, S., Meiser, J., Nickels, S., Träger, C., Meilenbrock, R.-L., Brockhaus, J., Schreitmüller, M., Missler, M. and Schwamborn, J. C. (2015). Rapid and robust generation of long-term self-renewing human neural stem cells with the ability to generate mature astroglia. *Scientific Reports*, *5: 16321*.

Pellerin, L., Bouzier-Sore, A.-K., Aubert, A., Serres, S., Merle, M., Costalat, R., and Magistretti, P. J. (2007). Activity-Dependent Regulation of Energy Metabolism by Astrocytes: An Update. *Glia*, *55*, 1251–1262.

Pellerin, L., and Magistretti, P. J. (1994). Glutamate uptake into astrocytes stimulates aerobic glycolysis: a mechanism coupling neuronal activity to glucose utilization. *Proceedings of the National Academy of Sciences of the United States of America*, *91*(22), 10625–10629.

Phatnani, H., and Maniatis, T. (2015). Astrocytes in Neurodegenerative Disease. *Cold Spring Harbor Perspectives in Biology*, *7*(6), a020628.

Rouach, N., Koulakoff, A., Abudara, V., Willecke, K., and Giaume, C. (2008). Astroglial Metabolic Networks Sustain Hippocampal Synaptic Transmission. *Science*, *322*, 1551–1555.

Sá, J. V., Duarte, T. M., Carrondo, M. J. T., Alves, P. M., and Teixeira, A.

P. (2015). Metabolic Flux Analysis: A Powerful Tool in Animal Cell Culture. In M. Al-Rubeai (Ed.), *Animal Cell Culture* (Vol. 521–539, p. 785). Springer International Publishing.

Sauer, U. (2006). Metabolic networks in motion: 13C-based flux analysis. *Molecular Systems Biology*, *2*(62).

Seri, B., Garcı, J. M., Mcewen, B. S., and Alvarez-buylla, A. (2001). Astrocytes Give Rise to New Neurons in the Adult Mammalian Hippocampus. *The Journal of Neuroscience*, *21*(18), 7153–7160.

Simard, M., and Nedergaard, M. (2004). The neurobiology of glia in the context of water and ion homeostasis. *Neuroscience*, *129*(4), 877–896.

Ullian, E. M., Sapperstein, S. K., Christopherson, K. S., and Barres, B. a. (2001). Control of synapse number by glia. *Science (New York, N.Y.)*, *291*, 657–661.

Vander Heiden, M. G., Cantley, L. C., and Thompson, C. B. (2009). Understanding the Warburg Effect : Cell Proliferation. *Science*, *324*, 1029–1034.

Walls, A. B., Bak, L. K., Sonnewald, U., Schousboe, A., and Waagepetersen, H. S. (2014). Metabolic Mapping of Astrocytes and Neurons in Culture Using Stable Isotopes and Gas Chromatography-Mass Spectrometry (GC-MS). In HirrlingerJohannes & H. S. Waagepetersen (Eds.), *Brain Energy Metabolism* (pp. 73–105).

Westergaard, N., Banke, T. U. E., Wahl, P., Sonnewaldt, U., and Schousboe, A. (1995). Citrate modulates the regulation by Zn2 + of N-methyl-D-aspartate receptor-mediated channel current and neurotransmitter release, *92*(April), 3367–3370.

Westergaard, N., Sonnewald, U., Unsgård, G., Peng, L., Hertz, L., and Schousboe, A. (1994). Uptake, release, and metabolism of citrate in

neurons and astrocytes in primary cultures. *Journal of Neurochemistry*, *62*(5), 1727–33.

Wiechert, W. (2001). 13C metabolic flux analysis. *Metabolic Engineering*, *3*(3), 195–206.

Yeo, H., Lyssiotis, C. a, Zhang, Y., Ying, H., Asara, J. M., Cantley, L. C., and Paik, J.-H. (2013). FoxO3 coordinates metabolic pathways to maintain redox balance in neural stem cells. *The EMBO Journal*, *32*(19), 2589–602.

Young, J. D. (2014). INCA: A computational platform for isotopically nonstationary metabolic flux analysis. *Bioinformatics (Oxford, England)*, *30*, 11–13.

Young, J. D., Walther, J. L., Antoniewicz, M. R., Yoo, H., and Stephanopoulos, G. (2008). An elementary metabolite unit (EMU) based method of isotopically nonstationary flux analysis. *Biotechnology and Bioengineering*, *99*(3), 686–99.

Zhang, J., Nuebel, E., Daley, G. Q., Koehler, C. M., and Teitell, M. A. (2012). Metabolic regulation in pluripotent stem cells during reprogramming and self-renewal. *Cell Stem Cell*, *11*(5), 589–95.

Zwingmann, C., and Leibfritz, D. (2003). Regulation of glial metabolism studied by 13C-NMR. *NMR in Biomedicine*, *16*(6-7), 370–99.

7. Supplementary Material

Supplementary Table 2.1 – Specific uptake and secretion rates of extracellular metabolites and their standard deviations (nmol/h/10^6cell) from replicate wells of NSCs and astrocytes. The rates were calculated by linear regression of extracellular metabolite concentration profiles along 24 h after label administration. NaN represents undetermined transport rates.

Metabolite	Neural Stem Cells	Astrocytes
Glucose	-256.3 ± 1.3	-175.7 ± 17.9
Lactate	237.8 ± 10.1	348.6 ± 9.6
Aspartate	-2.6 ± 0.7	-11.9 ± 5.8
Glutamate	-1.8 ± 0.4	-10.5 ± 3.4
Serine	-2.8 ± 1.4	-4.1 ± 1.7
Asparagine	-0.6 ± 0.3	-1.6 ± 0.3
Glycine	2.4 ± 1.1	NaN
Glutamine	26.1 ± 6.5	10.4 ± 2.2
Histidine	NaN	-3.4 ± 1.0
Threonine	NaN	0.9 ± 0.6
Arginine	NaN	1.7 ± 0.3
Alanine	9.0 ± 1.4	-6.6 ± 3.1
Proline	0.3 ± 0.1	NaN
Tyrosine	-3.3 ± 1.9	NaN
Valine	-3.0 ± 2.2	NaN
Methionine	-0.8 ± 0.4	-1.9 ± 0.3
Isoleucine	-3.7 ± 2.2	-1.5 ± 0.7
Leucine	-3.9 ± 2.3	NaN
Phenylalanine	NaN	2.1 ± 0.8

Citrate	NaN	6.6 ± 0.9
Pyruvate	-12.9 ± 5.1	-48.0 ± 4.4

Supplementary Table 2.2 – Mass isotopomer distributions of intracellular metabolites for [1-^{13}C] glucose experiments measured by GC-MS. Data was corrected for natural isotope abundances.

	Neural Stem Cells				*Astrocytes*			
	0.33 h	**3 h**	**12 h**	**24 h**	**0.33 h**	**3 h**	**12 h**	**24 h**
3PG (M0)	0.639	0.787	0.604	0.564	0.586	0.568	0.667	0.582
3PG (M1)	0.361	0.213	0.396	0.436	0.414	0.432	0.333	0.418
PEP (M0)	0.695	0.771	0.618	0.578	0.608	0.639	0.754	0.674
PEP (M1)	0.305	0.229	0.382	0.422	0.392	0.361	0.246	0.326
Lac (M0)	0.906	0.882	0.891	0.844	0.992	0.986	0.968	0.824
Lac (M1)	0.094	0.118	0.109	0.156	0.008	0.014	0.032	0.176
Lac (M2)	0	0	0	0	0	0	0	0
Ala (M0)	0.782	0.726	0.667	0.646	0.861	0.828	0.791	0.710
Ala (M1)	0.218	0.274	0.333	0.354	0.139	0.172	0.209	0.290
Ala (M2)	0	0	0	0	0	0	0	0
Cit (M0)	0.812	0.713	0.677	0.656	0.894	0.880	0.775	0.726
Cit (M1)	0.186	0.261	0.270	0.282	0.106	0.119	0.189	0.227
Cit (M2)	0.002	0.025	0.047	0.056	0	0.002	0.034	0.046
Cit (M3)	0	0	0.006	0.006	0	0	0.002	0.001
Suc (M0)	0.974	0.945	0.934	0.923	0.993	0.993	0.983	0.959

Suc (M1)	0.026	0.054	0.063	0.070	0.007	0.007	0.017	0.036
Suc (M2)	0	0.001	0.003	0.007	0	0	0.001	0.004
Suc (M3)	0	0	0	0	0	0	0	0
Fum (M0)	0.965	0.898	0.854	0.820	0.991	0.955	0.881	0.872
Fum (M1)	0.031	0.093	0.126	0.153	0.008	0.043	0.103	0.116
Fum (M2)	0.004	0.009	0.020	0.026	0.001	0.002	0.016	0.011
Fum (M3)	0	0	0.001	0.002	0	0	0	0.001
Mal (M0)	0.964	0.894	0.825	0.809	0.994	0.952	0.810	0.767
Mal (M1)	0.035	0.101	0.156	0.167	0.006	0.048	0.174	0.213
Mal (M2)	0	0.003	0.017	0.022	0	0	0.016	0.020
Mal (M3)	0	0.001	0.001	0.002	0	0	0	0
Asp (M0)	0.976	0.910	0.826	0.817	1	0.957	0.877	0.869
Asp (M1)	0.024	0.089	0.158	0.163	0	0.043	0.116	0.124
Asp (M2)	0	0.001	0.015	0.018	0	0	0.006	0.005
Asp (M3)	0	0	0.001	0.001	0	0	0.001	0.002
Glu (M0)	0.941	0.867	0.796	0.798	0.980	0.922	0.664	0.616
Glu (M1)	0.057	0.121	0.173	0.167	0.020	0.077	0.285	0.321
Glu (M2)	0.001	0.011	0.029	0.032	0	0.001	0.050	0.062
Glu (M3)	0	0	0.002	0.003	0	0	0.001	0.001
Gln (M0)	1	0.995	0.993	0.994	1	0.964	0.789	0.716
Gln (M1)	0	0.005	0.007	0.006	0	0.036	0.184	0.240
Gln (M2)	0	0	0	0	0	0	0.026	0.043

Gln (M3)	0	0	0	0	0	0	0	0

Supplementary Table 2.3 – Metabolic fluxes and associated 95% confidence intervals (nmol/h/10^{6}cell) estimated after [1-^{13}C]glucose administration to NSCs and astrocytes. For flux estimation, experimentally determined errors were associated with the extracellular rates and an error of 1.5 mol% was attributed for the MS measurements. Flux estimation solutions with statistically accepted fits were obtained for both cell populations. For NSC the sum of square residuals (SSR) was 36.0 (the system has 86 degrees of freedom; assuming the minimized SSR follows a χ^2-distribution, the expected 95% confidence region of SSR is [62.2, 113.5]. For astrocytes the SSR was 89.1 (the expected SSR interval was [51.3, 98.5], with 73 degrees of freedom).

#	Reaction		NSC		Astrocytes	
			Flux	***95% Confidence Interval***	***Flux***	***95% Confidence Interval***
R1	G6P ↔ F6P	net	246.7	[239.7, 257.8]	147.3	[129.9, 163.2]
	G6P ↔ F6P	exch	7734.4	[0, Inf]	2646.0	[0, Inf]
R2	F6P → FBP		253.1	[249.6, 257.7]	152.8	[135.8, 170.7]
R3	FBP ↔ DHAP + GAP	net	253.1	[249.6, 257.7]	152.8	[135.8, 170.7]
	FBP ↔ DHAP + GAP	exch	1E-7	[0, Inf]	1E-7	[0, Inf]
R4	DHAP ↔ GAP	net	253.1	[249.6, 257.7]	152.8	[135.8, 170.7]
	DHAP ↔ GAP	exch	120.9	[0, Inf]	119.0	[0, Inf]
R5	GAP ↔ 3PG	net	509.3	[503.5, 516.6]	308.4	[274.3, 342.8]
	GAP ↔ 3PG	exch	0.6	[0, Inf]	1E-7	[0, Inf]
R6	3PG ↔ PEP	net	509.3	[503.5, 516.6]	308.4	[274.3, 342.8]
	3PG ↔ PEP	exch	1E-7	[0, Inf]	0.2	[0, Inf]

R7	PEP → Pyr.c		509.3	[503.5, 516.6]	308.4	[274.3, 342.8]
R8	G6P → P5P + CO_2		9.5	[NaN, 16.1]	8.3	[4.2, 13.9]
R9	P5P + P5P ↔ GAP + S7P	net	3.2	[NaN, 5.3]	2.8	[1.4, 4.6]
	P5P + P5P ↔ GAP + S7P	exch	277.5	[172.5, 404.7]	1E-7	[0, Inf]
R10	S7P + GAP ↔ E4P + F6P	net	3.2	[NaN, 5.3]	2.8	[1.4, 4.6]
	S7P + GAP ↔ E4P + F6P	exch	1E-7	[0, 15.6]	1E-7	[0, Inf]
R11	E4P + P5P ↔ GAP + F6P	net	3.2	[NaN, 5.3]	2.8	[1.4, 4.6]
	E4P + P5P ↔ GAP + F6P	exch	1E-7	[0, 4.1]	1E-7	[0, Inf]
R12	Pyr.c ↔ Lac	net	239.3	[217.9, 262.1]	354.1	[323.8, 384.1]
	Pyr.c ↔ Lac	exch	139.2	[0, 204.7]	77.8	[0, 236.7]
R13	Pyr.c ↔ Ala	net	9.0	[6.1, 12.3]	-6.5	[-12.7, -0.3]
	Pyr.c ↔ Ala	exch	73.1	[0, Inf]	10329	[8.3, Inf]
R14	Pyr.m → AcCoA.m + CO_2		318.0	[290.2, 353.5]	9.1	[3.2, 20.0]
R15	Pyr.m + CO_2 → OAC		57.7	[22.8, 323.0]	39.2	[18.8, 106.4]
R16	OAC + AcCoA.m → Cit		347.1	[306.6, 391.9]	17.9	[13.2, 30.2]
R17	Cit ↔ AKG + CO_2	net	-27.7	[-42.1, 56.1]	11.2	[6.8, 17.3]
	Cit ↔ AKG + CO_2	exch	54545.1	[19.5, Inf]		
R18	AKG → SucCoA + CO_2		0.08	[0, 83.0]	1E-7	[-2.8E-15, 5.5]
R19	SucCoA ↔ Suc	net	0.08	[0, 83.0]	1E-7	[0, 5.5]
	SucCoA ↔ Suc	exch	1E-7	[0, Inf]	50.3	[0, Inf]
R20	Suc ↔ Fum	net	6.7	[0.4, 87.6]	3.4	[2.0, 21.0]
	Suc ↔ Fum	exch	4.0	[0, 10.9]	1E-7	[0, 36.4]
R21	Fum ↔ Mal	net	10.2	[2.6, 94.1]	5.2	[2.2, 11.7]
	Fum ↔ Mal	exch	64.8	[14.2, 815.3]	5.8	[1.7, 43.6]
R22	OAC ↔ Mal	net	88.7	[43.7, 345.9]	32.4	[6.5, 98.4]
	OAC ↔ Mal	exch	1E-7	[0, Inf]	1E-7	[0, 48.9]
R23	Mal → Pyr.m + CO_2		98.9	[52.2, 358.9]	37.6	[10.5, 103.9]
R24	Cit → OAC + AcCoA.c		374.8	[331.4, 425.5]	1E-7	[0, NaN]
R25	Gln ↔ Glu	net	25.9	[13.1, 38.6]	-9.5	[-14.0, -5.5]

	Gln ↔ Glu	exch	1.1	[0, 185.9]	1E-7	[0, 2.4]
R26	Glu ↔ AKG	net	27.8	[14.5, 43.0]	-11.2	[-16.5, -6.9]
	Glu ↔ AKG	exch	53.5	[15.8, 387.6]	404.5	[0, Inf]
R27	Asn ↔ Asp	net	0.6	[0.08, 1.2]	1.6	[1.0, 2.1]
	Asn ↔ Asp	exch	260.2	[0, Inf]	2600.3	[0, Inf]
R28	Asp ↔ OAC	net	3.3	[1.8, 5.0]	11.0	[1.3, 20.5]
	Asp ↔ OAC	exch	103.5	[14.3, Inf]	11.2	[2.6, 69.5]
R29	Ser → Pyr.c		2.9	[0.05, 5.8]	4.1	[0, 11.4]
R30	Ser ↔ Gly + C1	net	-0.8	[-2.1, 0]	-1.9	[-8.5, 3.8]
	Ser ↔ Gly + C1	exch	26.4	[0, Inf]	0.02	[0, Inf]
R31	Glu ↔ Pro	net	0.3	[0.08, 0.5]	1E-7	[-0.5, 1.3]
	Glu ↔ Pro	exch	0.3	[0, Inf]	1E-7	[0, Inf]
R32	Val + CO_2 → Suc + CO_2 + CO_2		2.4	[0, 8.2]	1E-7	[0, 1.8]
R33	Ile + CO_2 → Suc + AcCoA.m + CO_2		3.5	[0, 7.8]	1.6	[0.2, 2.9]
R34	Leu + CO_2 → AcCoA.m + AcCoA.m + AcCoA.m + CO_2		3.9	[0, 9.0]	0.5	[0, 2.0]
R35	Thr → AcCoA.m + Gly		2.3	[0, 4.5]	0.09	[0, 1.3]
R36	Phe → Tyr		0.7	[0, 3.5]	0.2	[0, 1.7]
R37	Tyr → Fum + AcCoA.m + AcCoA.m + CO_2		3.5	[0, 8.7]	1.8	[0., 5.2]
R38	Met + Ser + CO_2 → Suc + Cys.snk + CO_2 + C1		0.7	[0, 1.6]	1.9	[1.3, 2.5]
R39	Lys → CO_2 + CO_2 + AcCoA.m + AcCoA.m		2.2	[0, 7.9]	0.9	[0, 3.3]
R40	His → Glu + C1		0.1	[0, 1.1]	1E-7	[0, 1.1]
R41	Arg → Glu + Urea.snk		72.3	[0, 1325.4]	1E-7	[0, 42.7]
R42	Glu + CO_2 → Arg		72.1	[0, 1338.0]	1.7	[1.0, 73.3]
R43	Pyr.c ↔ Pyr.m	net	276.8	[251.6, 303.7]	10.8	[-1.2, 25.0]
	Pyr.c ↔ Pyr.m	exch	1E-7	[0, Inf]	516.1	[239.1, 791.6]
R44	CO_2 ↔ CO_2.ext	net	279.4	[-890.7, 398.2]	29.0	[-44.2, 50.9]
	CO_2 ↔ CO_2.ext	exch	1E-7	[0, Inf]	1E-7	[0, 43.6]

R45	Glc.ext → G6P		256.2	[253.8, 258.7]	155.7	[138.5, 172.9]
R46	Lac ↔ Lac.ext	net	239.3	[215.5, 262.1]	354.1	[323.8, 384.1]
	Lac ↔ Lac.ext	exch	542.8	[344.5, 721.8]	1E-7	[0, 135.6]
R47	Ala ↔ Ala.ext	net	9.0	[6.1, 12.3]	-6.5	[-12.7, -0.3]
	Ala ↔ Ala.ext	exch	1E-7	[0, 113.9]	1E-7	[0, 88.3]
R48	Pyr.ext ↔ Pyr.c	net	12.8	[5.0, 21.9]	45.9	[35.4, 56.5]
	Pyr.ext ↔ Pyr.c	exch	0.2	[0, 35.5]	1E-7	[0, 93.0]
R49	Cit → Cit.ext				6.7	[4.1, 9.4]
R50	Gln ↔ Gln.ext	net	-25.9	[-38.6, 13.1]	9.5	[5.5, 14.0]
	Gln ↔ Gln.ext	exch			2.1	[0, 5.2]
R51	Glu ↔ Glu.ext	net	-1.8	[-2.7, -1.0]	-1E-7	[-0.5, 1.7]
	Glu ↔ Glu.ext	exch	14.5	[0, 157.5]	1E-7	[0, 1.8]
R52	Asp ↔ Asp.ext	net	-2.6	[-4.0, -1.2]	-9.4	[-19.3, 0.3]
	Asp ↔ Asp.ext	exch	5.4	[0, 121.7]	1E-7	[0, 50.1]
R53	Asn ↔ Asn.ext	net	-0.6	[-1.2, -0.08]	-1.6	[-2.1, -1.0]
	Asn ↔ Asn.ext	exch	0.7	[0, 158.7]	1E-7	[0, Inf]
R54	Ser.ext ↔ Ser	net	2.8	[-0.4, 5.6]	4.1	[0.7, 7.6]
	Ser.ext ↔ Ser	exch	1E-7	[0, Inf]	0.03	[0, Inf]
R55	Gly ↔ Gly.ext	net	1.5	[-0.5, 3.8]	-1.9	[-8.4, 3.9]
	Gly ↔ Gly.ext	exch	0.005	[0, Inf]	1E-7	[0, Inf]
R56	Pro.ext ↔ Pro	net	-0.3	[-0.5, -0.08]	-1E-7	[-1.3, 0.5]
	Pro.ext ↔ Pro	exch	0.9	[0, Inf]	1.0	[0, Inf]
R57	Val.ext → Val		2.4	[0, 8.2]	1E-7	[0, 1.8]
R58	Ile.ext → Ile		3.5	[0, 7.8]	1.6	[0.2, 2.9]
R59	Leu.ext → Leu		3.9	[0, 9.0]	0.5	[0, 2.0]
R60	Thr.ext → Thr		2.3	[0, 4.5]	0.09	[0, 1.3]
R61	Phe.ext → Phe		0.7	[0, 3.5]	0.2	[0, 1.7]
R62	Tyr.ext → Tyr		2.8	[0, 7.1]	1.6	[0, 4.8]
R63	Met.ext → Met		0.7	[0, 1.6]	1.9	[1.3, 2.5]
R64	Lys.ext → Lys		2.2	[0, 7.9]	0.9	[0, 3.3]
R65	His.ext → His		0.1	[0, 1.1]	1E-7	[0, 1.1]
R66	Arg.ext ↔ Arg	net	0.2	[-2.6, 3.3]	-1.7	[-2.4, -1.0]
	Arg.ext ↔ Arg	exch	1E-7	[0, 305.4]	1E-7	[0, Inf]

3

Unveiling Dynamic Metabolic Signatures in Human Induced Pluripotent and Neural Stem Cells

This chapter was adapted from:

Sá, JV, Simão, D; Terrasso, A.P.; Silva, M.M; Brito, C., Isidro, I.A.; Alves, PM.; Carrondo, M.J.T (2019) Unveiling Dynamic Metabolic Signatures in Human Induced Pluripotent and Neural Stem Cells. *PLOS Comp Biol* (*Accepted)*

Author contributions to this chapter:

João Sá participated in the experimental setup and design, participated in experiment execution and in the analytical measurements, performed the computational analyses and wrote this chapter.

Table of Contents

Abstract

Metabolism plays an essential role in cell fate decisions. However, the methods used for metabolic characterization and for finding potential metabolic regulators are still based on characterizing cellular metabolic steady-state which is dependent on the extracellular environment. In this work, we hypothesized that the response dynamics of intracellular metabolic pools to extracellular stimuli is controlled in a cell type-specific manner. We applied principles of process dynamics and control to human induced pluripotent stem cells (hiPSC) and human neural stem cells (hNSC) subjected to a sudden extracellular glutamine step. The fold-changes of steady-states and the transient profiles of metabolic pools revealed that dynamic responses were reproducible and cell type-specific. Importantly, many amino acids had conserved dynamics and readjusted their steady state concentration in response to the increased glutamine influx. Overall, we propose a novel methodology for systematic metabolic characterization and identification of potential metabolic regulators.

1. Introduction

Over the last decade, the paradigm of metabolism being simply the engine for metabolic constituents has been dramatically shifted. Metabolism generates regulatory responses (McKnight, 2010) that affect all other molecular levels, from epigenome to proteome, through diverse action mechanisms (e.g. DNA methylation, histone acetylation) (Bulusu and Aulehla, 2016; Harvey et al., 2016; Zhang et al., 2018). Those regulatory responses modulate key cell decisions such as proliferation, differentiation and death (Gerosa and Sauer, 2011). From this relationship between metabolism and cell fate, it follows that each cell type may have a unique metabolic phenotype.

Inspecting the activity of metabolic pathways is an appealing approach for cell characterization. This approach can pose significant limitations, as recent literature has shown that cells not only fine-tune their intracellular fluxes according to momentaneous needs (Zhang et al., 2016) but can also change their sources of carbon and nitrogen (Pavlova et al., 2018). For instance, it was found that asparagine uptake in mammalian cells preferentially occurs in a glutamine-deficient environment and does not occur when glutamine is present (Pavlova et al., 2018).

In an attempt to better characterize metabolic cell status, several studies have explored intracellular metabolic pool quantification. However, dependency of intracellular metabolic pools on extracellular environment was also observed (Rehberg et al., 2014; Zhang et al., 2016). Furthermore, metabolic pools involved in epigenetic regulation are usually identified by looking into substrates of epigenetic enzymes (Cai et al., 2011; Kaelin and McKnight, 2013; TeSlaa et al., 2016). This has the shortcoming of leaving out

metabolites that, although apparently unrelated to those enzymes, could influence them due to the complex dynamics of metabolic and regulatory networks. Another limitation of stationary quantitative approaches is that potentially relevant metabolites might be masked if the response to a change in conditions is transient and the metabolite concentration returns to the same levels of the previous cell state (TeSlaa et al., 2016). Consequently, not only are the methods used for characterization of cell metabolism dependent on extrinsic factors but can also lead to limited deductions as these are typically based on steady-state data, meaning that transient dynamics and potential regulators are not experimentally observed.

In this work, we hypothesized that cells must be able to maintain homeostasis and stable conditions to prevent small environmental variations from causing substantial changes in cell phenotype. Therefore, the metabolic phenotype of a cell is displayed by the dynamics of metabolite pools and consequently metabolites with a very efficient or robust control of their concentration are potentially key for the cell homeostasis. Observing pool dynamics instead of flux dynamics should improve the accuracy of cell characterization as pools directly affect several molecular levels such as proteins, DNA and histones which in turn influence cell fate (Bulusu and Aulehla, 2016; Zhang et al., 2018). In order to test our hypothesis, two human induced pluripotent stem cell (hiPSC) lines and two human neural stem cell (hNSC) lines were exposed to a step increase in extracellular glutamine concentration. With this challenge, the intracellular dynamic profiles were determined for up to 201 metabolites, covering most of the central carbon metabolism and lipidic pathways. The dynamic profiles were compared between hiPSC and hNSC using process dynamics and control concepts. This approach allowed for the identification of metabolic dynamics

conserved and unique for each cell type. Overall, we propose an unbiased and systematic methodology to characterize cells metabolic signatures and to identify potential metabolic pools involved in cell fate decision.

2. Materials and Methods

2.1. Cell culture

Primed hiPSC IMR90-4 (RRID: CVCL_C437) were purchased from WiCell and WTC-11 (RRID: CVCL_Y803) were obtained from The J. David Gladstone Institutes, designated throughout the text by hiPSC 1 and hiPSC 2 respectively. Primed hiPSC were maintained under feeder-free conditions with Matrigel (Corning® Matrigel® hESC-Qualified Matrix and Corning® Matrigel® Growth Factor Reduced (GFR) Basement Membrane Matrix, BD Biosciences) and fed daily with mTeSR1™ medium (STEMCELL Technologies). Versene (Gibco Life Technologies) and Accutase (STEMCELL Technologies) were used to enzymatically dissociate hiPSCs into single cells for hiPSC 1 and hiPSC 2, respectively. At cell passage, mTeSR1™ was also supplemented with 5 µM of ROCK inhibitor Y-27632 (Calbiochem). Complete medium exchange was performed every day. Cells were maintained under humidified atmosphere with 5 % CO_2, at 37 °C.

hNSC 1 was derived from hiPSC 1 IMR90-4 using a dual SMAD inhibition protocol (Chambers et al., 2009). Briefly, hiPSC differentiation was induced by supplementing the culture media with 10 µM SB431542 and 1 µM LDN193189 (both from STEMCELL Technologies) for 10 days. hNSC 2 was originally derived from hiPSC line RIi001-A (RRID: CVCL_C888), as previously described (Simão et al., 2018) and designated throughout the text as hNSC 2.

hNSC were expanded in DMEM/F12 (Invitrogen) with Glutamax, N2 and B27 supplements (Invitrogen), 20 µg/mL insulin and 20 ng/mL of bFGF (Peprotech) and of EGF (Sigma). Half of culture media volume was exchanged every other day (Simão et al., 2018). hNSC were maintained under humidified atmosphere with 5 % CO_2 and 3 % O_2, at 37 °C.

2.2. Stirred-tank bioreactor cultures

hiPSC and hNSC were inoculated in 200 mL of media as single cell suspensions of $0.25x10^6$ cell/mL and $0.4x10^6$ cells/mL, respectively, into software-controlled stirred-tank DASGIP® Bioblock bioreactor system (Eppendorf). hiPSC 1, hiPSC 2, hNSC 1 and hNSC 2 were used for these experiments at cell passage number P40, P36, P12 and P34, respectively (four bioreactor runs in total). Bioreactor temperature was set to 37 ºC, dissolved oxygen to 15%, pH to 7.4, aeration rate to 0.1 vvm and the agitation rate to a range from 70 to 100 rpm (Abecasis et al., 2017; Simão et al., 2016). Perfusion was initiated after inoculation and interrupted just before the perturbation experiment. Perfusion rates of hiPSC and hNSC were 1.3 day^{-1} and 0.33 day^{-1}, respectively. Cells were allowed to aggregate for 2 to 3 days before performing the perturbation experiment.

2.3. Perturbation experiments and sampling for metabolomics

Before initiating the perturbation experiment, perfusion was interrupted. Glutamine concentration in the culture medium was determined using an YSI 7100 MBS analyser (YSI Life Sciences,

Yellow Springs, Ohio USA) offline. The glutamine pulse was induced by adding the required volume of glutamine concentrated solution (L-Glutamine, 200 mM, Gibco) to attain a concentration of 15 mM in the culture media. Changes in osmolarity of the culture medium of bioreactor cultures were later determined using a K-7400S Semi-Micro Osmometer (KNAUER Wissenschaftliche Geräte GmbH, Germany). Sampling was performed before the glutamine step and at several time-points after the step: immediately (0 min), 5 min, 10 min, 15 min, 30 min, 1 h and 2 h after. A sample of 15 mL of culture was collected per time-point sample and distributed equitably in three 50 mL tubes, containing ice-cold PBS to quench cell metabolism, generating three technical replicates that were processed independently. After centrifugation at 300*xg* for 3 min at 4 ºC, a sample of supernatant was stored for later quantification of extracellular glutamine, glucose, lactate and ammonia. The remaining supernatant was discarded and the cell pellet was washed with ice-cold PBS and centrifuged again. The supernatant was removed and a solution of 40:40:20 acetonitrile:methanol:water was added to extract intracellular metabolites from the cell pellet. Sonication was performed to guarantee a complete cell lysis. The extracts were transferred to microcentrifuge tubes and centrifuged at 20000 x g at 0 ºC for 15 minutes. Supernatant was collected, snap-frozen in liquid nitrogen and stored at -80 ºC until metabolomic analysis. The pellet was also snap-frozen in liquid nitrogen and stored at -80 ºC until protein quantification. Protein was dissolved in lysis buffer containing 2% SDS (v/v) and quantified using a Microplate BCA Protein Assay Kit (Thermo Scientific). Ammonia was quantified using the Ammonia Assay Kit (Megazyme).

2.4. Cell viability

Cell viability in spheroids was analysed before the glutamine perturbation experiment by staining the spheroids with fluorescein diacetate (FDA) in PBS (0.02 mg/mL) and propidium iodide (PI) in PBS (0.002 mg/mL), followed by visualization by fluorescence microscopy using an inverted phase contrast microscope (Leica Microsystems GmbH).

2.5. Flow cytometry

Single-cell suspensions of hiPSC were prepared by Versene/Accutase treatment of cell spheroids. Cell density was determined and $0.5x10^6$ cells were transferred to a microcentrifuge tube, centrifuged at 300*xg* for 5 min and washed with 2% FBS in PBS. The cells were resuspended in 50 µl of a solution containing the primary antibody: TRA-1-60 (Santa Cruz Biotechnology, sc-21705, dilution 6:100) or SSEA4 (Santa Cruz Biotechnology, sc-21704, dilution 1:10). Cells were incubated with the primary antibody solution for 1 hour at 4 ºC, washed with 2% FBS in PBS and centrifuged twice, followed by 30 minutes at 4 ºC incubation with AlexaFluor 488 secondary antibodies (Invitrogen, A21042 for TRA-1-60 and A11001 for SSEA4, dilution 1:1000). Cells were washed and centrifuged twice with 2% FBS in PBS, and finally resuspended in 500 uL of 2% FBS in PBS for flow cytometry analysis. Data was collected on a CyFlow Space flow cytometer from Partec. Cells were gated on forward and side scatter dot plots. 10,000 events per sample were acquired and the data were analyzed with FloMax software (version 3.0).

2.6. Immunofluorescence microscopy

hNSC spheroids were plated on sterile glass coverslips inserted on 24-well plates and left for adherence at 37 ºC and 5% CO_2. Each coverslip containing spheroids were washed once with cold PBS +/+ and then fixed in 500 µL of 4% paraformaldehyde + 4% sucrose in phosphate-buffered saline (PBS) for 20 min at room temperature. Before storage, fixed cells were washed twice with 500 µL PBS. Cells were blocked and permeabilized with 0.2% FSG (Gelatin from cold water fish skin, Sigma, G7765) + 0.1% TritonX-100 in PBS for 20 minutes at room temperature. Primary antibodies were diluted in 0.125% FSG in PBS + 0.1% TritonX-100 and added to fixed spheroids for an incubation of 2 hours at room temperature. Afterwards, cells were washed twice with PBS and incubated with secondary antibodies diluted in 0.125% FSG in PBS for 1 hour and protected from light. Primary and secondary antibodies were used as follows: anti-nestin (Merck Millipore, AB5922), anti-Sox2 (Merck Millipore, AB5603), anti-βIII-tubulin (Merck Millipore, 1:200, MAB1637), AlexaFluor 488 goat anti-rabbit IgG (Invitrogen, A11008), AlexaFluor 594 goat anti-mouse IgG (Invitrogen, A11005). Coverslips were mounted in ProLong Gold antifade reagent with DAPI (Invitrogen, P36935) for staining of cell nuclei. Preparations were visualized on an inverted microscope Leica DMI6000 B (Leica Microsystems). The obtained images were processed using FIJI software (Schindelin et al., 2012) and relying solely on linear adjustments.

2.7. Metabolomic analysis of intracellular extracts

Targeted and quantitative metabolomic analysis was performed using the AbsoluteIDQ® p180 kit and the Energy Metabolism Assay (Biocrates Life Sciences AG, Innsbruck, Austria). The two assays quantify a total of 201 metabolites from different biological classes, including amino acids, biogenic amines, acylcarnitines, lysophosphatidylcholines, phosphatidylcholines, sphingomyelins and several metabolites of the energy metabolism. For the first assay, analyses were carried out after phenylisothiocyanate (PITC)-derivatization in the presence of internal standards by flow-injection tandem mass spectrometry (FIA-MS/MS, for quantification of acylcarnitines, (lyso-) phosphatidylcholines, sphingomyelins, hexoses) and liquid chromatography-tandem mass spectrometry (LC-MS/MS, for amino acids, biogenic amines) using a SCIEX 4000 QTRAP® (SCIEX, Darmstadt, Germany) and a Xevo TQ-S Micro (Waters, Vienna, Austria) instrument with an electrospray ionization (ESI) source. The experimental metabolomics measurement technique is described in detail by patent US 2007/0004044 (accessible online at http://www.freepatentsonline.com/20070004044.html). For the second assay, after derivatization to their corresponding methoxime-trimethylsilyl (MeOx-TMS) derivatives, energy metabolites were determined by gas chromatography-mass spectrometry (GC-MS) using an Agilent 7890 GC/5975 MSD (Agilent, Santa Clara, USA) system. Pretreated samples were evaporated to complete dryness and subjected to a two-step methoximation-silylation derivatization. N-methyl-N-(trimethylsilyl) trifluoroacetamide (MSTFA) was used as silylation reagent. Split injection was performed and chromatograms were recorded in selected ion monitoring (SIM) mode. External

standard calibration curves and ten internal standards were used to calculate concentrations of individual energy metabolites. Data were quantified using the appropriate MS software (Agilent, Masshunter) and imported into Biocrates MetIDQ™ software for further analysis.

2.8. Data pre-processing and statistical analyses

Absolute metabolic values were normalized by the protein content of the cell pellet for each replicated sample (Supplementary Table 3.2). Metabolites with more than 62.5% of missing values or with coefficients of variation greater than 15% were excluded.

For unsupervised analyses, normalized and averaged metabolic values per time-point were z-scored by subtracting to each value the mean for each metabolite-cell and then dividing by the respective standard-deviation. Principal component analysis and hierarchical clustering was performed in Matlab R2015b (MathWorks, Natick MA) and in Perseus software (Tyanova et al., 2016), respectively.

Steady-state fold changes were statistically tested by performing a two-sample t-test, two-sided, at the 5% significance level, assuming the two samples comes from independent random samples from normal distributions with equal means and equal but unknown variances. The Benjamini-Hochberg method was used to correct for multiple testing errors using a false discovery rate of 5% (Benjamini and Hochberg, 1995). These fold-changes were log2-transformed for depiction in volcano plots and in the Pearson Correlation matrices. These statistical tests and correlations were performed in Matlab R2015b (MathWorks, Natick MA).

2.9. Dynamic modelling and characterization of parameters

A classical model from process dynamics and control based on two liquid surge tanks placed in series (Seborg et al., 2011) was used for modelling the dynamical metabolic profiles. The specific model, named second order with numerator dynamics, has different equations for two scenarios: one for an underdamped process and another for an overdamped process, both displayed below and derived after Laplace transformation with its complex variable *s*.

$$Overdamped: y'(s) = \frac{KM(\tau_a s + 1)}{(\tau_2 s + 1)(\tau_1 s + 1)} \quad (1)$$

$$Underdamped: y'(s) = \frac{KM(\tau_a s + 1)}{\tau^2 s^2 + 2\zeta\tau s + 1} \quad (2)$$

Metabolic profiles were fit to these two equations by minimization of the sum of squared residuals. The scenario that presented the lowest residual was chosen. The parameter *M* was calculated based on the concentration of extracellular concentration of glutamine (Supplementary Table 3.1). Fitting of the four other parameters, the steady-state gain K, the numerator coefficient τ_A, the response time τ and the damping coefficient ζ, was performed in MATLAB using lsqnonlin and nlinfit functions. The former function was used to get a first estimation of model parameters which would serve as initial parameters to the latter, as the latter function accepts standard-deviations as weights for fitting. Fits with residual norm above 4% were not considered. The fitting of intracellular glutamine for the four cell lines, instantly subjected to the sudden extracellular glutamine step, using the same model parameters except one, display considerable resemblance and very low average fitting error (Supplementary Figure 3.6). So, to tackle randomness variable

affecting the quantification of moles of metabolites per protein quantity between time-points, experimental values of hNSC (especially affected by the mentioned random variable) were normalized to the shared glutamine profile by multiplying the ratio of simulated value per experimental value of glutamine at that time-point and for that cell line (for all i, g and y, Met normalized $_{\text{i,cell line g, time-point y}}$ = Met $_{\text{i,cell line g, time-point y}}$ x (Gln simulated $_{\text{cell line g, time-point y}}$ / Gln experimental $_{\text{cell line g, time-point y}}$).

The settling time of each fitting curve was determined by finding the time-point after which the metabolic pool value would remain inside a band whose width is equal to ±5% of the final metabolic pool concentration.

The damping coefficient in the overdamped case was calculated directly from the model parameters obtained for each metabolite:

$$In\ Overdamped: \zeta = \frac{\tau_1 + \tau_2}{2\sqrt{\tau_1 \tau_2}}$$

3. Results

3.1 Glutamine perturbation experiments of stem cells in stirred-tank bioreactors

For time-series metabolomics, two cell lines of hiPSC and two cell lines of hiPSC-derived neural stem cells (hNSC) were used (see Materials and Methods). Considering the risk of finding false differences due to cell origin and not due to cell phenotype, one of the hNSC lines used was derived from one of the hiPSC lines (hiPSC 1 and hNSC 1). Cells were cultured as spheroids in stirred-tank bioreactors, displaying high cell viability (Figure 3.1A). This culture

system presents several advantages considering our experimental design, as it allows for a fast and multiple sampling while providing controlled conditions (temperature, pH and pO_2) that maximize the biological reproducibility between replicates (Simão et al., 2016). Cell spheroids of hiPSC and hNSC maintained their phenotype features for the 3 days of the experiment. In hiPSC cultures, over 95% of cells were positive for pluripotency surface markers Tra-1-60 and SSEA4 (Figure 3.1B). The neural progenitor markers nestin, SOX2 and vimentin were detected in hNSC cultures, with rare neuronal βIII-tubulin-positive cells (Figure 3.1C).

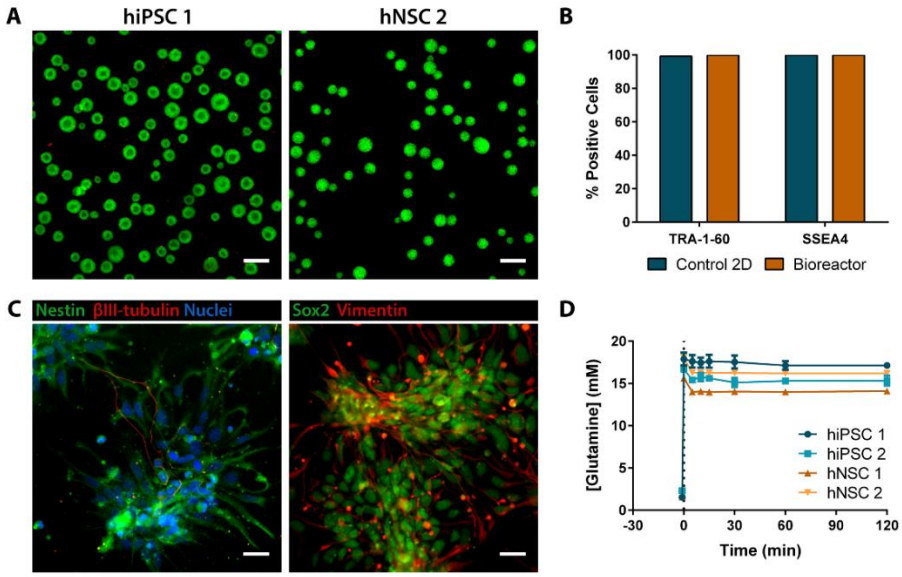

Figure 3.1 – Perturbation experiments of spheroids of hiPSC and hNSC in controlled bioreactors with a sudden glutamine perturbation step. **(A)** Viability analysis of hiPSC 1 and hNSC 2 spheroids in bioreactors by staining with FDA (in green, live cells) and PI (in red, non-viable cells). Scale bars, 200 μm. **(B)** Phenotypic analysis of hiPSC 1 by detection of the pluripotency markers TRA-1-60 and SSEA4 by flow cytometry. **(C)** Phenotypic analysis of hNSC 1 for four neural stem cells markers: Nestin, βIII-tubulin, Sox2 and

Vimentin by immunofluorescence microscopy. Scale bars, 25 µm. **(D)** Glutamine concentration profile: the extracellular glutamine perturbation step was performed from an initial extracellular concentration up to 2.5 mM until a final concentration of around 15 mM at 0 min. Data are represented as mean of sampling replicates and error bars represent standard deviation.

Glutamine, a metabolite critical for hPSC (Tohyama et al., 2016) and hNSC survival (Kleiderman et al., 2015; Palm et al., 2015; Yeo et al., 2013), was chosen for the extracellular perturbations. Indeed, this amino acid, a versatile donor of nitrogen and carbon atoms for diverse biosynthetic reactions, is preferentially consumed by proliferating mammalian cells in comparison with other amino acids (Pavlova et al., 2018). Nucleotides, non-essential amino acids and the anaplerotic substrates of the TCA cycle are all major biosynthetic products of glutamine in human cells (Heiden and Deberardinis, 2017). The intensity of the glutamine step is also important. On one hand, a low intensity could conceal metabolic differences as these would come close to error values of technical sampling replicates. On the other hand, a too high intensity could eventually cause an irreversible homeostatic disruption of intracellular metabolic pools to which cells could not naturally respond and possibly cause phenotypic changes such that metabolic adaptation would not be seen, only the outcome of an uncontrollable disruption. Studies on *E.coli* with glucose steps used an increase of extracellular concentration from 10 to 35 fold (De Mey et al., 2010; Taymaz-Nikerel et al., 2011, 2013). However, with glucose being the initial metabolite of the highly active metabolic pathway of glycolysis, cell dynamics might be more robust to glucose steps than to glutamine

steps, despite glutaminolysis being also an important and active metabolic pathway for hPSC (Tohyama et al., 2016) and hNSC (Kleiderman et al., 2015; Palm et al., 2015; Yeo et al., 2013). The glutamine concentration after the perturbation step was set to 15 mM, i.e., a step increase of at least 6 times over the initial glutamine concentrations of 2.5 mM, which decreased slightly over time due to consumption (Supplementary Table 3.1). The absence of ammonia accumulation after the perturbation step (Supplementary Figure 3.1) corroborates that the final concentration of glutamine is not cytotoxic, as previously reported in murine PSC (Baptista et al., 2013). Furthermore, the quantity of glutamine added did not alter significantly the osmolarity or the ammonia concentration (Supplemental Figure 3.1) or the concentration of glucose and lactate in bioreactor culture media (data not shown). Sampling was done until 2 hours after the glutamine step, as by that time most metabolic pools reached their new steady-state (Supplementary Figure 3.2). Moreover, cell phenotype does not seem to change after glutamine perturbation: pluripotency markers and cell viability of 2D hiPSC cultures have remained unchanged for 72 hours after glutamine perturbation in subsequent experiments.

3.2 Steady-state changes reveal different metabolic phenotypes between hiPSC and hNSC

To study the effects of an extracellular glutamine perturbation step (Figure 3.1D) in the intracellular metabolic network, a set of 201 metabolites from different metabolic classes were analysed over time: amino acids, biogenic amines, acylcarnitines, phosphatidylcholines, lysophosphatidylcholines, sphingomyelins and TCA cycle intermediates. For each sample, metabolic pools

were quantified, normalized to protein content and then averaged per time-point. Two types of pre-processing operations were performed: (i) at sample level, for removing samples that were considered as mistreated during sample preparation/processing (*i.e.*, presenting metabolite concentrations systematically far from its equivalent replicates) and (ii) at metabolite level, for removing metabolites that could not be quantified with accuracy or at all (*i.e.*, presenting null values or below the limit of detection). For the first operation, samples that caused a relative standard deviation (RSD) over 10% on protein normalized concentration for each metabolite and for each time-point, across all metabolites, were considered outliers and removed from analysis (two outliers in hiPSC 1, hiPSC 2 and hNSC 2 and one outlier in hNSC 1, in a total of 8 time-points x 3 replicates for each cell line). Metabolites that had 5 or more time-points with values under the detection limit or with a RSD on averaged molar quantity per protein above 15 % were removed (from 201 measured metabolites for each cell line, 145 metabolites were used in hiPSC 1, 165 in hiPSC 2, 159 in hNSC 1 and 114 in hNSC 2; Supplementary Table 3.3). High variation in average values for different time-points was considered indicative of inadequate extraction or analytical method.

A simple descriptor of steady-state change was determined for each metabolic profile. For each metabolite, changes in steady-states were determined by calculating the ratio of final to initial average molar quantities per protein (fold-change). In order to identify statistically significant changes in steady-states, steady-state values, before the initial glutamine step increase and 2 hours after, were statistically compared by a two-sample t-test at 5% significance level. If null hypothesis prevailed, the steady-states before and after glutamine step were considered to be the same.

Volcano plots of steady-state changes indicate a decrease in the metabolic pools of amino acids for both hiPSC and hNSC. These plots also suggest a trend towards an increase in central energy metabolic pools for hiPSC, while in hNSC lipids, mainly phosphatidylcholines, appear to be affected in their steady-state value (Figure 3.2A). These differences were reproducible between the 2 cell lines of each cell type, with Pearson correlation coefficients above 0.7 (Figure 3.2B). Principal Component Analysis (PCA) showed that most metabolic classes were not clustered in specific regions in the new components space and metabolic classes do not cluster together (Supplementary Figure 3.3A). Hierarchical clustering further demonstrates the heterogeneity of metabolic profiles (Supplementary Figure 3.3B). Thus, unsupervised analyses indicate that responses to glutamine step were dependent on the metabolite and not on the metabolic class, suggesting that a glutamine perturbation is an adequate experiment to inspect the characteristic metabolic dynamics of each metabolic pool. Overall, these results substantiated our initial hypothesis that steady-state analysis is a relevant method for phenotypic identification.

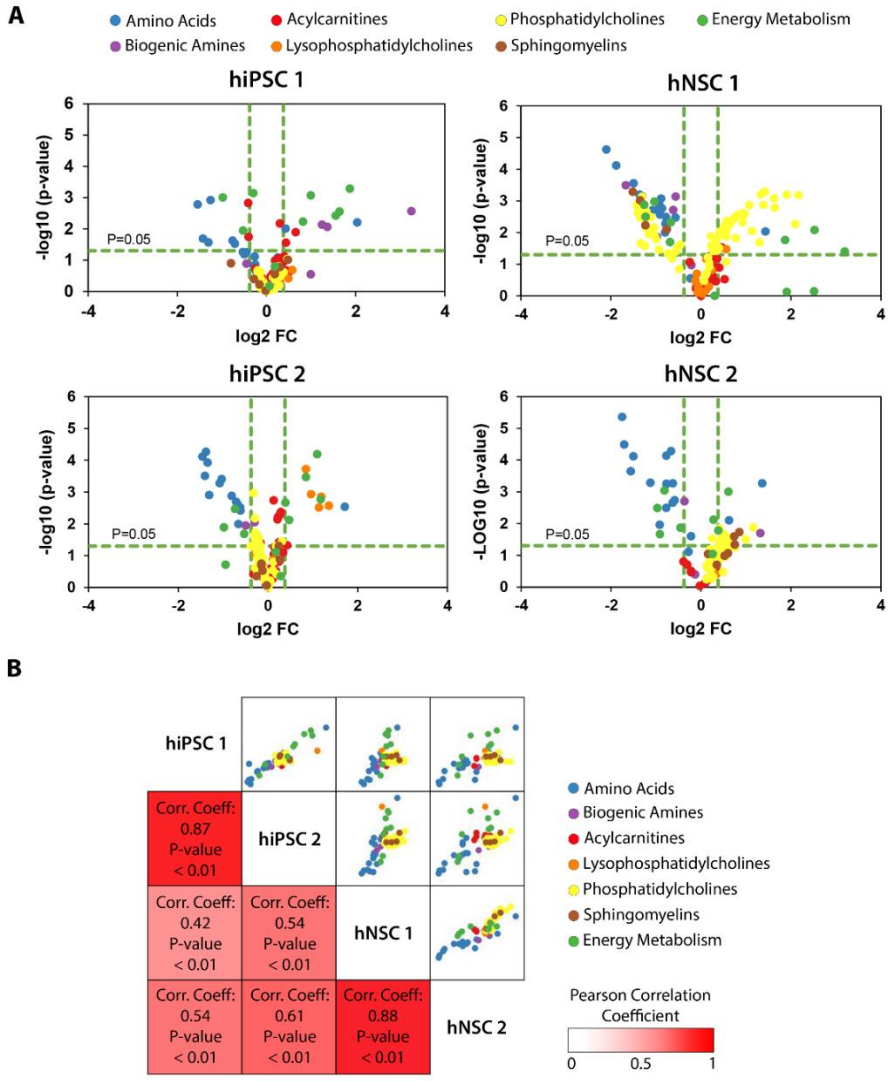

Figure 3.2 – Steady-state changes of hiPSC and hNSC reveal different and conserved responses to the glutamine step. (A) Volcano plots of steady-state changes of metabolites. The threshold for Type I error (α) is 0.05, with a p-value corrected for multiple testing hypothesis (see Materials and Methods), and for a relevant fold-change is 30% difference from initial steady-state. Positive fold-change means increase of intracellular metabolic pool level after glutamine step. **(B)** Pearson correlation matrix of fold-changes of

steady-states of metabolites. Pearson correlation coefficient spans from -1 to 1 where -1 is perfect negative linear correlation, 1 is perfect positive linear correlation and 0 no linear correlation. Typically, Pearson correlation coefficients between 0.7 and 1 denote a strong positive association.

Mapping the steady-state changes onto a metabolic network exposed the global changes in hiPSC and hNSC metabolism after the glutamine step (Figure 3). Preferred metabolic pathways used to tackle the glutamine influx were indirectly inferred for each cell type. In hiPSC, the glutamine step was absorbed by the lower part of the TCA cycle (from alpha-ketoglutarate to malate). The fueling of this section of the TCA cycle in hiPSC was clearly demonstrated by carbon-labelling in the pivotal work of TeSlaa et al. (TeSlaa et al., 2016). On the contrary, in hNSC, the glutamine shock had no effect on increasing the metabolites in the downstream section of the TCA cycle. Instead, the number of lipidic pools for which the steady-state increased was much higher in hNSC than in hiPSC, suggesting an increase in metabolic flux through the upstream section of the TCA cycle. These observations corroborated our previous findings in metabolic flux studies which predicted reductive carboxylation of α-ketoglutarate to fuel fatty acids biosynthesis in NSC (Sá et al., 2017). In contrast to the overall response of TCA cycle intermediates and lipids, most amino acid pools decreased their absolute levels (Figure 3.3). Alanine, arginine and lysine reached far lower steady-states in hNSC. On the other hand, for other amino acids differences were not observed (e.g. threonine) or were observed with fold-changes which were not consistent (e.g. tryptophan).

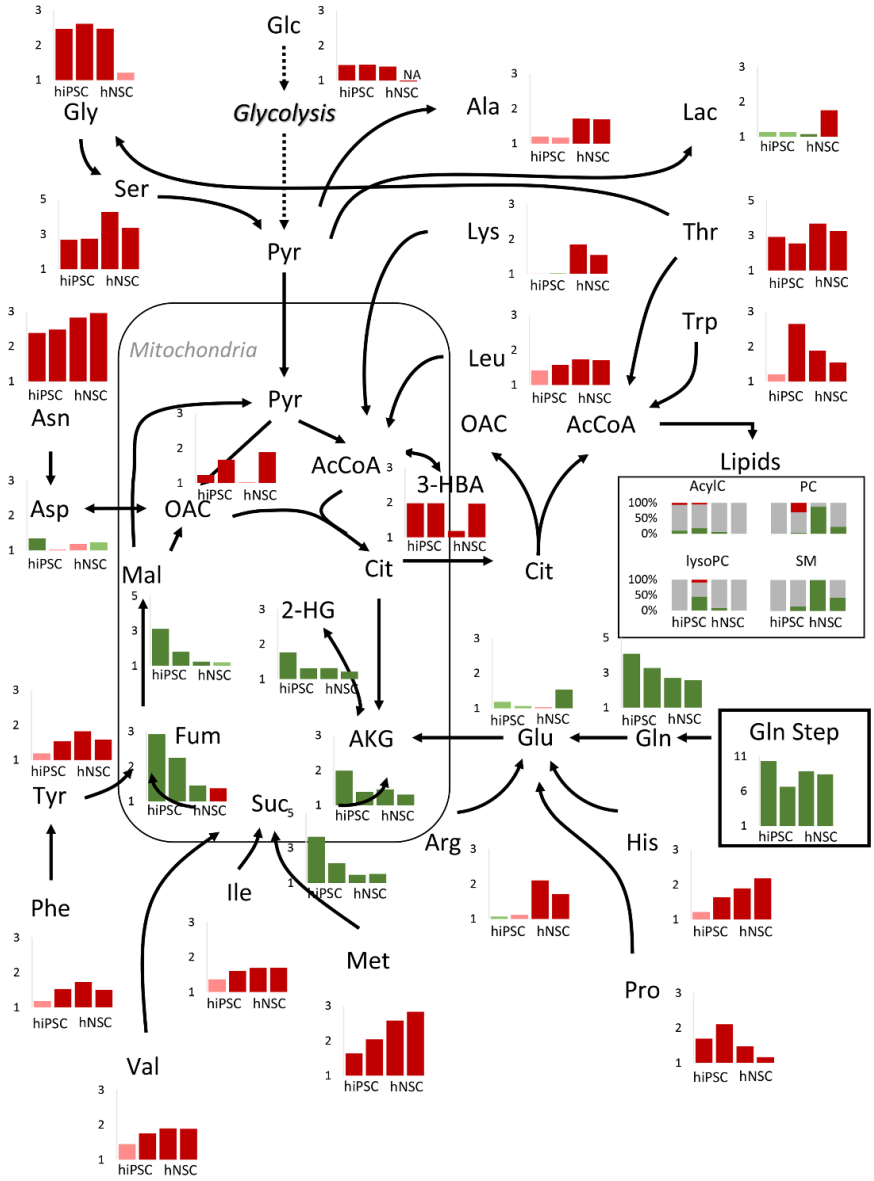

Figure 3.3 – Steady-state fold-changes mapped onto a metabolic network indicate that global responses of intracellular metabolites to glutamine step are cell-dependent. In each graph, fold-changes bars are depicted in the order hiPSC 1, hiPSC 2, hNSC 1 and hNSC 2. Green bars denote positive fold-changes, red bars denote negative fold-changes, dark colored bars

denote fold-changes statistically significant at 5% significance level, light colored bars for fold-changes which are not statistically significant at 5% significance level. In the lipids box, grey bars denote the percentage of lipids that maintained their steady-state, green bars denote the percentage of lipids that reached higher steady-states and red bars the percentage of lipids that reached lower steady-states, at 5% significance level. AcylC: Acylcarnitines, PC: Phosphatidylcholines, LysoPC: Lysophosphatidylcholines, SM: Sphongomyelins.

3.3 Fitting metabolic profiles with a classical process control model exposes conserved transient dynamics

Our data suggests that steady-state changes are cell type-specific, indicative of preferred or active metabolic pathways. We then analysed the transient dynamic profiles of metabolic pools by employing the two liquid surge tanks in series model, typical in the field of process dynamics and control (Seborg et al., 2011). This model was chosen based on the analogy of metabolic pools as liquid tanks and enzymatic reactions connecting the metabolic pools as tubes connecting liquid tanks. Due to the intricacy and redundancy of the metabolic network that naturally leads to the phenomena of inertia in metabolic pools, a numerator factor was added to the model (see Materials and Methods). The obtained second-order model is still able to fit dynamic models of unknown processes (Seborg et al., 2011), in spite of biological systems incorporating both feedforward and feedback control, along with multiloop and multivariable properties (Bhartiya et al., 2006; Seborg et al., 2011). After modelling, mathematical fits with high residual norm were filtered out

(see Materials and Methods and Supplementary Table 3.3). A total of 99, 134, 116 and 71 metabolites for hPSC 1, hPSC 2, NSC 1 and NSC 2 respectively, were fitted to a mean fitting error below 5% (Supplementary Table 3.3). The model successfully fitted at least 60% of the metabolites for each cell line. Moreover, it was flexible enough to represent metabolites that reached different steady-states and that presented distinct dynamics such as initial overshoots and oscillations over time (Figure 3.4). More complex or different types of modelling approaches could be considered. However, to accurately fit the additional parameters of such models, one would need additional sampling points, which in this system would be difficult to achieve as we were near the maximum experimentally possible number of samples.

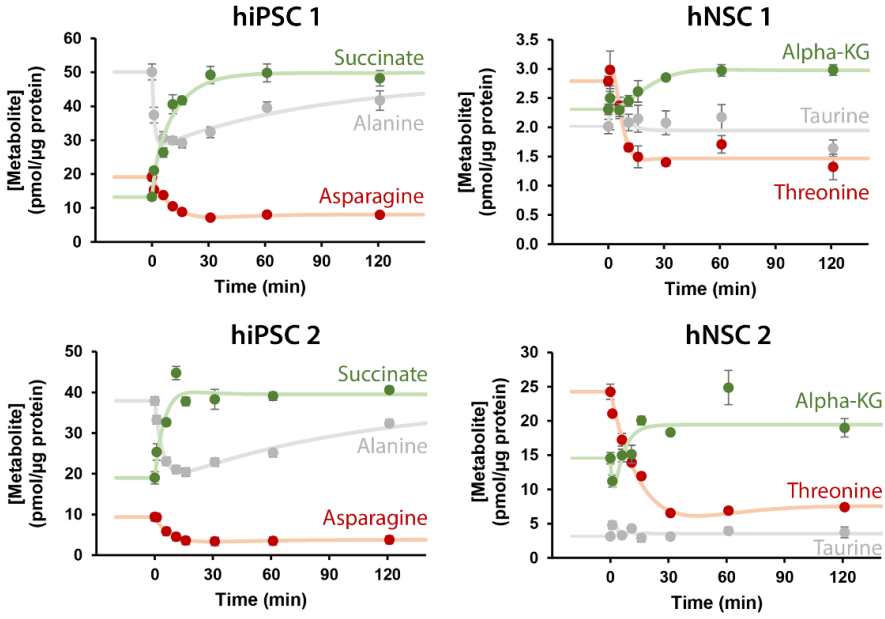

Figure 3.4 – Mathematical model can simulate different types of dynamic responses. In green, examples of intracellular metabolites that reach a new and higher steady-state after the glutamine step, in red examples of metabolites that reach a new and lower steady-state

and in grey examples of metabolites that keep the same steady-state. Data are represented as mean of sampling replicates and error bars represent standard deviation. Solid lines represent the mathematical fitting to the experimental data.

The modelling of transient dynamic metabolic profiles captures a layer of information that is not present in analysis of dynamics by fold-changes of steady-states. Indeed, using the fold-change of steady-states for discriminating between hiPSC and hNSC increases the quality of the classification model with an area under the curve of 0.79, better than using initial or final steady-states alone (Figure 3.5A). A classification model is considered good when its area under the curve is above 0.8, where the accuracy of identification is no longer penalized by a high number of false positives. Alternatively, inspecting transient dynamics may contribute to reveal more precisely distinct conserved metabolic features in hiPSC and hNSC (Figure 3.5B). As depicted for alanine and histidine, transient dynamics reveal metabolic characteristics such as the overall robustness and speed of the response which fold-change of steady-states cannot (Figure 3.5B). Even when considering the more sophisticated tool of fold-changes of steady-states, it is entirely possible that the same metabolite, in both cell types, can have the same fold-change but in one cell type show oscillations or overshoots while in the other cell type that behaviour is not observed. Therefore, the ability of distinction between cell types is increased when profiling transient dynamics.

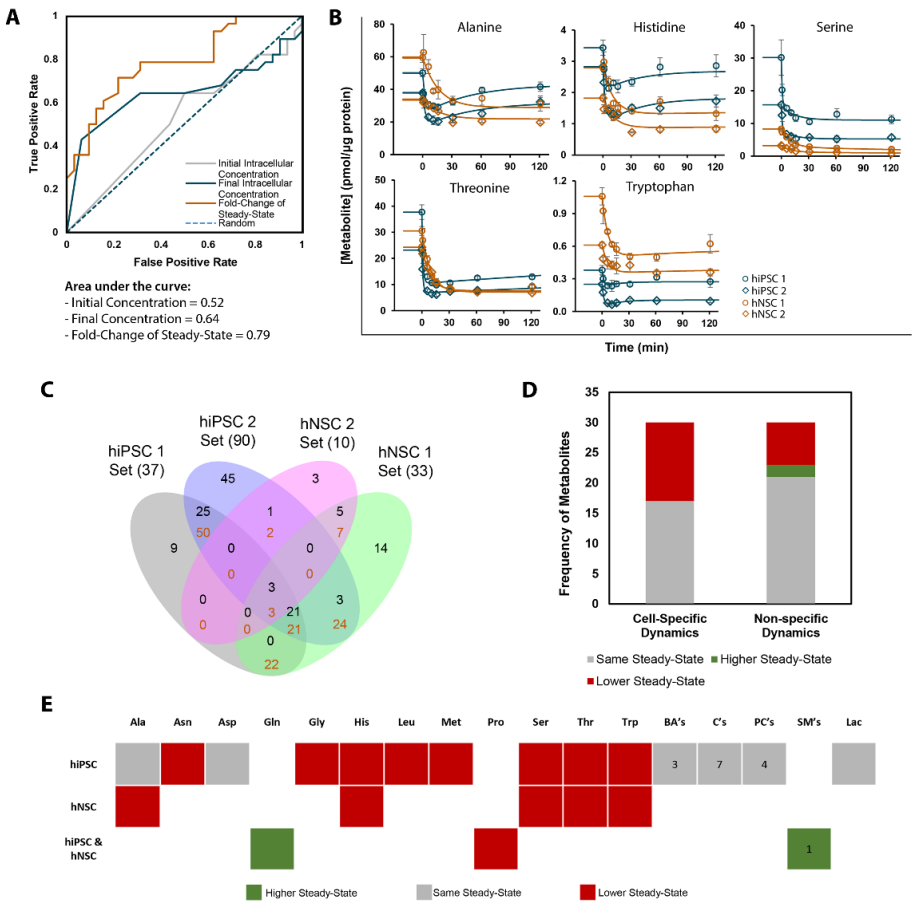

Figure 3.5 – Identification of metabolites with cell type-specific-dynamics reveals the amino acid class as highly conserved in hiPSC and hNSC and that most of the cell type-specific amino acids decreased their steady-state upon glutamine step increase. (A) Receiver operating characteristic (ROC) curves show the fraction of metabolic pairs correctly/incorrectly identified as deriving from different cells by the application of three models: one based on comparison of initial intracellular concentration, another based on comparison of final intracellular concentration, and the last one based on the fold-change of steady-state after the glutamine step. **(B)** Metabolic profiles of all metabolites with cell type-specific

dynamics in hNSC and their respective cell type-specific dynamics in hiPSC. Experimental points: hiPSC 1 – blue round circles, hiPSC 2 – blue diamonds, hNSC 1 – orange round circles and hNSC 2 – orange diamonds. Adjusted models for cell type-specific dynamics: hiPSC in blue lines and hNSC in orange lines. Data are represented as mean of sampling replicates and error bars represent standard deviation. **(C)** Venn diagram of metabolites with common dynamics. In each intersection, only metabolites with a mean fitting error below 4% are accepted. Black numbers indicate the number of simulated metabolic profiles which fit, specifically to that region and not to any other region with the same or higher number of intersections. Orange numbers indicate the number of all simulated metabolic profiles that fit to that region, regardless of fitting to other regions with the same or higher number of intersections. **(D)** Distribution of simulated metabolic profiles according to the steady-state outcome for metabolites with cell type-specific dynamics and with non-specific dynamics (acceptable fits between at least two cell lines of different cell types). **(E)** Heatmap of metabolites with unique dynamics for hiPSC and for hNSC and of metabolites with dynamics shared by all cells lines, divided in steady-state outcome. Lipids were lumped in classes and the numbers inside its boxes are the number of lipids from that class with dynamics which are cell type-specific or are common to hiPSC and hNSC. BA's: Biogenic Amines; C's: Acylcarnitines; PC's: Phosphatidylcholines; SM's: Sphingomyelins. (See Supplementary Table 3.5 for the total list of metabolites with conserved dynamics).

3.4 Amino acids show conserved dynamics and readjust their intracellular pools without resorting to oscillations

Following the evidence that metabolic dynamics were generally reproducible between cell lines of the same cell type but not between cell types, metabolites from the same cell type were fit using the same model parameters, except for the parameter process gain, in order to identify which metabolites had conserved dynamics in hiPSC and hNSC (additional details in the Materials and Methods). However, the definition of an acceptable fitting error threshold, adequate for claiming a different dynamic metabolic response between cells, has to be rationally evaluated.

Therefore, the number of metabolites fitted in all cell lines with acceptable fitting error and included after the pre-filtering step (Supplementary Table 3.3), was graphed over the threshold fitting error (Supplementary Figure 3.4). Each metabolite was fit to all possible combinations for four, three and two cell lines. At a large threshold, all fits of common metabolites belonged to the case of simultaneous fitting to the four cell lines. As the threshold reached to 4% of fitting error, the number of metabolites with fit to the four cells scenario decreases while the fit to hiPSC cell lines and to hNSC cell lines scenario reached their maximum (Supplementary Figure 3.4A-B). With this threshold for fitting error, the Venn diagram of all metabolic fits showed a relevant amount of metabolites with conserved dynamics, especially for hiPSC (Figure 5C).

When comparing these cell type-specific metabolic profiles with the metabolic profiles that were shared, at least, between two cell lines of hiPSC and hNSC, control characteristics such as settling time and damping coefficient could not discriminate those groups

(Supplementary Figure 3.5). Settling time is the time a perturbed process takes to stabilize to a 5% margin of its final steady-state. The damping coefficient relates to the oscillatory behavior. Lower than but close to one means the process is slightly oscillatory in order to reach the region of the new steady-state faster. Above one means that the process is more sluggish and therefore robustness of response is preferred over fastness. This means that damped processes tend to be more stable to unmeasured and unexpected disturbances. Then, for metabolites with unique and shared dynamics, robustness and stable responses seem to be preferred over response speed (Supplementary Figure 3.5).

In terms of steady-state outcome, a substantial fraction of the metabolites with cell type-specific dynamics adjusted their set-point to a lower value after the glutamine step (Figure 3.5D). This fraction was significantly lower in metabolites with shared dynamics across hiPSC and hNSC. Interestingly, all of these metabolites were amino acids, many with characteristic and distinct dynamics in hiPSC and hNSC (Figure 3.5B, Figure 3.5E and Supplementary Table 3.5).

4. Discussion

Control of metabolic pools is paramount for cell homeostasis as metabolism has a strong effect on the epigenome, transcriptome, proteome, metabolome and fluxome through varied mechanisms of action. Mathematical modelling of all the interactions of metabolism with other cellular components is still very challenging and appropriate mathematical tools are not yet available. Thus, an understanding of what is the identity of metabolic phenotype when metabolism can adjust itself to environmental changes is slim. Our hypothesis changes the focus from modelling the general to

modelling the particular, considering each metabolic pool individually. We resorted to a perturbation experiment where an extracellular glutamine step was applied and dynamic intracellular metabolomics was assessed. The observation of metabolic changes allowed an analysis of the essential and constant metabolic features of the cells, and of the key metabolites that seemed to govern the metabolic response. To our knowledge, this is the first time an experiment of this type is performed in human stem cells to uncover intrinsic dynamics of metabolic pools, while other works have mainly been focused on transition to new metabolic programs. Dynamic metabolomics on adipocytes upon insulin stimulation reported on metabolic rearrangements in central carbon metabolism (Krycer et al., 2017) and a sudden reactive oxygen species stress to *E. coli* unravelled novel allosteric regulations in glycolysis and in pentose phosphate pathway (PPP) (Christodoulou et al., 2018).

In our study, most metabolites in hiPSC and in hNSC had their most relevant dynamics for 30 min after the glutamine step, similar to what was obtained for metabolites upon insulin stimulation in adipocytes (Krycer et al., 2017). In *E. coli*, metabolites responded quickly to extracellular changes and achieved the new steady-state in less than 40 seconds (Christodoulou et al., 2018; Taymaz-Nikerel et al., 2013). Mammalian cells are larger in size, more compartmentalized and with much slower dynamics. Studies of this type on human cells should be designed to perform intensive sampling during the first 30 minutes after the challenge with time intervals as short as possible. Nevertheless, perturbation steps with metabolites are easier to implement than perturbation of fluxes by overexpressing enzymes (Tanner et al., 2018). Given the limited time frame, the dynamic response observed in this work should not be regulated at the gene expression level, as protein synthesis rate

in mammalian cells is usually in the time frame of hours (Kristensen et al., 2013), but rather by regulation of enzyme activity. Future studies focused on the proteome and post-translational modifications could contribute to clarify what are the main responsible molecular regulators Also, correlation with gene expression data (at wider time frames) would be valuable in attempting to understand the downstream impact of the metabolic perturbations and its effect on cell phenotype.

The exploratory approach of this study required broad metabolomics coverage. Different classes of metabolites were quantified, especially from pathways close to the glutamine pathway where the external perturbation was performed: TCA intermediates, amino acids, biogenic amines and lipids. Previous works, in E.coli and human skin cells, sharing related concepts or objectives usually focused on glycolysis and PPP (Christodoulou et al., 2018; Kuehne et al., 2015). Herein, the focus was on TCA cycle, amino acid metabolism and lipidic pathways, as these pathways have higher probability of being cell type-specific than foundational pathways such as glycolysis and PPP. Indeed, it has been previously reported that TCA intermediates influence hPSC differentiation (TeSlaa et al., 2016), amino acids and biogenic amines influence the cell fate of hiPSC (Shiraki et al., 2014), of T-cells (Geiger et al., 2016) and of oligodendrocyte precursor cells (Beyer et al., 2018). Lipid levels have been found to be changed between hiPSC and ESC (Panopoulos et al., 2012) and to promote important signalling for insulin-glucose homeostasis (Yore et al., 2014). The Pearson correlation for fold-change of steady-state demonstrated these features were very well conserved in hiPSC and hNSC, independently of the metabolic class. Importantly, this successful correlation demonstrates the potential of simple steady-state fold-

change analysis as a method for phenotypic characterization, in contrast with using intracellular metabolic levels for discriminating different cell types, as used recently in cancer cell lines (Li et al., 2019). Moreover, steady-state changes from dynamic analysis allowed for a systemic perspective on the metabolic response of hiPSC and hNSC to the glutamine perturbation. We identified a systemic response towards specific metabolic pathways instead of a uniform flux distribution. This type of behavior has been also observed for adipocytes (Krycer et al., 2017). Interestingly, our results closely match the data obtained by carbon-labelling experiments, usually more expensive and labor-intensive (Sá et al., 2017; TeSlaa et al., 2016). Thus, the use of perturbation experiments could be developed in the future to benefit metabolic flux studies.

The correlation of metabolic steady-state fold-changes between hiPSC and hNSC was still high and statistically significant. In order to prove with greater confidence that metabolic dynamics are cell type-specific, analysis of transient dynamics was used. The chosen model for fitting was the simplest one that could incorporate inertia in response. In order to get 100% of successful fittings, more complex models (and different types) would have to be used. That would allow us to detect different groups of dynamic response but would require more sampling points, as the number of parameters to be fitted would increase. Nevertheless, the relatively simple model permitted the identification of metabolites with cell type-specific dynamics. Half of them decreased their intracellular metabolic steady-state against one quarter of the metabolites with shared dynamics across cell types. Interestingly, all of those metabolites with cell type-specific dynamics and with decreased steady-state were amino acids. Some of the identified amino acids are known to have important cell regulatory functions. A controlled level of

intracellular methionine and of the enzymes involved in its metabolism has been shown to be crucial for maintenance of pluripotency in hiPSC (Shiraki et al., 2014). In a specific subtype of breast cancer with stem-cell like properties, asparagine has been pointed out as a key factor for governing metastasis (Knott et al., 2018). Asparagine has also been shown as regulator of protein synthesis in mammalian cells (Pavlova et al., 2018). Serine supports proliferation of the breast cancer cells (Labuschagne et al., 2014). In addition, serine as well as glycine, are involved in one-carbon metabolism that influence epigenetics in human cells (Locasale, 2013). Besides the biological importance of the identification of amino acids having dynamics which are cell-type specific, this result suggests that targeted approaches for identification of amino acid dynamics may be sufficient for cell identity characterization, instead of the more complex and expensive untargeted metabolomics studies. Moreover, the prevalence of amino acids in metabolic response is advantageous as respective analytical methods are easier, amino acid pool levels tend to be large allowing a simulation fit of dynamic data, and many experimental means are available to the researcher such as label tracers or enzymatic activation/inhibition chemicals.

In the near future, the analysis of dynamics by control parameters such as damping coefficient and settling time might be decisive for ranking the metabolites as potential targets for cell homeostasis regulation. This would tackle another problem concerning classical comparative metabolomics where it is unclear how to accurately identify which molecule among the numerous changed metabolic pools is likely to be the most effective phenotype modulator (Guijas et al., 2018). The manipulation of effective phenotype modulators to induce cell fate decisions would bring

enormous advances in cell therapy and regenerative medicine. After all, reprogramming somatic cells into pluripotent stem cells, expanding stem cells, differentiating stem cells and transdifferentiating cells constitute bioprocesses that are often time-consuming, inefficient and expensive.

Overall, we propose a methodology with considerable specificity for metabolic characterization and for the identification of metabolites characteristic of a cell phenotype by modelling dynamic metabolomics. In this work, we identified metabolic signatures of stemness of hiPSC and of NSC that can potentially be used to solve lingering doubts about differences in phenotype related to cell origins, in the pluripotent and neural stem cell fields. The unbiased nature of the proposed method allows it to be expanded to many other metabolic pathways by performing perturbation steps with different metabolites and by performing more comprehensive untargeted metabolomics, which is increasingly improving its sensitivity and throughput (Guijas et al., 2018). Coupling these dynamic studies with mathematical modelling in future investigations will lead to a better metabolic understanding on cell regulation and opens an avenue for cell fate manipulation.

5. Author contributions

J.V.S., D.S., I.I. and P.M.A. conceived the project. J.V.S., D.S., A.P.T., M.M.S., C.B. and I.I devised the adequate methodology. J.V.S. created the Matlab scripts for the statistical analysis and mathematical fitting of the experimental data.; J.V.S. and D.S. applied other statistical tools to analyse and synthesize experimental data. J.V.S, D.S., A.P.T. and M.M.S. carried out the experiments. A.P.T., M.M.S, C.B., P.M.A. and M.J.T.C provided all study

materials, reagents, instrumentation and computing resources. J.V.S. wrote the original draft. J.V.S, D.S., I.I., C.B. P.M.A. and M.J.T.C. reviewed and edited the manuscript. J.V.S., D.S. and I.I. devised how the data should be visualized. I.I., C.B., P.M.A. and M.J.T.C supervised and guided the research planning and execution. All authors read and approved the final manuscript.

6. Acknowledgments

We gratefully acknowledge Dr Tomo Šaric (University of Cologne, Germany) for the supply of hNSC 2. We thank Francisca Arez (iBET) for assistance with sample processing. We also thank Rui M.C. Portela (GSK Vaccines) and Marta Abreu Paiva (iBET) for insightful discussions.

7. Availability of data and materials

Data have been deposited at the MetaboLights database (https://www.ebi.ac.uk/metabolights/) with the accession number MTBLS1349.

8. References

Abecasis, B., Aguiar, T., Arnault, É., Costa, R., Gomes-Alves, P., Aspegren, A., Serra, M., and Alves, P.M. (2017). Expansion of 3D human induced pluripotent stem cell aggregates in bioreactors : Bioprocess intensification and scaling-up approaches. J. Biotechnol. *246*, 81–93.

Baptista, R.P., Fluri, D.A., and Zandstra, P.W. (2013). High density continuous production of murine pluripotent cells in an acoustic

perfused bioreactor at different oxygen concentrations. Biotechnol. Bioeng. *110*, 648–655.

Benjamini, Y., and Hochberg, Y. (1995). Controlling the False Discovery Rate : A Practical and Powerful Approach to Multiple Testing. J. R. Stat. Soc. Ser. B *57*, 289–300.

Beyer, B.A., Fang, M., Sadrian, B., Montenegro-Burke, J.R., Plaisted, W.C., Kok, B.P.C., Saez, E., Kondo, T., Siuzdak, G., and Lairson, L.L. (2018). Metabolomics-based discovery of a metabolite that enhances oligodendrocyte maturation. Nat. Chem. Biol. *14*, 22–28.

Bhartiya, S., Chaudhary, N., Venkatesh, K. V, and Doyle, F.J. (2006). Multiple feedback loop design in the tryptophan regulatory network of Escherichia coli suggests a paradigm for robust regulation of processes in series. J. R. Soc. Interface *3*, 383–391.

Bulusu, V., and Aulehla, A. (2016). Metabolic Control of Cellular Differentiation. Dev. Cell *39*, 286–287.

Cai, L., Sutter, B.M., Li, B., and Tu, B.P. (2011). Acetyl-CoA induces cell growth and proliferation by promoting the acetylation of histones at growth genes. Mol. Cell *42*, 426–437.

Chambers, S.M., Fasano, C. a, Papapetrou, E.P., Tomishima, M., Sadelain, M., and Studer, L. (2009). Highly efficient neural conversion of human ES and iPS cells by dual inhibition of SMAD signaling. Nat. Biotechnol. *27*, 275–280.

Christodoulou, D., Link, H., Fuhrer, T., Kochanowski, K., Gerosa, L., and Sauer, U. (2018). Reserve Flux Capacity in the Pentose Phosphate Pathway Enables Escherichia coli's Rapid Response to Oxidative Stress. Cell Syst. *6*, 1–10.

Geiger, R., Rieckmann, J.C., Wolf, T., Zamboni, N., Sallusto, F., Lanzavecchia, A., Geiger, R., Rieckmann, J.C., Wolf, T., Basso, C., et al. (2016). L-Arginine Modulates T Cell Metabolism and Enhances Survival and Anti-tumor Activity. Cell *167*, 829–842.

Gerosa, L., and Sauer, U. (2011). Regulation and control of metabolic fluxes in microbes. Curr. Opin. Biotechnol. *22*, 566–575.

Guijas, C., Montenegro-Burke, J.R., Warth, B., Spilker, M.E., and Siuzdak, G. (2018). Metabolomics activity screening for identifying metabolites that modulate phenotype. Nat. Biotechnol. *36*, 316–320.

Harvey, A.J., Rathjen, J., and Gardner, D.K. (2016). Metaboloepigenetic Regulation of Pluripotent Stem Cells. Stem Cells Int.

Heiden, M.G. Vander, and Deberardinis, R.J. (2017). Understanding the Intersections between Metabolism and Cancer Biology. Cell *168*, 657–669.

Kaelin, W.G., and McKnight, S.L. (2013). Influence of Metabolism on Epigenetics and Disease. Cell *153*, 56–69.

Kleiderman, S.M., Sá, J. V, Teixeira, A.P., Brito, C., Gutbier, S., Evje, L.G., Hadera, M.G., Glaab, E., Henry, M., Agapios, S., et al. (2015). Functional and phenotypic differences of pure populations of stem cell-derived astrocytes and neuronal precursor cells. Glia *64*, 1–21.

Knott, S.R.V., Wagenblast, E., Khan, S., Kim, S.Y., Soto, M., Wagner, M., Turgeon, M., Fish, L., Erard, N., Gable, A.L., et al. (2018). Asparagine bioavailability governs metastasis in a model of breast cancer. Nature *554*, 378–381.

Kristensen, A.R., Gsponer, J., and Foster, L.J. (2013). Protein synthesis rate is the predominant regulator of protein expression

during differentiation. Mol. Syst. Biol. *9*, 1–12.

Krycer, J.R., Yugi, K., Hirayama, A., Fazakerley, D.J., Quek, L.-E., Scalzo, R., Ohno, S., Hodson, M.P., Ikeda, S., Shoji, F., et al. (2017). Dynamic Metabolomics Reveals that Insulin Primes the Adipocyte for Glucose Metabolism. Cell Rep. *21*, 3536–3547.

Kuehne, A., Emmert, H., Soehle, J., Winnefeld, M., Fischer, F., Wenck, H., Gallinat, S., Terstegen, L., Lucius, R., Hildebrand, J., et al. (2015). Acute Activation of Oxidative Pentose Phosphate Pathway as First-Line Response to Oxidative Stress in Human Skin Cells. Mol. Cell *59*, 359–371.

Labuschagne, C.F., van den Broek, N.J.F., Mackay, G.M., Vousden, K.H., and Maddocks, O.D.K. (2014). Serine, but Not Glycine, Supports One-Carbon Metabolism and Proliferation of Cancer Cells. Cell Rep. *7*, 1248–1258.

Li, H., Ning, S., Ghandi, M., Kryukov, G. V., Gopal, S., Deik, A., Souza, A., Pierce, K., Keskula, P., Hernandez, D., et al. (2019). The landscape of cancer cell line metabolism. Nat. Med. *25*, 850–860.

Locasale, J.W. (2013). Serine, glycine and one-carbon units: cancer metabolism in full circle. Nat. Rev. Cancer *13*, 572–583.

McKnight, S.L. (2010). On Getting There from Here. Science *330*, 1338–1339.

De Mey, M., Taymaz-Nikerel, H., Baart, G., Waegeman, H., Maertens, J., Heijnen, J.J., and van Gulik, W.M. (2010). Catching prompt metabolite dynamics in Escherichia coli with the BioScope at oxygen rich conditions. Metab. Eng. *12*, 477–487.

Palm, T., Bolognin, S., Meiser, J., Nickels, S., Träger, C., Meilenbrock, R.-L., Brockhaus, J., Schreitmüller, M., Missler, M., and

Schwamborn, J.C. (2015). Rapid and robust generation of long-term self-renewing human neural stem cells with the ability to generate mature astroglia. Sci. Rep. *5*, 1–16.

Panopoulos, A.D., Yanes, O., Ruiz, S., Kida, Y.S., Diep, D., Tautenhahn, R., Herrerías, A., Batchelder, E.M., Plongthongkum, N., Lutz, M., et al. (2012). The metabolome of induced pluripotent stem cells reveals metabolic changes occurring in somatic cell reprogramming. Cell Res. *22*, 168–177.

Pavlova, N.N., Hui, S., Ghergurovich, J.M., Fan, J., Intlekofer, A.M., White, R.M., Rabinowitz, J.D., Thompson, C.B., and Zhang, J. (2018). As Extracellular Glutamine Levels Decline, Asparagine Becomes an Essential Amino Acid. Cell Metab. *27*, 1–11.

Rehberg, M., Rath, A., Ritter, J.B., Genzel, Y., and Reichl, U. (2014). Changes in intracellular metabolite pools during growth of adherent MDCK cells in two different media. Appl. Microbiol. Biotechnol. *98*, 385–397.

Sá, J. V., Kleiderman, S., Brito, C., Sonnewald, U., Leist, M., Teixeira, A.P., and Alves, P.M. (2017). Quantification of Metabolic Rearrangements During Neural Stem Cells Differentiation into Astrocytes by Metabolic Flux Analysis. Neurochem. Res. *42*, 244–253.

Schindelin, J., Arganda-Carreras, I., Frise, E., Kaynig, V., Longair, M., Pietzsch, T., Preibisch, S., Rueden, C., Saalfeld, S., Schmid, B., et al. (2012). Fiji: An Open Source platform for biological image analysis. Nat. Methods *9*, 676–682.

Seborg, D.E., Edgar, T.F., Mellichamp, D.A., and Doyle III, F.J. (2011). Process Dynamics and Control (New Dehli: Wiley).

Shiraki, N., Shiraki, Y., Tsuyama, T., Obata, F., Miura, M., Nagae,

G., Aburatani, H., Kume, K., Endo, F., and Kume, S. (2014). Methionine Metabolism Regulates Maintenance and Differentiation of Human Pluripotent Stem Cells. Cell Metab. *19*, 780–794.

Simão, D., Arez, F., Terasso, A.P., Pinto, C., Sousa, M.F.Q., Brito, C., and Alves, P.M. (2016). Perfusion Stirred-Tank Bioreactors for 3D Differentiation of Human Neural Stem Cells. In Bioreactors in Stem Cell Biology, E. Turksen, ed. (New York, NY: Humana Press), pp. 129–142.

Simão, D., Silva, M.M., Terrasso, A.P., Arez, F., Sousa, M.F.Q., Mehrjardi, N.Z., Šaric, T., Gomes-Alves, P., Raimundo, N., Alves, P.M., et al. (2018). Recapitulation of Human Neural Microenvironment Signatures in iPSC-Derived NPC 3D Differentiation. Stem Cell Reports *11*, 1–13.

Tanner, L.B., Goglia, A.G., Wei, M.H., Sehgal, T., Parsons, L.R., Park, J.O., White, E., Toettcher, J.E., and Rabinowitz, J.D. (2018). Four Key Steps Control Glycolytic Flux in Mammalian Cells. Cell Syst. *7*, 49–62.

Taymaz-Nikerel, H., van Gulik, W.M., and Heijnen, J.J. (2011). Escherichia coli responds with a rapid and large change in growth rate upon a shift from glucose-limited to glucose-excess conditions. Metab. Eng. *13*, 307–318.

Taymaz-Nikerel, H., Mey, M. De, Baart, G., Maertens, J., Heijnen, J.J., and van Gulik, W. (2013). Changes in substrate availability in Escherichia coli lead to rapid metabolite, flux and growth rate responses. Metab. Eng. *16*, 115–129.

TeSlaa, T., Chaikovsky, A.C., Lipchina, I., Escobar, S.L., Hochedlinger, K., Huang, J., Graeber, T.G., Braas, D., Teitell, M.A., Birsoy, K., et al. (2016). α-Ketoglutarate Accelerates the Initial

Differentiation of Primed Human Pluripotent Stem Cells. Cell Metab. *24*, 485–493.

Tohyama, S., Fujita, J., Hishiki, T., Matsuura, T., Hattori, F., Ohno, R., Kanazawa, H., Seki, T., Nakajima, K., Kishino, Y., et al. (2016). Glutamine Oxidation Is Indispensable for Survival of Human Pluripotent Stem Cells. Cell Metab. *23*, 663–674.

Tyanova, S., Temu, T., Sinitcyn, P., Carlson, A., Hein, M.Y., Geiger, T., Mann, M., and Cox, J. (2016). The Perseus computational platform for comprehensive analysis of (prote)omics data. Nat. Methods *13*, 731–740.

Yeo, H., Lyssiotis, C. a, Zhang, Y., Ying, H., Asara, J.M., Cantley, L.C., and Paik, J.-H. (2013). FoxO3 coordinates metabolic pathways to maintain redox balance in neural stem cells. EMBO J. *32*, 2589–2602.

Yore, M.M., Syed, I., Moraes-Vieira, P.M., Zhang, T., Herman, M.A., Homan, E.A., Patel, R.T., Lee, J., Chen, S., Peroni, O.D., et al. (2014). Discovery of a Class of Endogenous Mammalian Lipids with Anti-Diabetic and Anti-inflammatory Effects. Cell *159*, 318–332.

Zhang, H., Badur, M.G., Divakaruni, A.S., Parker, S.J., Jäger, C., Hiller, K., Murphy, A.N., and Metallo, C.M. (2016). Distinct Metabolic States Can Support Self-Renewal and Lipogenesis in Human Pluripotent Stem Cells under Different Culture Conditions. Cell Rep. *16*, 1536–1547.

Zhang, J., Zhao, J., Dahan, P., Lu, V., Zhang, C., Li, H., and Teitell, M.A. (2018). Metabolism in Pluripotent Stem Cells and Early Mammalian Development. Cell Metab. *27*, 332–338.

9. Supporting Information

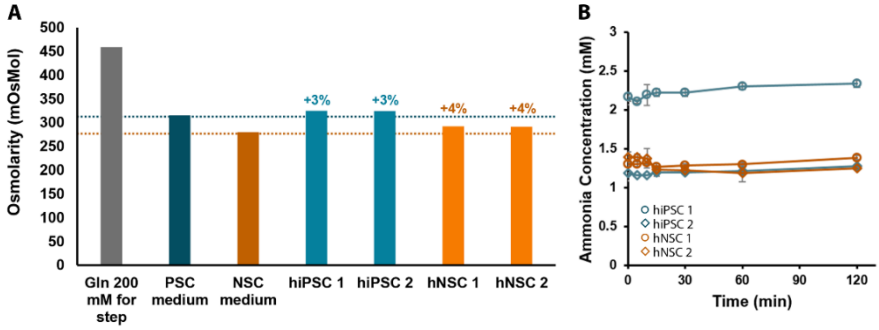

Supplementary Figure 3.1 – Effect of glutamine steps in hiPSC and hNSC bioreactors on extracellular environment. (A) Osmolarity of the solution of glutamine used for the perturbation step, of the cell culture media used for hiPSC and hNSC and of the culture media of the four bioreactor cultures immediately after the glutamine perturbation step. Changes in osmolarity after perturbation step are indicated in percentage on top of each bar. Osmolarity after the glutamine step changed less than 5%. **(B)** Ammonia concentration in bioreactors culture media.

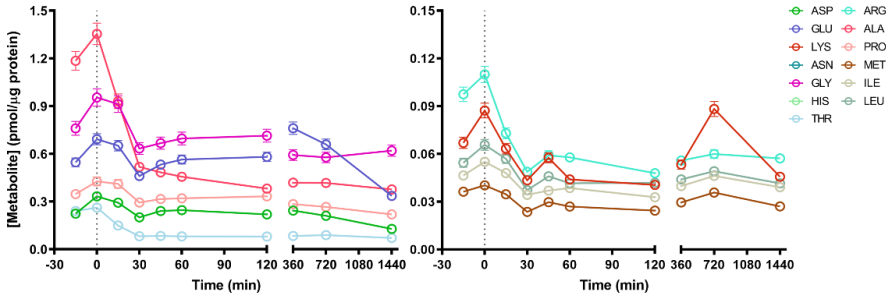

Supplementary Figure 3.2 – Intracellular metabolites reach their steady-state after approximately 2 hours. Metabolic profiles of different amino acids in an experiment covering up to 24 hours after

the glutamine step increase hNSC 1 demonstrating that 2 hours is sufficient to reach a new metabolic steady-state.

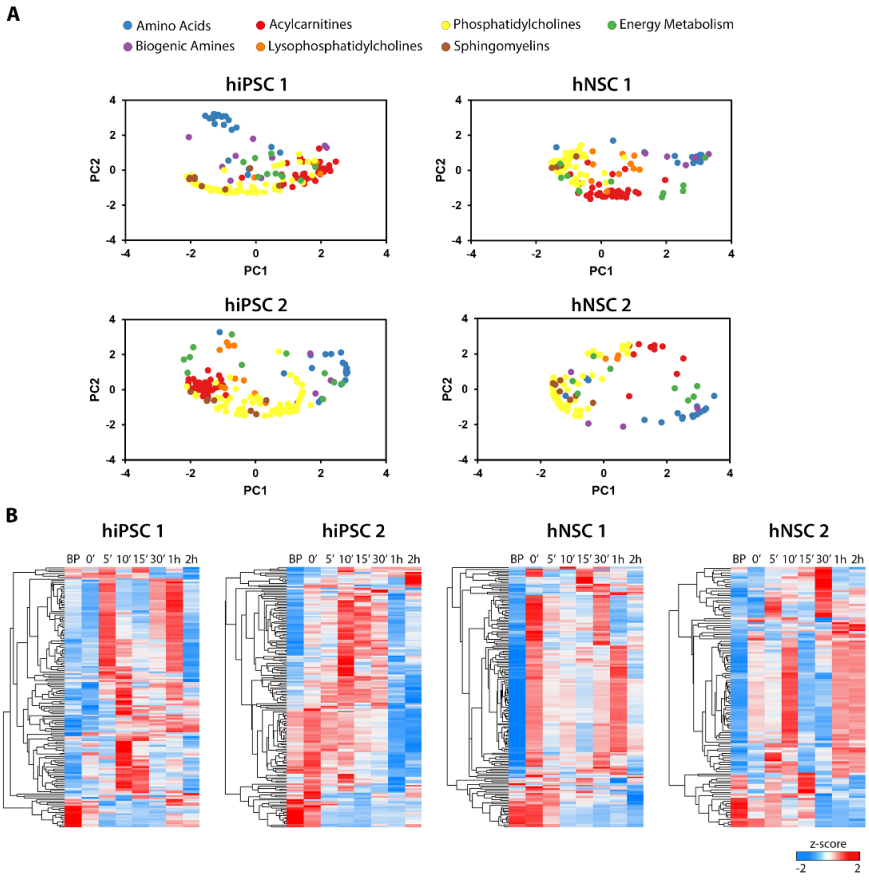

Supplementary Figure 3.3 – Unsupervised analysis of dynamic profiles of intracellular metabolites after glutamine step perturbation. The dynamic profiles of molar quantities per protein were normalized by a z-score procedure (see Materials and Methods). **(A)** Principal component analysis of metabolic profiles. **(B)** Hierarchical clustering of metabolic profiles. Rows represent the different metabolites, while each column represents one time point (BP – before pulse, 0, 5, 10, 15, 30 min, 1, 2 hours).

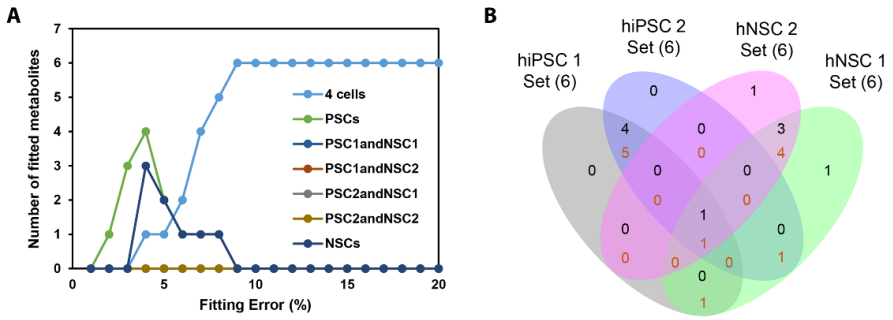

Supplementary Figure 3.4 – Selecting the ideal fitting error threshold to allow a confident identification of metabolites with cell type-conserved dynamics. (A) Frequency of fitted metabolites along the threshold of the fitting error, to several combinatorial groups of cells. **(B)** Venn diagram of metabolites, present in all four cell lines, with fits below a 4% error to all cell types. Orange numbers indicate the number of all simulated metabolic profiles that fit to that region, regardless of fitting to other regions with the same or higher number of intersections.

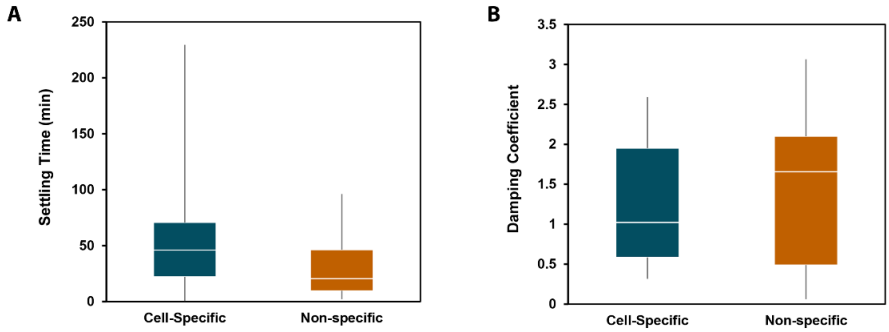

Supplementary Figure 3.5 – Comparison of control-related parameters of simulated metabolic responses between metabolites with cell type-specific dynamics and with shared dynamics across cell types. (A) Boxplot of settling time of simulated metabolic profiles between cell type-specific and shared

dynamics (non-specific). **(B)** Boxplot of damping coefficient of simulated metabolic profiles between cell type-specific and shared dynamics (non-specific).

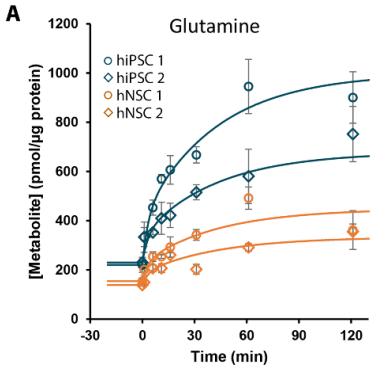

B

Damping Coefficient, ζ	Response Time, τ (min)	Numerator Coefficient, τ_A (min)
1.98	11.58	12.87

C

	Average Fitting Error (%)	Steady-State Gain, K (pmol / μg_{prot} / mM_{step})	Settling Time (min)
hiPSC 1	2.94	778.88	105.25
hiPSC 2	3.50	448.17	98.75
hNSC 1	4.51	294.07	92.00
hNSC 2	4.82	194.85	83.50

Supplementary Figure 3.6 – Modeling glutamine dynamic profile for all cells using the same model parameters, except of steady-state gain. (A) Metabolic profile over two hours for each cell line. Experimental points: hiPSC 1 – blue round circles, hiPSC 2 – blue diamonds, hNSC 1 – orange round circles and hNSC 2 – orange diamonds. Simulated profiles: hiPSC in blue lines and hNSC in orange lines. Experimental data are represented as mean of sampling replicates and error bars represent standard deviation. **(B)** Parameters used for modeling glutamine profiles. **(C)** Step-response descriptors from glutamine modeling for each cell line.

Supplementary Table 3.1 – Step inputs of extracellular glutamine concentration for the different bioreactors.

	Before Pulse (mM)	After Pulse (mM)	Step input (mM) $[Gln]_{ext,final}$ - $[Gln]_{ext,\ initial}$
hiPSC 1	1,46	15,04	13,58
hiPSC 2	2,33	15,43	13,1

hNSC 1	1,59	14,04	12,45
hNSC 2	1,77	14,88	13,11

Supplementary Table 3.2 – Complete metabolic quantification dataset for each cell line.

The Supplementary Table 3.2 is too large to insert here therefore check please the online version of the paper.

Supplementary Table 3.3 – Number of metabolites after each data processing for each cell line. The "Pre-filtered" step refers to the step where metabolites that had 5 or more time-points with values under the detection limit or with a relative standard deviation on averaged molar quantity per protein above 15%, were discarded. Metabolic profiles were then fitted to an equation model and those with a mean fitting error above 5% were discarded.

	hiPSC 1	hiPSC 2	hNSC 1	hNSC 2
Experimental Data	201	201	201	201
Pre-filtered	145	165	159	114
Filtered to a fitting error below 5%	99	134	116	71
	-68%	-81%	-73%	-62%

Supplementary Table 3.4 – Model parameters for simulated metabolite profiles of each cell line shared in article: Sá, JV, Simão, D; Terrasso, A.P.; Silva, M.M; Brito, C., Isidro, I.A.; Alves,

PM.; Carrondo, M.J.T (2019) Unveiling Dynamic Metabolic Signatures in Human Induced Pluripotent and Neural Stem Cells. PLOS Comp Biol.

Supplementary Table 3.5 – Metabolites with unique dynamics for hiPSC, hNSC and metabolites with dynamics shared by all cells lines, divided in steady-state outcome. Metabolites which have characteristic dynamics for hiPSC and also have characteristic dynamics for hNSC are underlined.

	hiPSC	**hNSC**	**hiPSC + hNSC (all 4 cell lines)**
Same Steady-State	Ala	-	-
	Asp		
	ADMA		
	Kynurenine		
	Taurine		
	C2		
	C3-DC (C4-OH)		
	C5:1		
	C6:1		
	C12-DC		
	C16:1-OH		
	C18:1-OH		

	PC aa C34:1		
	PC aa C40:4		
	PC ae C38:4		
	PC ae C42:5		
	Lac		
New and Higher Steady-State	-	-	Gln
			SM C18:1
New and Lower Steady-State	Asn	Ala	
	Gly	His	
	His	Ser	
	Leu	Thr	
	Met	Trp	
	Ser		
	Thr		
	Trp		

4

Discussion and Perspectives

Há tempos de coruja e tempos de falcão

D. João II

Author contributions to this chapter:

João Sá wrote this chapter.

Table of Contents

1. Discussion

The application of stem cell-derived products for human health is still below its potential. Different applications of stem cell bioprocesses – cell therapy, discovery of new targets for regenerative medicine, disease modeling, drug and toxicity testing – have common hurdles. The most relevant hurdle is the lack of quality of cell products due to inefficient and ineffective stem cell differentiation. Differentiated cells *in vitro* do not behave similarly to mature cells *in vivo* despite presenting similar surface and intracellular protein biomarkers. Lack of cell functionality and therefore inadequate for cell therapy, disease modeling, drug testing and toxicity, lies in weak understanding of cell "behavior". Cells communicate with the environment and with neighboring cells, usually through secreted factors and through metabolites. This communication is guaranteed by an adjustable and controlled internal system in which metabolism is extremely important. Therefore, as complement to protein biomarkers, stem cell bioprocesses should be monitored and optimized by evaluating metabolic systemic characteristics. Thus, metabolism can constitute the needed toolbox for understanding and for improving stem cell bioprocesses.

The work developed in this thesis aimed firstly to demonstrate how metabolic systems biology can differentiate between different stages in a neural differentiation process, and secondly, based on the obtained results, to propose new metabolic-based strategies to optimize stem cell bioprocesses. For this, two different metabolic characterization approaches were pursued (Figure 4.1): metabolic flux analysis of neural stem cells and astrocytes in **Chapter 2**, and dynamic metabolomics of pluripotent and neural stem cells in **Chapter 3**.

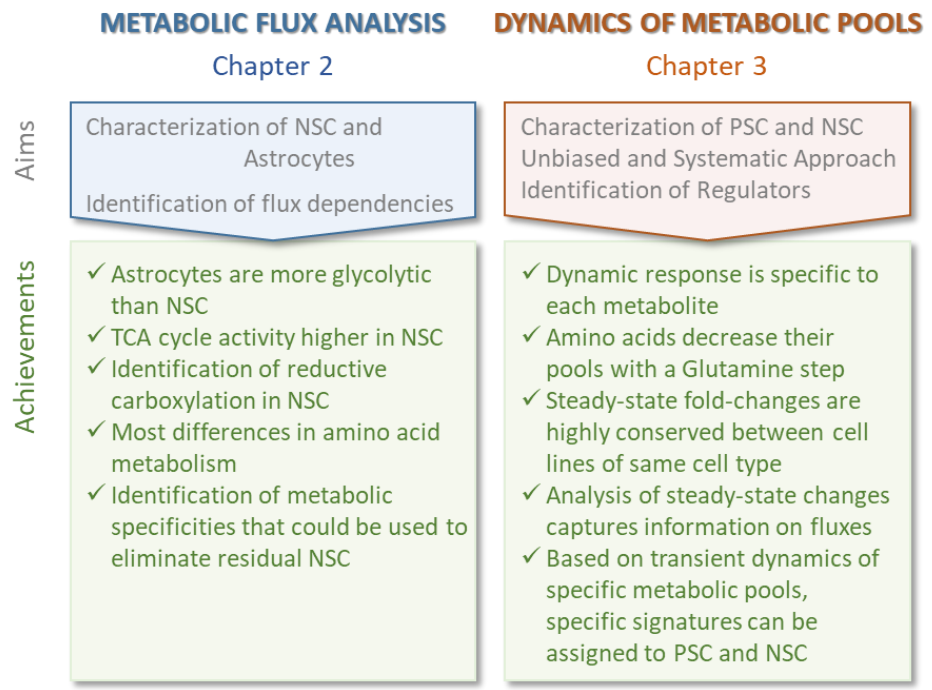

Figure 4.1 – Schematic representation of the major aims of the thesis and the achievements of each chapter (2-3). NSC – Neural Stem Cells; TCA – tricarboxylic acid cycle; PSC – pluripotent stem cells;

Methods for metabolic characterization of stem cells and bioproducts require sufficient accuracy and precision. Ideally, a method for cell characterization also needs to be simple, fast and inexpensive so that it can be better incorporated in stem cell bioprocesses. These quality and process-related objectives in one method has not been yet achieved. In this section, the methods employed in **Chapter 2** and **Chapter 3** will be analyzed under this view. Additionally, in each subsection, optimization strategies will be proposed for improving stem cell bioprocesses, based on the cell characterization achieved in each chapter.

1.1. Metabolic Flux Analysis for Stem Cell Bioprocesses

In **Chapter 2**, ^{13}C-MFA was used to show that the fluxomes of NSC and of astrocytes are distinct. The observed astrocytic fluxome shows a significant glycolytic rate, citrate release, glutamine synthesis and secretion and residual TCA cycle activity. Relevant fluxomic characteristics of NSC include reductive carboxylation, significant lipid synthesis and high upstream TCA cycle activity. The differences between NSC's fluxome and astrocytes' fluxome could be exploited to optimize neural stem cell bioprocessing. To increase the safety of a putative astrocytic therapeutic product, or just increasing purity to enable more precise drug testing and toxicity results, glutamine deprivation or enzymatic blockage of fatty acid synthesis could be employed to starve off NSC. After all, it has been shown that NSC die when deprived of glutamine (Kleiderman et al., 2015).

The intensity of fluxes suggests which metabolic pathways are preferred by a given cell. Metabolic fluxes represent much more than fulfilling energetic, anabolic or redox needs of a cell. These fluxes, and the consequent metabolic pools, also represent a homeostatic regulatory level over the functioning of a cell. This knowledge might be powerful for optimizing stem cell bioprocesses. Firstly, identification of especially active metabolic pathways provides guidance for the design of culture media. Secondly, a metabolic flux map is a phenotypic feature which means that MFA could be used for cell characterization during the process and as product quality control. Thirdly, MFA can reveal metabolic dependencies which might be exploited for removing undesired cells such as residual stem cells in a cardiomyocytes product (Tohyama et al., 2013).

However, metabolic flux analysis (MFA), in its current state, faces relevant technological challenges. MFA uses an algorithm for matching

carbon labelling data, secretion and uptake rates, and quantified metabolic pools, with a metabolic network. Unfortunately, the human metabolic network is still under construction, with new enzymes, new metabolites and new enzymatic reactions being discovered (Sévin et al., 2016). This means that the metabolic network that is given to the algorithm is not complete or may be missing some enzymatic reactions that are important for quantifying accurately and with low error a given cell fluxome. Moreover, MFA methods require knowledge on atom transitions in each enzymatic reaction which is uncertain for many reactions. It should be noted that the metabolic network given to the algorithm cannot be bigger than the available experimental data or the mathematical solution would be undetermined. Thus, a metabolic network has to be shortened to a number of unknown variables and then trimmed by trial-and-error by solving the mathematical system until a reasonable result with a low error is obtained. Additionally, the dimension of the metabolic network is also kept reduced due to metabolite compartmentalization in mammalian cells or the utilization of multiple labelled substrates which increases the number of compounds that need to be experimentally measured (Niklas and Heinzle, 2012). On top of all these hurdles it is still unclear if the obtained result is unique or multiple, this is, if there are multiple metabolic flux maps for the same given set of experimental data. Here, scientists and engineers from the life sciences need further developments on network mathematics, a highly complex field (Pržulj and Malod-Dognin, 2016).

Beyond technological challenges, a reasonable argument can be made against the accuracy of MFA in describing the systemic metabolism of a given cell. Metabolic fluxes are adjustable and can even reverse directions to accommodate different extracellular environments (Pavlova et al., 2018; Zhang et al., 2016). Therefore, through a snapshot of

metabolic fluxes, it is unclear how to determine what is circumstantial and what is inherent and characteristic of the system.

Other problems hinder the applicability of MFA for stem cell in-process control bioprocesses. An important one is time. It usually takes at least a day of experimental work, plus the time for computational analysis. Expensive reagents and labor-intensive experiments limit its broader application.

1.2. Dynamic Metabolomics for Stem Cell Bioprocesses

In **Chapter 3**, a new characterization approach focused on unveiling the intracellular metabolic control of a cell was pursued. The hypothesis consisted that each type of cell present metabolic pools with specific, and therefore characteristic, control dynamics. This is based on the present knowledge of the influence of several metabolites in the fate of specific cells. To identify candidates with regulatory potential, an extracellular step stimulus was applied. A relatively large number of metabolites with a broad chemical range was followed after the extracellular pulse. The first important observation was that metabolic pools levels changed but cell phenotype did not. This means that “static” characterization methods quantifying metabolic pools are only focusing on one possible metabolic pool set. Secondly, some metabolic pool changes were conserved between different cell lines of hiPSC and hNSC, suggesting that some metabolic pools have controlled steady-state changes while other metabolic pools are “free” to change their level. Interestingly, when mapping the ratio of metabolic pool levels after and before the pulse onto a metabolic network, similarities to the metabolic flux map retrieved from literature and even from work in **Chapter 2** could be observed. The consequence is the use of this pulse approach to determine active fluxes, which consumes less computational time and is cheaper as ^{13}C-labelling

is not required. Finally, characterization at the metabolic level was achieved by modelling the dynamic data of each metabolic pool to a classical process dynamics equation. Dynamic simulation of most amino acid profiles showed a cell-specific curve. This means that the capture of the dynamic behavior of amino acid metabolic pools, over time after a perturbation, may be an important complement for cell characterization. After all, the analytical methods for amino acids are abundant, precise and accurate. Additionally, there are several molecular methods to probe and study amino acid metabolism. Of course the proposed method is also experimentally and computationally burdensome to which improved procedures, such as by use of robots, and algorithms are needed.

However, many questions raised during the work in **Chapter 3** were left unanswered. One of those questions was if metabolites could be compared in terms of response efficiency, i.e., which metabolites had a dynamic response to perturbation pertained as having a better control system design. A way to look into a “good” control is to determine the settling time, this is, the timing the metabolic pool takes until reaching a new steady-state level. Another parameter to consider is the dampening coefficient which describes how sluggish or oscillatory is the response, ideally the dynamic response should be a balance between those two extremes. These parameters were not determined with precision due to lack of experimental points. Thus, next experiments will have to include more experimental points which represents a challenge that needs a creative solution.

2. Conclusions and Perspectives

In this thesis, cells involved in a neural stem cell process were characterized using two distinct approaches: one starting from a network and determining the respective individual fluxes (a “top-down” approach) and another going from the particular observation to the overall observation of the system (“bottom-up” approach). The “bottom-up” approach, through the dynamic quantification of several metabolic pools after a sudden extracellular metabolic pulse (**Chapter 3**), illustrates a novel approach to metabolomics. Non only in being capable of describing and differentiating hiPSC from hNSC with some precision and accuracy, but also on reproducing some of the flux results obtained by ^{13}C-MFA (“top-down” approach, **Chapter 2**) for hNSC. Moreover, that reproduction of results was performed through experiments which were cheaper and whose result analysis does not require lengthy and labor-intensive computations.

Additionally, the observation of dynamic responses of each metabolic pool offers an extraordinary promise: the identification of key metabolic regulators. Some work was developed in attempting to identify those metabolic regulators by determining parameters associated with effective control of systems: settling time, the damping coefficient (data not shown). However, the available data was insufficient to determine parameters with a low associated error. This is something that can be solved by obtaining more time points during the dynamic metabolic response interval.

Nevertheless, ^{13}C-MFA can have a slightly different application which dynamic metabolomics cannot do on its own: unravelling the metabolic crosstalk between cells. This metabolic crosstalk might be relevant for stem cell bioprocess. During the natural development of human body, it is known that the majority of cells grow (and differentiate) in a neighborhood

with cells of different identity. This suggests that cells may only achieve functional maturity if a metabolic crosstalk is established. However, in bioprocesses it is preferred to have monocultures. Thus, this metabolic crosstalk has to be reproduced without the concurrent use of other cells. Here, ^{13}C-MFA applied to co-cultures constitute probably one of the few methods capable of deciphering its metabolic crosstalk. The design of such interconnected metabolic network needs some adjustments but those are feasible, though a much larger set of experimental data is needed. Once discovered the metabolites involved in crosstalk between cells, one possibility to reproduce those in monocultures is through the use of peptides. Peptides composed of amino acids involved in metabolic crosstalk can be cleaved and the resultant amino acids consumed in a rate and with an extracellular concentration close to an *in vivo* situation.

Ideally, a combination of these two approaches would be the most appropriate to gain knowledge on metabolic systems. Some authors are already attempting to combine network based models with dynamic responses (Christodoulou et al., 2018). Moreover, the metabolic network does not need to be solely created by the user, as dynamic data will help completing the desired network.

Overall, I hope that work in this thesis has demonstrated the value of metabolic systems biology as a cell characterization tool and its potential for the design of strategies for improving bioprocesses. In a more particular view, we have demonstrated, through two different metabolic characterization methods, that amino acids features, be it fluxes or intracellular pool dynamics, seem to be specific to each cell type. Importantly, the conjugation of amino acids being spread in a reasonable wide range over the metabolic network, and of analytical methods of amino acids being very well established, can help focus the search of metabolism-based strategies for optimizing stem cell processes.

3. References

Christodoulou, D., Link, H., Fuhrer, T., Kochanowski, K., Gerosa, L., and Sauer, U. (2018). Reserve Flux Capacity in the Pentose Phosphate Pathway Enables Escherichia coli's Rapid Response to Oxidative Stress. Cell Syst. *6*, 1–10.

Kleiderman, S.M., Sá, J. V, Teixeira, A.P., Brito, C., Gutbier, S., Evje, L.G., Hadera, M.G., Glaab, E., Henry, M., Agapios, S., et al. (2015). Functional and phenotypic differences of pure populations of stem cell-derived astrocytes and neuronal precursor cells. Glia *64*, 1–21.

Niklas, J., and Heinzle, E. (2012). Metabolic Flux Analysis in Systems Biology of Mammalian Cells. Adv. Biochem. Eng. Biotechnol. *127*, 109–132.

Pavlova, N.N., Hui, S., Ghergurovich, J.M., Fan, J., Intlekofer, A.M., White, R.M., Rabinowitz, J.D., Thompson, C.B., and Zhang, J. (2018). As Extracellular Glutamine Levels Decline, Asparagine Becomes an Essential Amino Acid. Cell Metab. *27*, 1–11.

Pržulj, N., and Malod-Dognin, N. (2016). Network analytics in the age of big data. Science *353*, 123–124.

Sévin, D.C., Fuhrer, T., Zamboni, N., and Sauer, U. (2016). Nontargeted in vitro metabolomics for high-throughput identification of novel enzymes in Escherichia coli. Nat. Methods *14*, 187–194.

Tohyama, S., Hattori, F., Sano, M., Hishiki, T., Nagahata, Y., Matsuura, T., Hashimoto, H., Suzuki, T., Yamashita, H., Satoh, Y., et al. (2013). Distinct metabolic flow enables large-scale purification of mouse and human pluripotent stem cell-derived cardiomyocytes. Cell Stem Cell *12*, 127–137.

Zhang, H., Badur, M.G., Divakaruni, A.S., Parker, S.J., Jäger, C., Hiller,

K., Murphy, A.N., and Metallo, C.M. (2016). Distinct Metabolic States Can Support Self-Renewal and Lipogenesis in Human Pluripotent Stem Cells under Different Culture Conditions. Cell Rep. *16*, 1536–1547.